Thermodynamic and Structural Analysis of Protein Aggregation and Amyloid Formation

DISSERTATION

zur Erlangung des Doktorgrades
der Naturwissenschaften
(Dr. rer. nat.)

eingereicht beim
Fachbereich Chemie
der Technischen Universität Dortmund

von

M. Sc. Vytautas Smirnovas

aus Visaginas, Litauen

Dortmund, 2007

Erstgutachter:	Prof. Dr. R. Winter
Zweitgutachter:	Prof. Dr. H. Rehage

Acknowledgements

Fist of all I would like to thank Prof. Dr. R. Winter for a chance to work on my PhD under his supervision. His guidance and support helped me to learn a lot of new things during my work. It was the first place where I had ability to use a number of different techniques and collaborate with a number of scientists all around the world. Thanks for all of this!

I would like to thank to Dr. W. Dzwolak for introducing me to topic of amyloid first, recommending me to Prof. Dr. R. Winter later and finally for collaboration during my work in Dortmund.

I want to thank Prof. Dr. E. Butkus – for encouraging me to go abroad for PhD studies.

I would like also to thank Prof. Dr. H. Rehage for being in my examination committee.

Many thanks go to all external scientists, I have ability to collaborate to: first of all, Dr. T. Funck, who introduced me to sound velocity measurements and his colleagues: Dr. H. Bierbaum, Dr. D. Gau, Dr. K. Born and Dr. S. Dickopf from TF Instruments, Heidelberg; M. Keerl and Prof. Dr. W. Richtering from RWTH Aachen for ability to learn a bit about polymers; Prof. Dr. S. Decatur from Mount Holyoke College, USA for ability to work on isotope-labeled peptides, Dr. O. Ces and his colleagues from Imperial College, London for a chance to use x-ray beam in ESRF.

Even more thanks I should address to the colleagues who worked around me. First of all I would like to thank PD, Dr. C. Czeslik for being the first one to answer any question and for being in my examination committee. Thanks to Dr. R. Jansen for collaboration and teaching AFM, Dr. J. Kraineva for collaboration and teaching high pressure FTIR and high pressure SAXS, Dr. S. Zhao and L. Mitra for help with DSC and PPC, Dr. S. Grudzielanek for a lot of fruitful collaboration and help with fluorescence and CD measurements, Dr. D. Lopes for interesting collaboration working on IAPP. Thanks to Dr. N. Smolin, Dr. G. Jackler, Dr. J. Baranski, Dr. E. Powalska, Dr. K. Voggt, Dr. M. Khurana, Dr. N. Javid, Dr. C. Nicolini, Dr. K. Weise, Dr. R. Mishra, Dr. R. Krivanek, M. Sulc, A. Gohlke, S. Jha, N. Periasamy, D. Sellin, G. Singh for all

the help and friendship during the years of working together or spending time after the work.

Special thanks for D. Radovan and M. Pühse for checking my PhD script, M. Andrews, for help with improving my English and C. Jeworrek for help with Zusammenfassung.

Thanks for Dr. W. Horstmann, frau B. Gruß and A. Kreusel for help everytime when I had problems with papers in German and for M. Saskovic and B. Schuppan for help with solving technical problems.

There are a lot of people I should thank and I hope I was able to remember all of them, but in case if you find yourself not mentioned here and you feel that I should have thanked you, I would like to thank you too!

Contents

Publications

Dzwolak W, **Smirnovas V**, Jansen R and Winter R: Insulin forms amyloid in a strain-dependent manner: An FT-IR spectroscopic study. PROTEIN SCI 13 (7): 1927-1932, 2004.

Dzwolak W, Jansen R, **Smirnovas V**, Loksztejn A, Porowski S and Winter R: Template-controlled conformational patterns of insulin fibrillar self-assembly reflect history of solvation of the amyloid nuclei. PHYS CHEM CHEM PHYS 7 (7): 1349-1351, 2005.

Dzwolak W and **Smirnovas V**: A conformational alpha-helix to beta-sheet transition accompanies racemic self-assembly of polylysine: an FT-IR spectroscopic study. BIOPHYS CHEM 115 (1): 49-54, 2005.

Dzwolak W, Grudzielanek S, **Smirnovas V**, Ravindra R, Nicolini C, Jansen R, Loksztejn A, Porowski S and Winter R: Ethanol-perturbed amyloidogenic self-assembly of insulin: Looking for origins of amyloid strains. BIOCHEMISTRY-US 44 (25): 8948-8958, 2005.

Smirnovas V, Winter R, Funck T and Dzwolak W: Thermodynamic properties underlying the alpha-helix-to-beta-sheet transition, aggregation, and amyloidogenesis of polylysine as probed by calorimetry, densimetry, and ultrasound velocimetry. J PHYS CHEM B 109 (41): 19043-19045, 2005.

Grudzielanek S, **Smirnovas V** and Winter R: Solvation-assisted pressure tuning of insulin fibrillation: From novel aggregation pathways to biotechnological applications. J MOL BIOL 356 (2): 497-509, 2006.

Smirnovas V, Winter R, Funck T and Dzwolak W: Protein amyloidogenesis in the context of volume fluctuations: A case study on insulin. CHEMPHYSCHEM 7 (5): 1046-1049, 2006.

Dzwolak W, Loksztejn A and **Smirnovas V**: New insights into the self-assembly of insulin amyloid fibrils: An H-D exchange FT-IR study. BIOCHEMISTRY-US 45 (26): 8143-8151, 2006.

Kraineva J, **Smirnovas V** and Winter R: Effects of lipid confinement on insulin stability and amyloid formation. LANGMUIR 23 (13): 7118-7126, 2007.

Grudzielanek S, Velkova A, Shukla A, **Smirnovas V**, Tatarek-Nossol M, Rehage H, Kapurniotu A and Winter R: Cytotoxicity of insulin within its self-assembly and amyloidogenic pathways. J MOL BIOL 370 (2): 372-384, 2007.

Grudzielanek S, **Smirnovas V** and Winter R: The effects of various membrane physical-chemical properties on the aggregation kinetics of insulin. CHEM PHYS LIPIDS 149 (1-2): 28-39, 2007.

Keerl M, **Smirnovas V**, Winter R and Richtering W: Interplay between synergistic hydrogen bonding and macromolecular architecture leading to unusual phase behaviour in thermosensitive ‘smart’ microgels. ANGEW CHEM, 2007, in press.

1. Introduction

1.1. Prions

The mystery behind scrapie, kuru and mad cow disease has finally been unraveled. Additionally, the discovery of prions has opened up new avenues to better understand the pathogenesis of other more common dementias, such as Alzheimer's disease [Petterson, 1997]. These words have been told 10 years ago when Stanley B. Prusiner recieved the Nobel Prize in medicine for his discovery of prions – a new biological principle of infection.

Prions are infectious proteins. In mammals, prions reproduce by recruiting normal cellular prion precursor protein (PrP^{C}) and thus stimulate its conversion to the disease-causing (scrapie) isoform (PrP^{Sc}). A major feature that distinguishes prions from viruses is that PrP^{Sc} is encoded by a chromosomal gene [Prusiner, 1998]. Limited proteolysis of PrP^{Sc} produces a smaller, protease-resistant molecule of approximately 142 amino acids, designated PrP 27–30, which polymerizes into amyloid [McKinley et al., 1991].

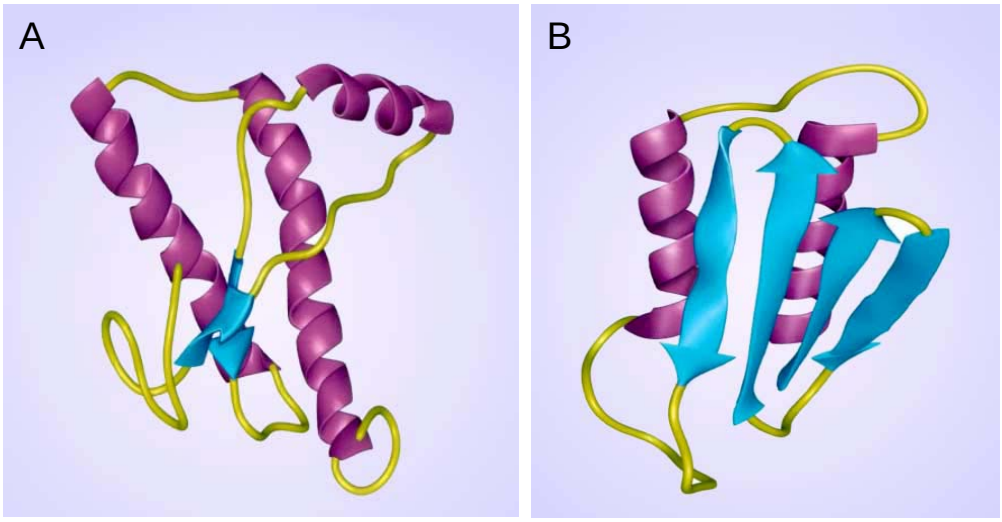

Figure 1: Structures of Prion Protein isoforms: panel A shows the α-helical structure of Syrian hamster recombinant PrP 90-231, which presumably resembles that of the cellular isoform (PrP^{C}); panel B shows a plausible model of the tertiary structure of human PrP^{Sc} [Prusiner, 2001].

The polypeptide chains of PrP^{C} and PrP^{Sc} are identical in composition but differ in their three-dimensional folded structures (conformations). PrP^{C} is rich in α-helixes and

has little β-sheet conformation, whereas the β-sheet conformation is the main component of PrP^{Sc} (Fig. 1) [Pan et al., 1993].

Several new concepts have emerged from studies of prions. First of all, prions are the only known example of nucleic acid-free infectious pathogens. All other infectious agents contain either RNA or DNA, which direct the synthesis of their proteins. Secondly, prion diseases (Table 1) are the only group of illnesses, which while caused by a single pathogen may manifest as infectious, genetic, or sporadic disorders. Thirdly, prion diseases result from the accumulation of PrP^{Sc}, which has a substantially different conformation from that of its precursor, PrP^{C}. Fourthly, PrP^{Sc} can have a variety of conformations, all of which seem to be associated with a specific disease. How a particular conformation of PrP^{Sc} is imparted to PrP^{C} during replication in order to produce a nascent PrP^{Sc} with the same conformation still remains unknown [Prusiner, 2001].

Table 1: Prion diseases [Prusiner, 1998].

Disease	Host	Mechanism of pathogenesis
Kuru	Fore people	Infection through ritualistic cannibalism
Iatrogenic Creutzfeldt-Jacob disease (CJD)	Humans	Infection from prion-contaminated human growth hormone (HGH)
Sporadic CJD	Humans	Somatic mutations or spontaneous conversion of PrP^{C} into PrP^{Sc}
Familial CJD	Humans	Germ-line mutations in PrP gene
New variant CJD	Humans	Infection from bovine prions
Fatal familial insomnia (FFI)	Humans	Germ-line mutations in PrP gene
Gerstmann-Sträusller-Sheinker disease (GSS)	Humans	Germ-line mutations in PrP gene
Fatal sporadic insomnia (FSI)	Humans	Somatic mutations or spontaneous conversion of PrP^{C} into PrP^{Sc}
Scrapie	Sheep	Infection of genetically susceptible sheep
Bovine spongiform encephalopathy (BSE)	Cattle	Infection with prion-contaminated meat and bone meal (MBM)
Transmissible mink encephalopathy (TME)	Mink	Infection with prions from sheep or cattle
Chronic wasting disease (CWD)	Deer, elk	Unknown
Feline spongiform encephalopathy (FSE)	Cats	Infection with prion-contaminated bovine tissues or MBM
Exotic ungulate encephalopathy	Greater Kudu, nyala	Infection with prion-contaminated MBM

The existence of prion strains raises the question of how heritable biologic information can be encrypted in a molecule other than a nucleic acid [Dickinson et al., 1968; Ridley and Baker, 1996]. Different strains of prions have been defined according to the rapidity with which they cause central nervous system damage and by the distribution of neuronal vacuolation [Dickinson et al., 1968]. Patterns of PrP^{Sc} deposition have also been used to characterize these strains [DeArmond et al., 1987; Bruce et al., 1989]. There is growing evidence that the diversity of prions is encoded in the conformation of the PrP^{Sc} protein [Telling et al., 1996; Safar et al., 1998]. Studies involving the transmission of fatal familial insomnia and familial Creutzfeldt–Jakob disease to mice expressing a chimeric human–mouse PrP transgene have shown that the tertiary and quaternary structure of PrP^{Sc} contains strain-specific information [Telling et al., 1996]. Studies of patients with fatal sporadic insomnia have extended these findings [Mastrianni et al., 1999], making it clear that PrP^{Sc} acts as a template for the conversion of PrP^{C} into nascent PrP^{Sc}.

1.2. Neurodegenerative diseases

Although prion diseases, due to possible infectivity, can become a major problem in the future, currently the number of cases is very low in comparison to other neurodegenerative diseases (Table 2). Alzheimer's disease is the most common neurodegenerative disorder followed by Parkinson's disease as the second most common one. According to the most current available data, there are more than 5 million Alzheimer's disease cases [www.alz.org] and more than 1 million Parkinson's disease cases [www.pdf.org] in the United States, which is more than 2 % of the whole population of the country.

Alzheimer's Association reports that currently 19 % Americans between age 75 and 84 and 42 % of those over age 85 are affected by this syndrome. As life expectancy continues to increase, the number of neurodegenerative diseases is growing. Although worldwide prevalence of Alzheimer's disease in 2006 was approximately 26.6 million, the forecast for 2050 suggest that more than 1 % of the world population will be affected [Brookmeyer et al., 2007].

There is increasing evidence, showing that different neurodegenerative diseases have common cellular and molecular mechanisms including protein aggregation. The aggregates usually consist of fibers containing misfolded protein with a dominant β-sheet conformation, termed amyloid [Ross and Poirier, 2004].

Table 2: Prevalence of neurodegenerative diseases in the United States in 2000 [Prusiner, 2001].

Disease	Number of cases	per 100000 of population
Prion disease	400	< 1
Pick's disease	5000	2
Spinocerebellar ataxias	12000	4
Progressive supranuclear palsy	15000	5
Amyotrophic lateral sclerosis	20000	7
Huntington's disease	30000	11
Frontotemporal dementia	40000	14
Parkinson's disease	1000000	360
Alzheimer's disease	4000000	1450

1.3. Amyloid

The definition of "amyloid" has varied over the years. Back in 1854, the German scientist Rudolf Virchow described iodine staining of the cerebral *corpora amylacea* that had an abnormal macroscopic appearance. As the sample showed typical starch-iodine reaction, he assumed that the substance contained a carbohydrate moiety [Virchow 1854] and named it amyloid. Later Friedreich and Kekulé proved the absence of carbohydrates along with the presence of a protein, and amyloid became known as a class of proteins [Sipe and Cohen, 2000]. Further studies made a more precise description possible. In clinical practice amyloid was characterized through its affinity to Congo red and green birefringence in polarized light after staining with Congo red [Jin et al., 2003]. Secondary structure studies showed a β-sheet rich structure [Glenner, 1980] and electron microscopy discovered that the amyloid material is made of ordered aggregates – filaments and fibers [Perutz et al., 2002]. Most recently, amyloid is defined as an extracellular deposit of protein fibrils with the specific organization, which has characteristic properties observed after staining with Congo red [Westermark et al., 2005]. It is suggested that the term "amyloid" would be restricted to the *in vivo*

material. Other fibrillar material should be called “amyloid-like” [Westermark, 2005]. Nevertheless, the term “amyloid fibrils” is widely used for any type of fibrillar aggregates [Dobson, 2003; Wetzel et al., 2007] and seems to be popular enough to override official guidelines.

For many years it was generally assumed that the ability to form amyloid fibrils was limited to the proteins, implicated in diseases, and that these proteins possess specific sequence motifs encoding the amyloid core. But during the last decade it was shown that many proteins, not associated with diseases can form amyloid-like fibrils [Fandrich et al., 2001; Nielsen et al., 2001; Munishkina et al., 2003]. Homopolypeptides, such as polylysine or polythreonine [Fandrich and Dobson, 2002], and even short oligopeptides, containing 4-6 amino acids [Lopez de la Paz et al., 2002; Baumketner and Shea, 2005] are able to be converted into amyloid fibers, as well.

Although amyloid precursor proteins are very different in amino acid sequence, secondary structure and size, the mature fibers show similar highly organized morphology and mechanisms of toxicity [Dobson, 2004]. It has been suggested that nearly all proteins have the ability to form amyloid under certain conditions, and that this can be considered a generic feature of polypeptide chains [Stefani and Dobson, 2003].

1.4. Structure of amyloid fibrils

A number of studies were aimed at obtaining an insight into the macromolecular structure of amyloid fibrils using atomic force microscopy [Jansen et al. 2005; Khurana et al. 2003], electron microscopy [Jimenez et al., 2001, 2002] and even fluorescence microscopy [Ban et al., 2006]. Despite the diversity of amyloid-forming proteins, structural studies agree that all fibrils are composed of protofilaments – the smallest fibrillar subunits. Protofilaments can assemble into protofibrils and fibrils. Dimensions of protofilaments and their assemblies depend on the substrate protein (Fig. 2). Although various models of fibril assembly from protofilaments can be supported by microscopy images of selected specimen, overall mature fibrils are too different and too inhomogenous to be described by a single model. Even the well-studied insulin amyloid

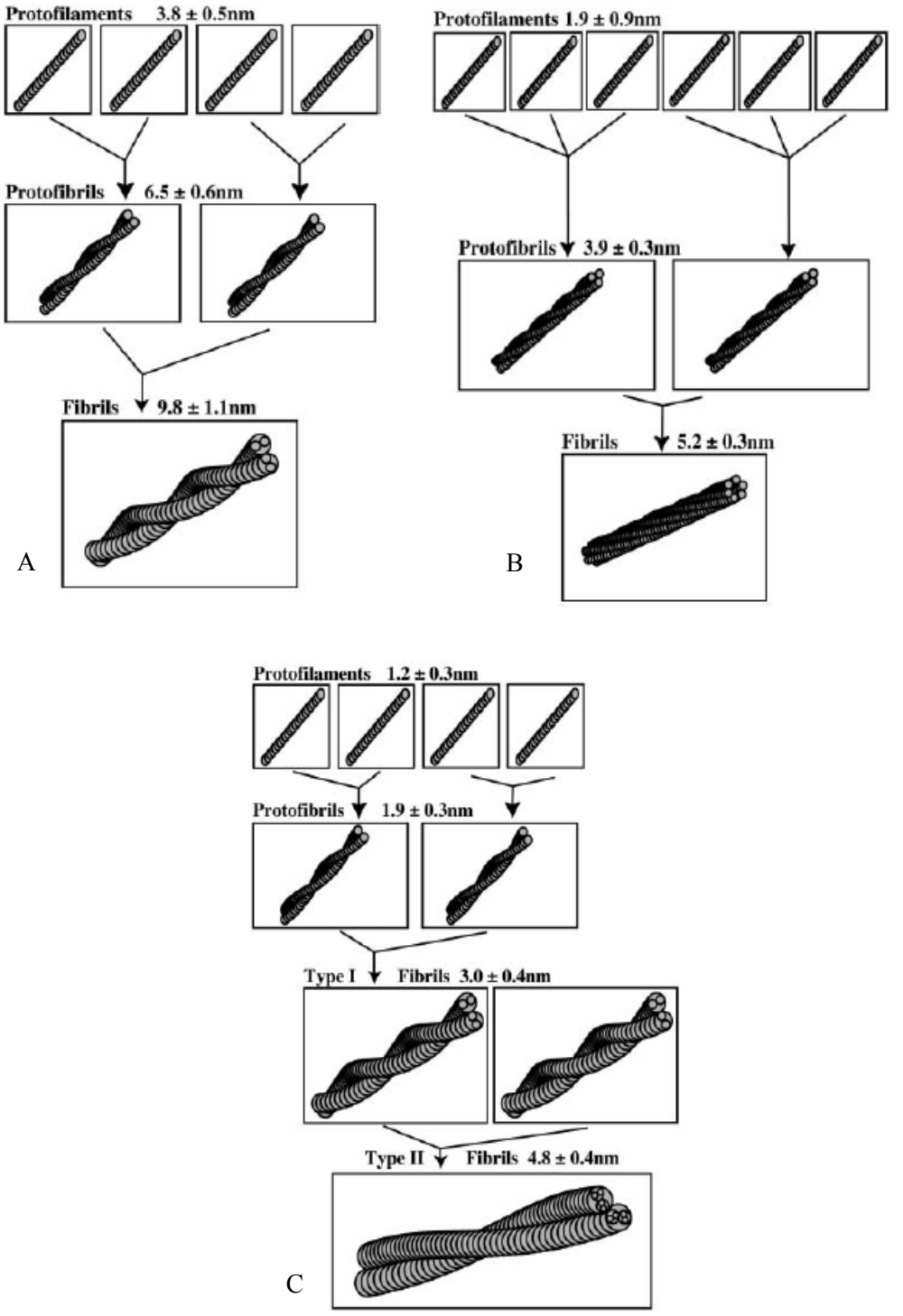

Figure 2: Models of hierarchical assembly of protofilaments into amyloid fibrils. Protofilament pairs wind together to form protofibrils, and each two protofibrils wind to form a fibril in case of α-synuclein (A); three protofilaments wind together to form a protofibril, and two protofibrils (or six protofilaments) wind to form a fibril in case of the B1 domain of protein G (B), and protofilament pairs wind together to form protofibrils, and each two protofibrils wind to form a type I fibril. Type II fibrils are the result of winding of type I fibrils in the case of insulin (C) [adapted from Khurana et al. 2003].

still raises a lot of questions in developing a common definition of the mature fibril structure due to its polymorphism (Fig. 3).

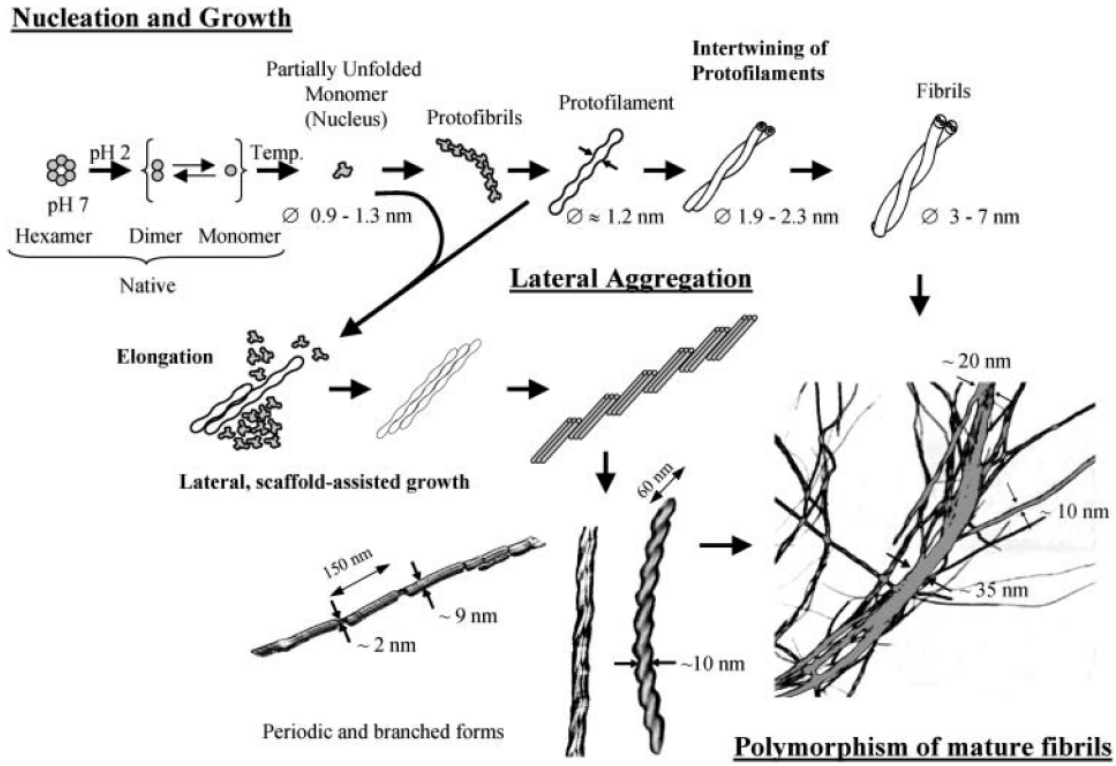

Figure 3: Generalized scheme of the multipathway fibrillization of insulin. The lateral interaction of early, prefibrillar forms with protofibrils and protofilaments, followed by the lateral association of protofilaments, is a self-assembly route alternative to the hierarchical intertwining of protofilaments. The observed polymorphism of mature amyloid samples suggests that, under the given conditions, insulin fibrillization proceeds from both pathways [Jansen et al., 2005].

The internal structure of amyloid protofilaments was studied mainly by X-ray diffraction [Geddes et al., 1968; Sunde et al., 1997] and solid state NMR [Tycko 2000, 2003]. The x-ray diffraction patterns of amyloid fibrils reveal a periodic molecular structure consisting of polypeptide chains in the extended β-conformation, forming hydrogen-bonded-β-sheets which run parallel to the long axis of the fibril, whereas the constituent β-strands are arranged perpendicular to this axis. This data has led establishing the cross-β structure model of amyloid protofilaments (Fig. 4). Although other models, such as the β-helix [Raetz and Roderick, 1995; Lazo and Downing, 1998] and predominantly native structures [Bouset et al., 2002; Inouye et al., 1998] were

described, the cross-β structure has a big support, including highly detailed structures for amyloid fibrils [Makin et al., 2005; Nelson et al., 2005].

Figure 4: Molecular model of the common core protofilament structure of amyloid fibrils. A number of β-sheets (four illustrated here) make up the protofilament structure. These sheets run parallel to the axis of the protofilament, with their component β-strands perpendicular to the fibril axis. With normal twisting of the β-strands, the β-sheets twist around a common helical axis that coincides with the axis of the protofilament, giving a helical repeat of 115.5 Å containing 24 β-strands (this repeat is indicated by the boxed region) [adapted from Sunde et al., 1997].

1.5. Mechanism of amyloid fibril formation

The most widely accepted and characterized mechanism of amyloid formation is the so-called "nucleation-elongation" or "nucleated growth" mechanism. Kinetic measurements of spontaneous aggregation usually show a lag phase, when no major changes are observed, followed by a rapid exponential growth phase [Nielsen et al., 2001; Serio et al., 2000]. The lag phase is defined as the time, required for the formation of "nuclei" – the structures which are able to grow into amyloid fibrils. Once the nucleus is formed, the fibril starts to grow by the attachment of either monomers or oligomers to the nucleus.

A lot of effort directed toward studying the nucleation process and the identification and characterization of the structures forming prior to fibrils has been made during the last decade. It has been shown that globular proteins need at least partial unfolding to be able to aggregate and form amyloid fibrils [Dobson, 1999; Uversky and Fink, 2004]. In some cases the presence of structured oligomers [Kayed et

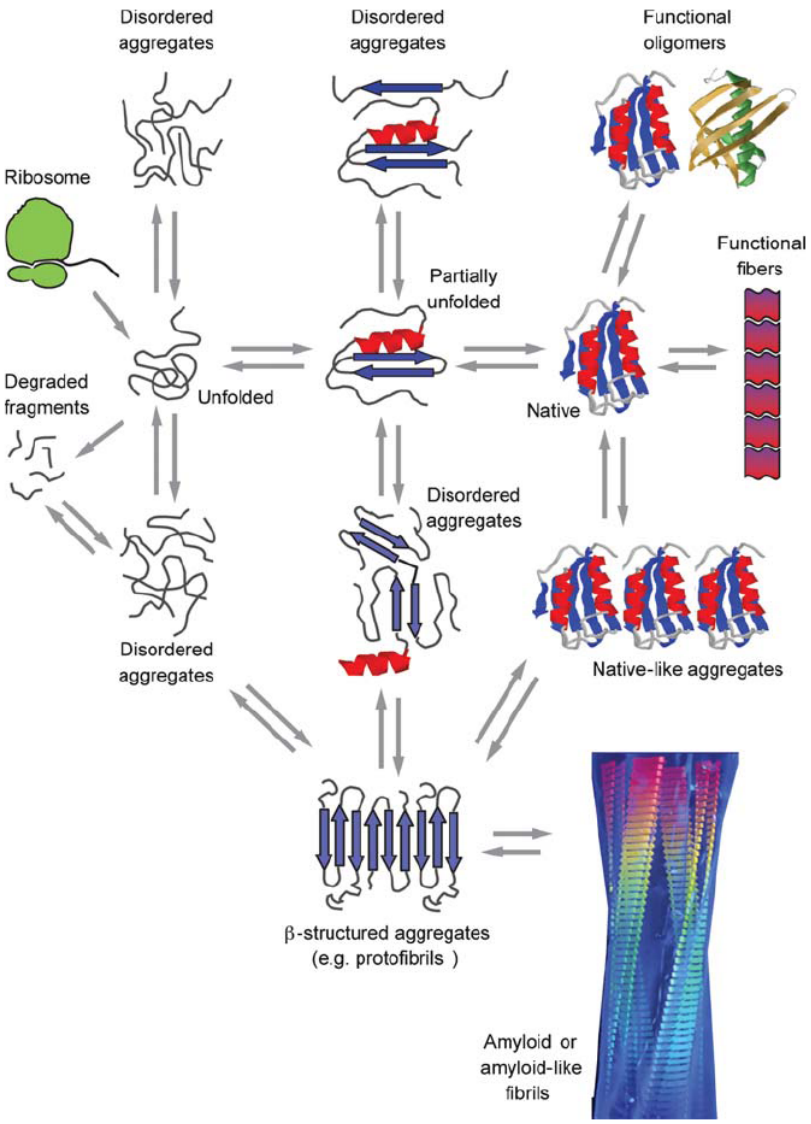

Figure 5: A schematic representation of some of the many conformational states that can be adopted by polypeptide chains. The transition from β-structured aggregates to amyloid fibrils can occur by addition of either monomers or protofibrils (depending on the protein) to preformed β-aggregates. All of these different conformational states and their interconversions are carefully regulated in the biological environment, much as enzymes regulate all the chemistry in cells, by using machinery such as molecular chaperones, degradatory systems, and quality control processes. Many of the various states of proteins are utilized functionally by biology, including unfolded proteins and amyloid fibrils, but conformational diseases will occur when such regulatory systems fail, just as metabolic diseases occur when the regulation of chemical processes becomes impaired [Chiti and Dobson, 2006].

al., 2004; Quintas et al., 2001] or unstructured aggregates [Kishnan and Lindquist, 2005; Modler et al., 2003] has been reported. Polypeptide chains can adopt different

conformational states and interconvert between them on a wide range of timescales. The network of equilibria, which link some of the most important of such states both inside and outside the cell, is schematically illustrated in figure 5 [Chiti and Dobson, 2006].

1.6. Seeding

A nucleated growth mechanism has been well studied in other contexts such as crystallization of molecules [Jarrett and Lansbury, 1993]. As in other processes dependent on a nucleation step, the addition of preformed fibrillar species to a protein sample under aggregation conditions causes shortening or complete elimination of the lag phase [Serio et al., 2000]. Such an effect is known as seeding. In the context of the nucleated growth model, the addition of preformed fibrillar species can be equated to addition of nuclei, so that the elongation process can start without the additional time (lag phase) required for the nuclei formation. In many cases, the formation of nuclei requires destabilization of protein; in the case of some familial forms of diseases it is the

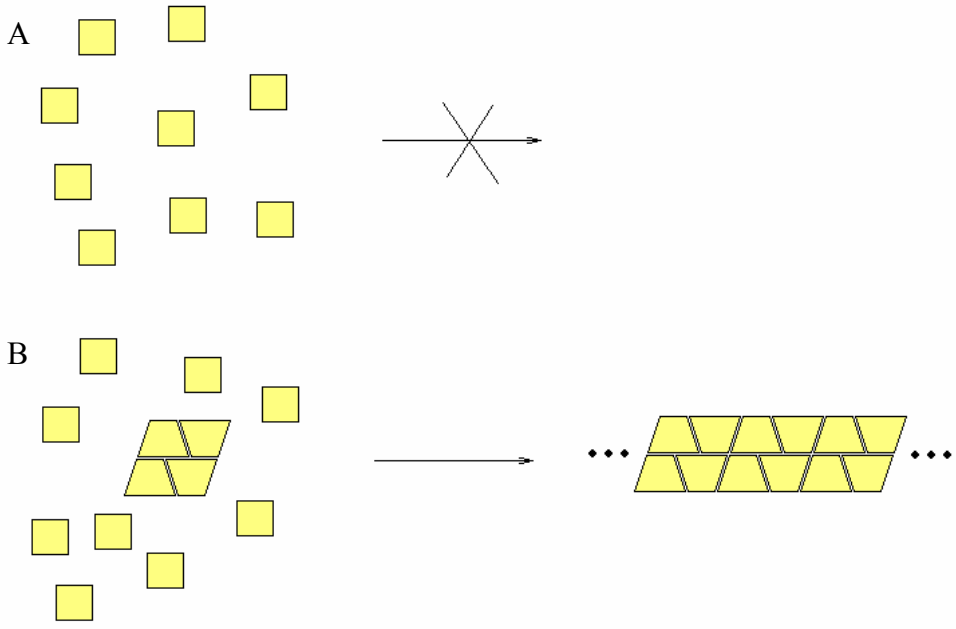

Figure 6: Under native conditions, the proteins are not able to form fibrils (A), but once preformed fibrillar species are added, elongation of fibrils occurs (B).

primary mechanism through which natural mutations mediate their pathogenicity [Canet et al., 2002]; but when preformed fibrillar species are added to a sample, elongation of fibrils can proceed even under conditions, which are normally not favorable for nuclei formation [Dzwolak et al., 2004a]. The ability of preformed amyloid fibrils to seed native proteins under native conditions (Fig. 6) opens a new page in the history of infectious particles by creating prions.

2. Materials and Methods

2.1. Materials

2.1.1. Chemicals

Chemicals, used for the experiments presented in this work are described in the following table (Table 3). For all experiemnts deionized water with (> 18 MΩ cm) was used, being obtained with the aid of an ELGA PURELAB Classic polisher system (ELGA LabWater, Celle, Germany).

Table 3: Chemicals, used for the experiments.

Material	Supplier
Insulin from bovine pancreas	Sigma-Aldrich, Steinheim, Germany
Poly-D-lysine, 27.2 kDa (PDL)	Sigma-Aldrich, Steinheim, Germany
Deuterium oxide, 99.9 atom % D (D_2O)	Sigma-Aldrich, Steinheim, Germany
Deuterium chloride, 99 atom % D (DCl)	Sigma-Aldrich, Steinheim, Germany
Ethyl alcohol-*d*, 99.5 atom % D (EtOD)	Sigma-Aldrich, Steinheim, Germany
Sodium deuteroxide, 99.5 atom % D (NaOD)	Sigma-Aldrich, Steinheim, Germany
Hydrochloric acid (HCl)	Merck, Darmstadt, Germany
Ethyl alcohol (EtOH)	Sigma-Aldrich, Steinheim, Germany
Sodium chloride (NaCl)	Merck, Darmstadt, Germany
Sodium phosphate, monobasic (NaH_2PO_4)	Sigma-Aldrich, Steinheim, Germany
Sodium phosphate, dibasic (Na_2HPO_4)	Sigma-Aldrich, Steinheim, Germany
Sodium hydroxide (NaOH)	Merck, Darmstadt, Germany
2,2,2-Trifluorethanol (TFE)	Merck, Darmstadt, Germany
Glycerol	Sigma-Aldrich, Steinheim, Germany
Thioflavin T (ThT)	Merck, Darmstadt, Germany
Chloroform ($CHCl_3$)	Merck, Darmstadt, Germany
Islet amyloid polypeptide (IAPP)	Calbiochem®, Merck, Darmstadt, Germany

2.1.2. Insulin

Insulin is a hormone produced by β cells in the pancreas. It has three important functions: it allows glucose to pass into cells, suppresses excess production of sugar in the liver and muscles and suppresses the breakdown of fat for energy.

Insulin is a rather small protein, with a molecular weight of 5740 Daltons. It is composed of two peptide chains, referred to as the A chain and B chain. The chains are linked together by two disulfide bonds, and an additional disulfide is formed within the A chain. In most species, the A chain consists of 21 amino acids and the B chain of 30 amino acids (Fig. 7).

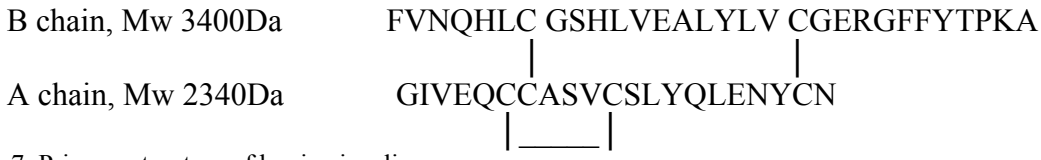

Figure 7: Primary structure of bovine insulin.

Although the amino acid sequence of insulin varies among species, certain segments of the molecule are highly conserved, including the positions of the three disulfide bonds, both ends of the A chain and the C-terminal residues of the B chain. The similar amino acid sequences of insulin lead to similar three dimensional conformations of protein from different species, and the insulin from one particular animal is very likely biologically active in other species, as well. Indeed, pig insulin has been widely used to treat human patients.

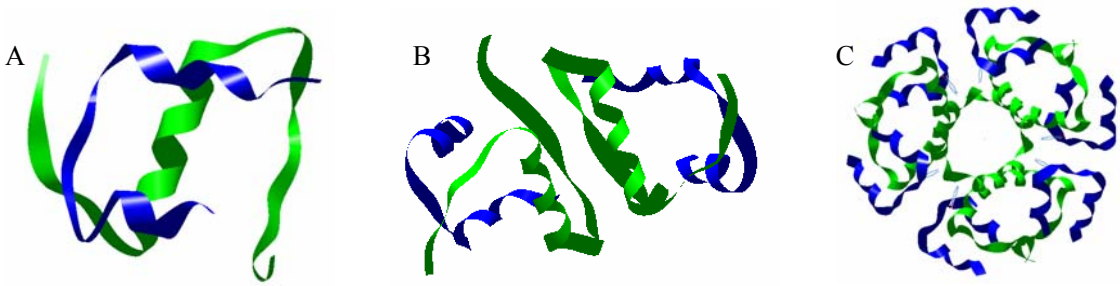

Figure 8: A molecular model of bovine insulin. Monomer (A), dimer (B) and hexamer (C), with the A chain colored blue and the larger B chain green [from the Protein data bank (file name 2a3g), picture created using Biodesigner software].

The secondary structure of insulin is predominantly α-helical. Insulin molecules have a tendency to form dimers in solution due to hydrogen-bonding between the C-termini of the B chains. Additionally, in the presence of zinc ions, insulin dimers associate into hexamers (Fig. 8).

The ability of insulin to form fibrils under certain conditions was reported in the middle of the last century [Waugh, 1946; Waugh et al., 1950]. After the discovery of prions, the interest in amyloid fibril formation increased and insulin became one of the most popular model protein for these studies. But despite these efforts, comprehensive mechanisms of insulin fibrillation are still lacking.

2.1.3. Polylysine

Polylysine is a synthetic polymer. There are two main reasons, for which polylysine is an excellent, probably even the simplest model for protein aggregation studies. It undergoes an α-helix-to-β-sheet transition, the hallmark of protein aggregation, and forms amyloid-like fibrils [Fuhrhop et al., 1987; Fändrich and Dobson, 2002; Dzwolak et al., 2004c]. The sequenceless character of the polypeptide permits exploring of the hypothesis that aggregation is as a common generic feature of proteins as polymers taking place when native protein tertiary contacts are overruled by main-chain interactions [Dobson, 2004].

2.1.4. Islet amyloid polypeptide (IAPP)

IAPP (also known as amylin) is a 37 amino acid residue peptide hormone [Lorenzo and Yankner, 1994] that is co-synthesized and co-secreted with insulin by pancreatic β-cells [Cooper et al., 1989]. Several functions have been associated with the soluble form of this hormone [Cooper et al., 1989; Johnson et al., 1992], including the control of hyperglycemia by restraining the rate at which dietary glucose enters the bloodstream. For reasons that are still not fully understood, IAPP aggregates in the extracellular matrix of the β-cells forming fibrillar amyloid deposits. These deposits are present in approximately 95 % of type II *diabetes mellitus* patients and are strongly

associated with degeneration and loss of islet β-cells [Westermark and Wilander, 1978; Hayden, 2002].

It has been proposed that the IAPP aggregation process has two distinct phases: a lateral growth of oligomers followed by longitudinal growth into mature fibrils [Kayed et al., 1999; Padrick and Miranker, 2001, 2002; Green et al., 2004], and it has been demonstrated that the initial stages of IAPP fibril formation are driven by the increase of solvent-exposure of hydrophobicity patches [Kayed et al., 1999]. However, the structural changes behind the fibrillization process are still poorly understood.

2.2. Methods

2.2.1. Atomic Force Microscopy (AFM)

All images were recorded on a MultiMode scanning probe microscope equipped with a Nanoscope IIIa Controller from Digital Instruments (Santa Barbara, California, USA). The microscope was coupled to an AS-12 E-scanner (13-μm) or J-scanner (100-μm) and an Extender Electronics Module EX-II (Santa Barbara, California, USA), which allows for acquisition of phase images. Typically used AFM-probes were aluminum-coated NCHR silicon SPM sensors (force constant = 42 N/m; length = 125 μm; resonance frequency ≈ 250-330 kHz; nominal tip radius of curvature ≤ 5 nm) from Nanosensors, Nanoworld or Budgetsensors. The AFM head with optical block and base was placed atop a commercially available active, piezo-actuated vibration-damping desk from Halcyonics (Göttingen, Germany). All measurements were done in the air using TappingMode™.

TappingMode™ (Fig. 9) AFM operates by scanning a tip attached to the end of an oscillating cantilever across the sample surface. The cantilever is oscillated at or near its resonance frequency with amplitude ranging typically from 20 nm to 100 nm. The tip lightly “taps” on the sample surface during scanning, contacting the surface at the bottom of its swing. The feedback loop maintains constant oscillation amplitude by maintaining a constant root mean square of the oscillation signal acquired by the split photodiode detector. The vertical position of the scanner at each (x,y) data point in

order to maintain a constant "setpoint" amplitude is stored by the computer to form the topographic image of the sample surface. By maintaining a constant oscillation amplitude, a constant tip-sample interaction is also preserved during imaging. The operation can take place in either ambient or liquid environment. When imaging in air, the typical amplitude of the oscillation allows the tip to contact the surface through the adsorbed fluid layer without getting stuck [Scanning probe microscopy training notebook, Digital Instruments].

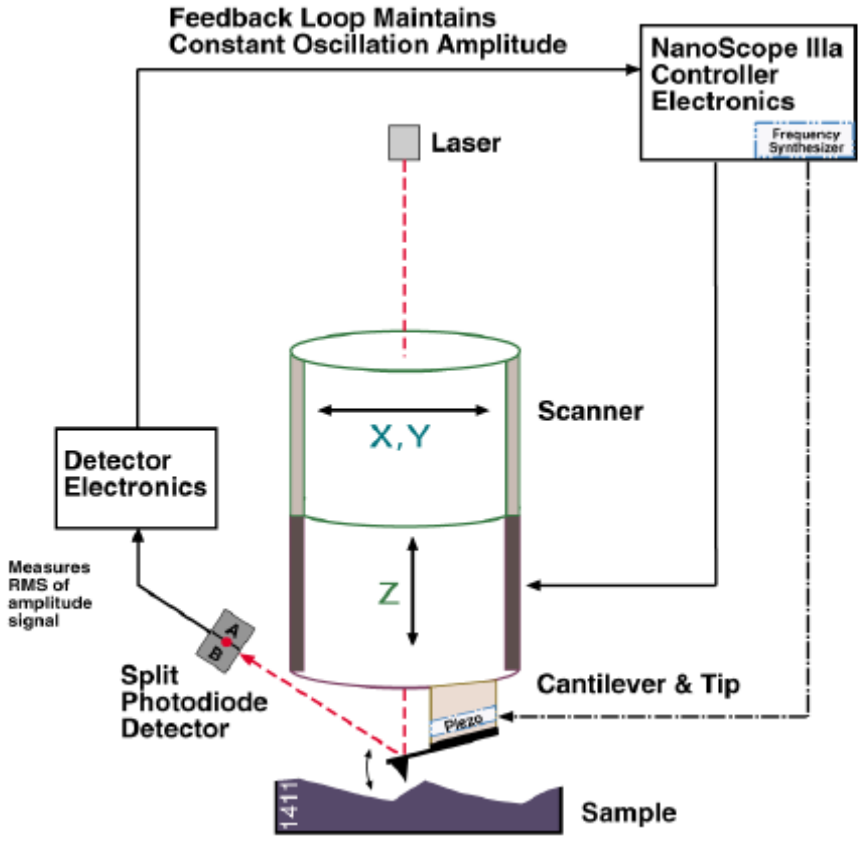

Figure 9: Scheme of AFM measurements using the TappingMode™ [adapted from the scanning probe microscopy training notebook, Digital Instruments].

Samples were diluted with deionized water to a final concentration of 0.5-2 µM, 10-30 µl were applied onto freshly cleaved muscovite mica and allowed to dry.

2.2.2. Fourier-transform infrared spectroscopy (FTIR)

The FTIR spectra were recorded using the Nicolet MAGNA 550, Nicolet NEXUS and Nicolet 5700 spectrometers from Thermo Scientific (Waltham, Massachusetts, USA) equipped with a liquid nitrogen cooled mercury-cadmium-telluride (MCT) detector. For all measurements, CaF_2 transmission windows and 0.05 mm Teflon or Mylar spacers were used. The temperature in the cell was controlled through an external water-circuit. For each spectrum, 256 interferograms of 2 cm^{-1} resolution were co added. The sample chamber was continuously purged with dry air. From the spectrum of each sample, a corresponding buffer spectrum was subtracted. All the spectra were baseline-corrected and normalized prior to further data processing. The plots of the progress of α-helix–to–β-sheet refolding upon aggregation were calculated as $(I - I_\alpha)/(I_\beta - I_\alpha)$, where I_α is spectral intensity at 1625 cm^{-1} (or 1622 cm^{-1} in EtOD) of the native insulin (corresponding to the first spectrum), I_β is the intensity after complete aggregation, and I is a transient intensity at this wavenumber. All data processing was performed with the GRAMS software (Thermo Scientific).

2.2.3. Ultrasonic resonator technology (URT)

The ultrasonic measurements were carried out using an ultrasonic resonator device (ResoScan system, TF Instruments GmbH, Heidelberg) with ultrasonic transducers made of single-crystal lithium niobate of a fundamental frequency of 9.5 MHz. The instrument comprises two independent cells for sample and reference with a path length of 7.0 mm. They are embedded into a metal block Peltier thermostat with a temperature stability of 0.001 °C. The resolution of the ultrasonic velocity measurements is 0.001 m s^{-1}. Ultrasonic velocities of the sample (U) and reference solvent (U_0) were measured over the same temperature range and at the same heating rate.

The fundamental pre-condition for the propagation of acoustical waves in media is the elastic coupling of the molecules to the media. For example, in solid phase materials the atomic bodies are thought to be coupled via “spring-like bonds”, while in liquids and gases elastic collisions are conceptualized as coupling intervals. In the absence of

sound, all these building elements are equally spaced, so that the mean force on them vanishes. Once this system is disturbed by a sudden and stepwise move of a rigid wall, the building blocks next to this wall get compressed and due to the described coupling, this compression propagates with the speed of sound (Fig. 10).

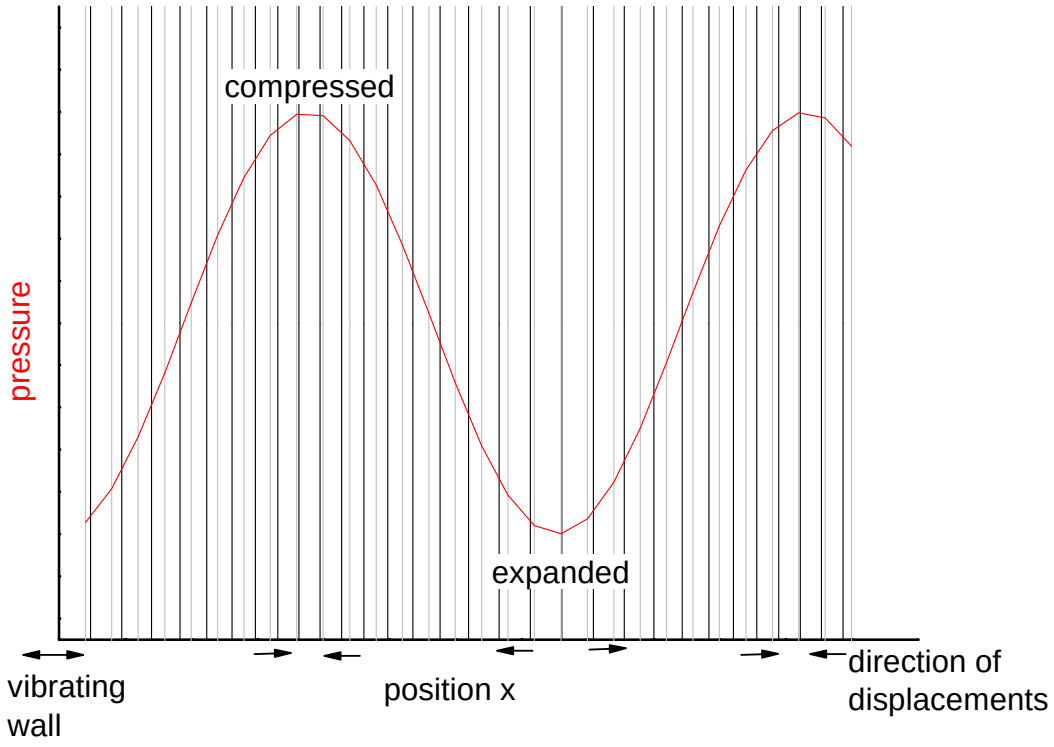

Figure 10: A periodically vibrating wall generates a wave field (black lines) were the displacements ξ of the building blocks results in areas of compressed and expanded density [Principles of sound measurement, TF Instruments].

If the wall moves periodically at the position x=0, a uniform wave field is created, which means that at a fixed position x the same phase of motion is reached after the time period T. The reciprocal of the time period T is the frequency f, usually expressed in Hz. At a snapshot at a fixed time t the wave field has the same phase of motion at points separated by the wavelength λ (along the direction of propagation). The wave is mathematically described by a function $\xi(x, t)$, which is the displacement of building blocks from the rest position at position x and time t. Wavelength λ and frequency f appear in this function as free parameters. Given the time period, T, for a propagation of a length, λ, the speed of sound can be found:

$$U=\lambda/T=\lambda f \qquad (1)$$

U is a constant for any material, which depends on the coupling strength between the building blocks of the medium.

The ResoScan system uses an acoustic resonator arrangement to measure the velocity of sound. The resonator consists of an ultrasonic sender and an ultrasonic receiver with the space between sender and transmitter filled with the sample fluid. A prerequisite for the high accuracy of measurements is the precise parallel alignment of sender and transmitter. Due to the reflection of sound at the transducers, a standing wave pattern can be established (Fig. 11A), but this is possible only at the ultrasonic wavelength λ_n, were the distance D between sender and receiver is (n is dependent on the standing wave pattern (Fig. 11B)):

$$D = n\frac{\lambda_n}{2} \qquad (2)$$

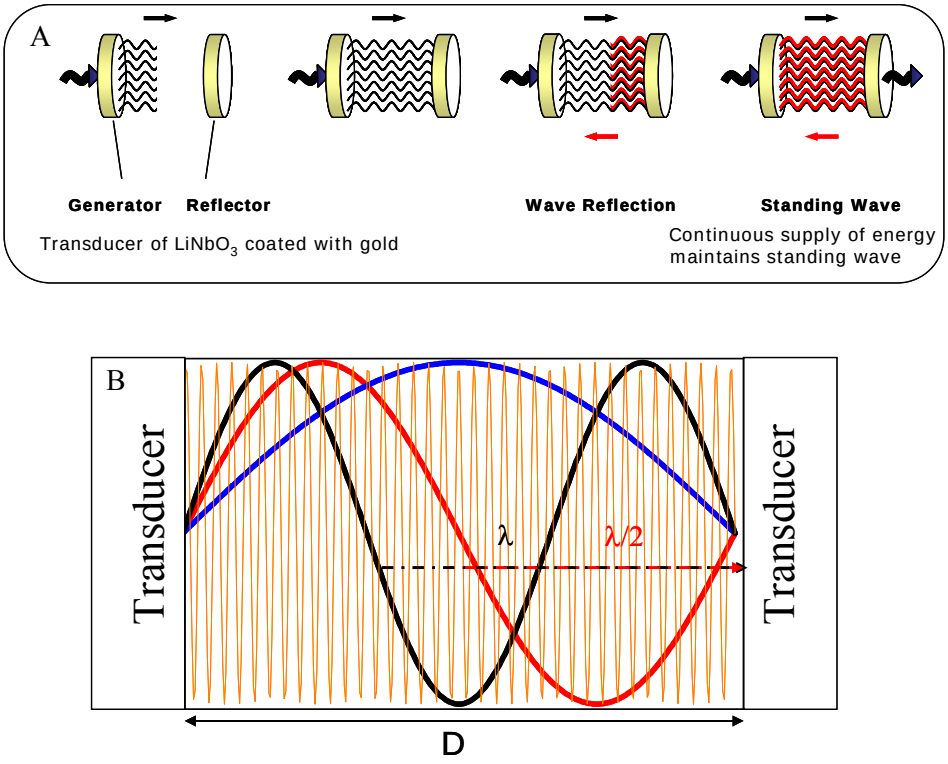

Figure 11: Establishing standing wave between transducers (A) and standing wave pattern for n=1, 2, 3 and 73 (B) [adapted from Short training course, TF Instruments].

On the other hand, the wavelength λ is linked to the frequency f, and the velocity of sound in liquid U_L, which is a characteristic for each wave transporting medium (here the fluid) via relation (1).

Since inside the resonator only standing waves with length λ_n are allowed, only discrete frequencies f_n may exist:

$$\lambda_n f_n = U_L \tag{3}$$

These frequencies f_n are the real quantities to be measured by the Resoscan. This is done due to the fact that mostly the frequencies can be measured with high accuracy, while the length D of the resonator is held fixed and measured only once by the manufacturer.

The combination of (2) and (3) yields the frequencies at which standing waves inside the resonator may exist:

$$f_n = n\frac{U_L}{2D} \tag{4}$$

In the terminology of ultrasonic interferometry, n is called the "peakorder". For example for our Resonator of D=7 mm, U_L=1498 m/s, one gets from (5) $f_n = n \cdot 107$ kHz, which means the first resonance is at 107 kHz, the second at 214kHz, the 78th at 8.346 MHz, etc. (Fig. 12). The spacing between resonances is called the base frequency f_L for the liquid:

$$f_L = f_{n+1} - f_n = \frac{U_L}{2D} \tag{5}$$

The above-mentioned approach implies the determination of the velocity of sound by measuring the difference between adjacent resonances f_n, as well as the length D of the resonator, followed by using (5) to calculate the velocity.

However, under real experimental conditions, the measured sequence of frequencies does not have exactly the same spacing (5) (due to the influence of the natural frequency of the transducers, which is in the same range as the measured frequencies of the fluid resonances). Since it is not obvious which of the several spacings is to be considered for the determination of the velocity, this results in a large error of the velocity determination.

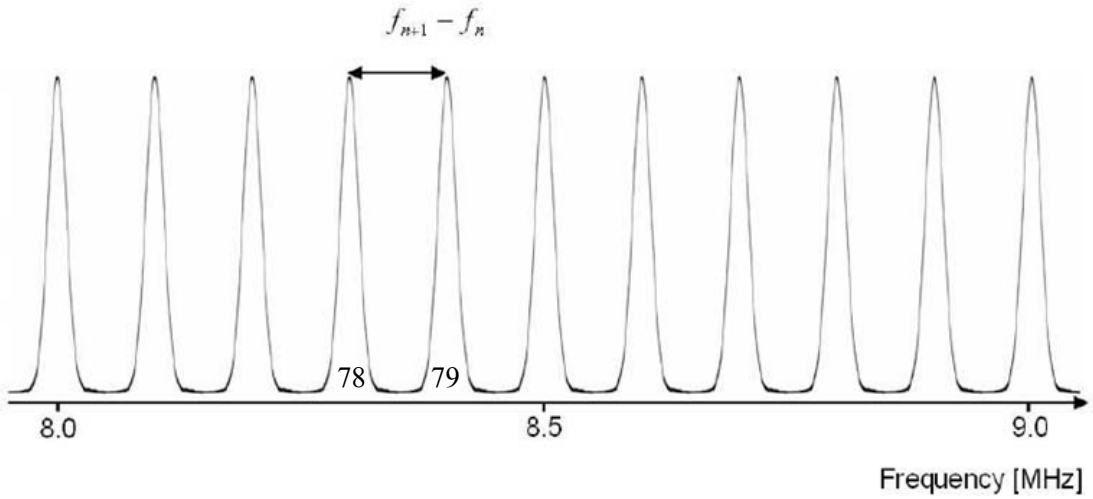

Figure 12: Schematic view of resonances in an ideal resonator with the dimensions of the ResoScan® System in the range from 8 to 9 MHz. Sample: water at 25.4 °C, U = 1498 m/s, D = 7.0 mm [Introduction into the Ultrasonic Resonator Technology, TF Instruments].

A theoretical model of the resonator shows that, in the vicinity of the "natural frequency" of the ultrasonic transducers f_R, significant deviations from the equal spaced model (4) exist. These deviations "y_n" of the measured frequencies from the harmonic row (4) can be described by a simulation function y_n:

$$y_k = \frac{U_L}{2D}\left(n - 2\,\Theta(f_n - f_R) + \frac{2}{\pi}\arctan\frac{z_L}{z_R \tan\left(\pi\frac{f_n}{f_R}\right)}\right) \qquad (6)$$

$$\text{with} \quad \Theta(f_n - f_R) = \begin{cases} 0 & \text{for} \quad f_n < f_R \\ 1 & \text{for} \quad f_n > f_R \end{cases}$$

where z_L is acoustical impedance of the fluid, z_R is acoustical impedance of the transducers, f_R is natural frequency of the transducers and f_n is measured frequency of order n.

Fitting the simulation function (6) to the measured deviations of the observed resonances to the harmonic row delivers the parameters of the function.

This method is used at the initial setup (at the manufacturer) of a new resonator, to determine for a fluid of known U_L and z_L, the following resonator-specific values: D, z_R and f_R. These parameters are fixed in the operating software.

Conversely, U_L and z_L of the investigated fluid can be determined with the already known parameters D, z_R and f_R of the resonator. This is done automatically during the initialization process of the operating software.

After the initialization process of the device, the velocity of sound in the fluid as well as the correction for every resonator mode is known. Therefore it is appropriate to measure a single Resonator mode repeatedly with high accuracy, to follow the velocity of sound in the sample with respect to time or temperature. The single repeatedly measured mode is called the "Master Peak".

The measurement of this single Master Peak is done in a so-called "phase scanning mode", were the resonator mode is sampled with very high accuracy. From the amplitude vs. frequency curve, a polynomial fit is done by the operation software to get the best value for the velocity of the sample [Principles of sound measurement, TF Instruments].

2.2.4. Densitometry

Density measurements were carried out with a DMA 58 density meter from Anton Paar (Graz, Austria) with a precision of $\pm 5 \cdot 10^{-5}$ g/cm^3, or DMA 5000 from Anton Paar GmbH (Graz, Austria) with a precision of $\pm 5 \cdot 10^{-6}$ g/cm^3.

Both density meters determine the density ρ of liquids and gasses by measuring the period of oscillation. To this end, the sample is introduced into a system which can oscillate and whose "natural frequency" is influenced by the mass of the sample. This system is a U-shaped tube which is excited to undamped oscillations by electronic means. Both straight sections of the U-shaped tube form the spring element of the oscillator. The direction of the oscillation is perpendicular to the plane of the U-shaped tube. The oscillating volume V is limited by the mounting points which are fixed. If the oscillator has been filled with the sample at least up to the mounting points, then the same known volume V of the sample also oscillates. The mass of the sample can therefore be considered as proportional to its density. If the oscillator has been filled beyond the mounting points, this has no effect on the measurement. For this reason, the oscillator can also measure the densities of samples flowing through it.

Assuming that the temperature is held constant, the density can be calculated from the period by considering a hollow body with mass M suspended on a spring constant s. The volume V of the hollow body is then filled with a sample of density ρ. The natural frequency of this spring mass system is:

$$f = \frac{1}{2\pi}\sqrt{\frac{s}{M+\rho V}} \tag{7}$$

and the period T is:

$$T = 2\pi\sqrt{\frac{M+\rho V}{s}} \tag{8}$$

Density dependent on the period T is:

$$\rho = \frac{T^2 s}{4\pi^2 V} - \frac{M}{V} \tag{9}$$

Using the abbreviations $A=c/4\pi^2 V$ and $B=M/V$, we arrive at

$$\rho = AT^2 - B \tag{10}$$

The constants A and B comprise the spring constant of the oscillator, the mass of the empty tube and the volume of the sample involved in the oscillation. A and B are therefore device constants for each individual oscillator. They can be derived from two period measurements when the oscillator has been filled with substances of known density [User manual, Anton Paar].

The partial specific volume of the protein has been calculated using

$$v^{o} = 1/c - (\rho - c)/\rho_0 c \tag{11}$$

ρ and ρ_0 are the densities of the solution and solvent, respectively; c is the specific concentration of the protein.

2.2.5. Differential scanning calorimtery (DSC) and Pressure perturbation calorimetry (PPC)

DSC and PPC measurements were carried out on a VP DSC calorimeter from MicroCal (Northampton, MA) equipped with the MicroCal's PPC accessory. For the DSC measurements, both cells of the calorimeter were first filled with buffer and a scan was performed. Immediately after the scan, the buffer was removed from the sample cell, replaced with ca. 0.5 mL sample and the measurement was performed. Buffer-

buffer data were subtracted from sample-buffer data. The specific heat capacity of the protein at constant pressure has been obtained from

$$c_p = \Delta C_p / m + v^{\circ} c_{p,0} / v_0^{\circ} \quad (12)$$

ΔC_p is the heat capacity difference between the sample solution and solvent reference cell as obtained by a the measurement; v° and v_0° are the partial specific volumes of the solute and solvent, respectively.

For the PPC measurements, gas (N_2) pressure jump applied to the samples was 5 bars. Under the same experimental conditions, a set of reference sample-buffer, buffer-buffer, buffer-water, and water-water measurements was carried out each time. The values of partial specific volumes used for volumetric calculations were obtained from density measurements.

2.2.6. Fluorescence Spectroscopy

Fluorescence measurements were carried out on a K2 multifrequency phase and modulation fluorometer (ISS, Urbana, IL). The measurements were performed within a high-pressure cell (ISS), equipped with sapphire windows, and the pressure was controlled by an automated pressure control system (APP, Ithaca, NY).

Insulin and the fibril-specific dye Thioflavine T (ThT) were dissolved in H_2O (pH 1.9) at a final protein to dye molar ratio of 50:1. The emission intensity at 482 nm was recorded upon excitation at 450 nm as a function of time *t*. The data were normalized by dividing the intensity at every point to the intensity recorded for the final aggregates.

2.2.7. Calculation of compressibilities

The most accurate method of determining the partial molar compressibility, K_S°, of a solute is based on the Newton-Laplace equation, which relates the coefficient of adiabatic compressibility of a medium,

$$\beta_S = -(1/V)(\partial V / \partial p)_S \quad (13)$$

with its density, ρ, and sound velocity, U [Gekko and Hasegawa, 1986,1989; Taulier and Chalikian, 2002; Chalikian, 2003]:

$$U^2 = (\beta_S \rho)^{-1} \tag{14}$$

For (infinitely) dilute solutions [Taulier and Chalikian, 2002; Chalikian, 2003],

$$K_S^o = \beta_{S0}\left(2V^o - 2[U] - M/\rho_0\right) \tag{15}$$

where

$$K_S^o = V^o \beta_S \tag{16}$$

and

$$V^o = (\partial V/\partial n)_{T,p} \tag{17}$$

is the partial molar volume of the solute, M its molar mass, and

$$[U] = (U\text{-}U_0)/(U_0 \cdot C) \tag{18}$$

is the relative molar sound velocity (increment) of the solute; U and U_0 are the sound velocities of the solute and solvent, respectively.

Experimental data on

$$\beta_T = K_T^o / V^o \tag{19}$$

of proteins are very scarce as it is technically challenging to measure the partial specific volume as a function of the pressure using densimetric techniques with high precision [Seemann et al. 2001]. However, the partial molar isothermal compressibility of the solute can be obtained from the adiabatic value by [Taulier and Chalikian, 2002; Chalikian, 2003]

$$K_T^o = K_S^o + \left(T\alpha_0^2/(\rho_0 c_{p0})\right)\left(2E^o/\alpha_0 - C_p^o/(\rho_0 c_{p0})\right) \tag{20}$$

where c_{p0} is the specific heat capacity at constant pressure of the solvent, α_0 is the coefficient of thermal expansion of the solvent, respectively, and

$$E^o = (\partial V^o/\partial T)_p \tag{21}$$

is the partial molar expansibility of the solute, which can be determined with high precision from pressure perturbation calorimetric measurements [Ravindra and Winter, 2003; Schreiner et al., 2004]. C_p^o is the partial molar heat capacity of the solute, and T is the absolute temperature.

3. Results and discussion

3.1. Insulin aggregation and amyloidogenesis

3.1.1. Effect of co-solvents

A 2% solution of insulin in D_2O with 0.1 M NaCl (with or without 20% ethanol, TFE or glycerol), pD-adjusted to 1.9 was used (pH-meter readout +0.4 [Makhatadze et al., 1995]). The temperature was increased continuously at a rate of 20 ºC/h.

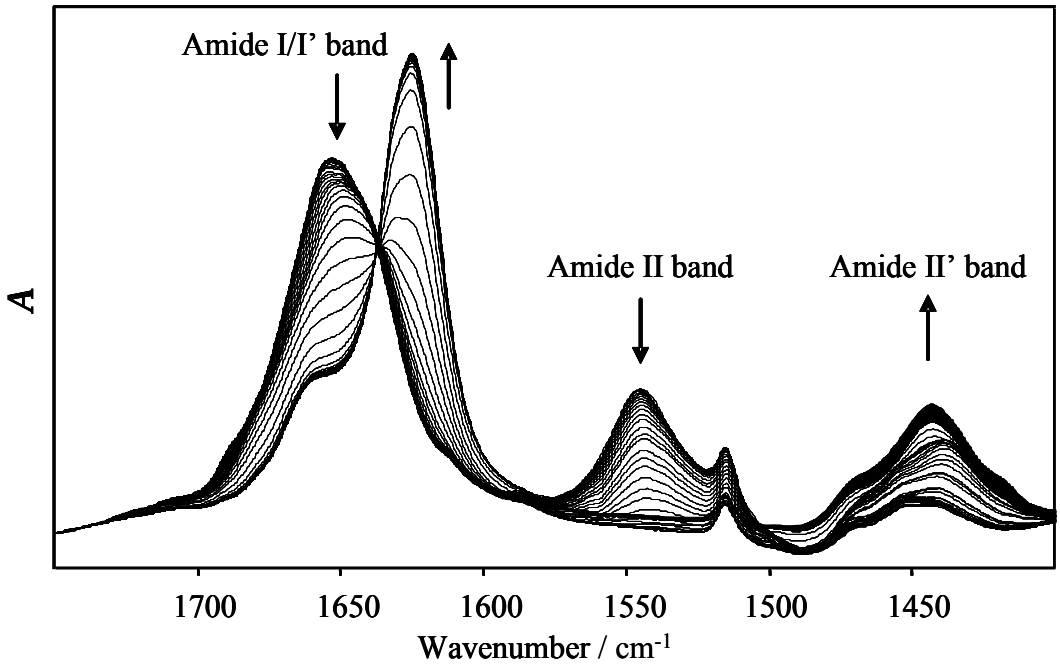

Figure 13: Time resolved FTIR spectra of insulin during heating and incubation at 60 ºC

With the increase of temperature, the amide II band (1543 cm^{-1}) decreases and amide II' (1445 cm^{-1}) increases because of H-D exchange (Fig. 13). Monitoring this process allows one to follow the exposure of the protein to the solvent, which is related to partial unfolding (Fig. 14). Experiments show that full H-D exchange in 20% ethanol is completed just below 45ºC, in 20% glycerol and in pure D_2O at around 47ºC, and in 20% TFE at about 50ºC. Ethanol seems to destabilize native α-helical structures of

insulin, TFE stabilizes them and glycerol seems to have no significant effect at this stage.

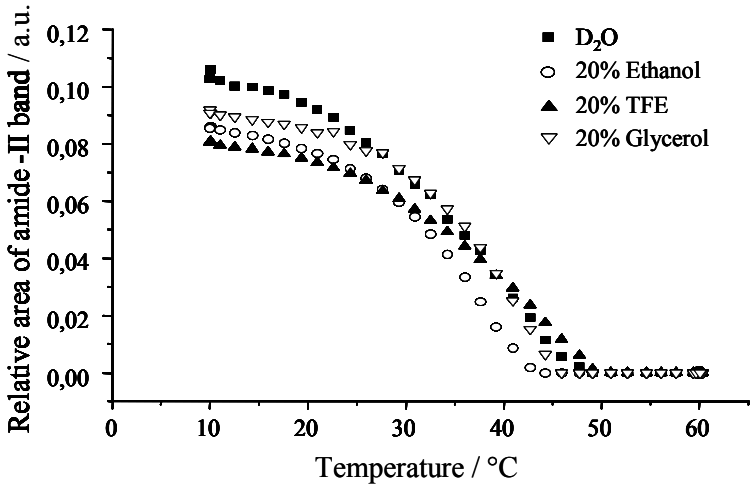

Figure 14: H-D exchange rate monitored in the presence of different co-solvents.

A further increase in temperature and further incubation at 60 ºC leads to changes of the secondary structure, from α-helix to β-sheet, which is reflected in the decrease of the peak around 1650 cm^{-1} and the increase of the peak in the region between 1620-1630 cm^{-1} of the amide I/I' band (Fig. 13). The kinetics of aggregation under different conditions was monitored by plotting the relative extent of α/β-transition (Fig. 15). The presence of glycerol or TFE seems to stabilize α-helical structures, while the aggregation curve in the presence of ethanol shows similar a midpoint when compared with the one in pure D_2O. The main difference is the faster rate of aggregation.

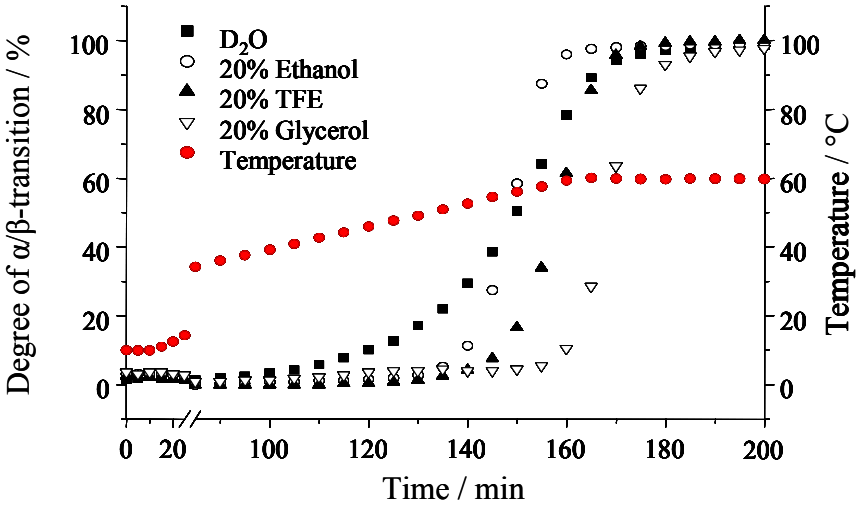

Figure 15: Aggregation kinetics of insulin monitored in the presence of different co-solvents

The final spectral positions of the amide I' band depend on the presence of co-solvents during the aggregation process (Fig 16). Amide I' band positions are as follows: in case of 20% TFE – 1621 cm^{-1}, 20% ethanol – 1622 cm^{-1}, pure D_2O – 1625 cm^{-1}, and 20% glycerol – 1626 cm^{-1}. A red shift of the band suggests stronger interstrand hydrogen bonds in the aggregates formed in the presence of ethanol and TFE, while the small blue shift suggests weaker interstrand hydrogen bonds in the aggregates formed in the presence of glycerol. Similar observations have been reported previously for insulin amyloids grown in the presence of ethanol [Dzwolak et al., 2004] and acetic acid [Nielsen et al., 2004]. Taken together, the data suggests the ability of insulin to form different final amyloid structures starting from the same amino acid sequence.

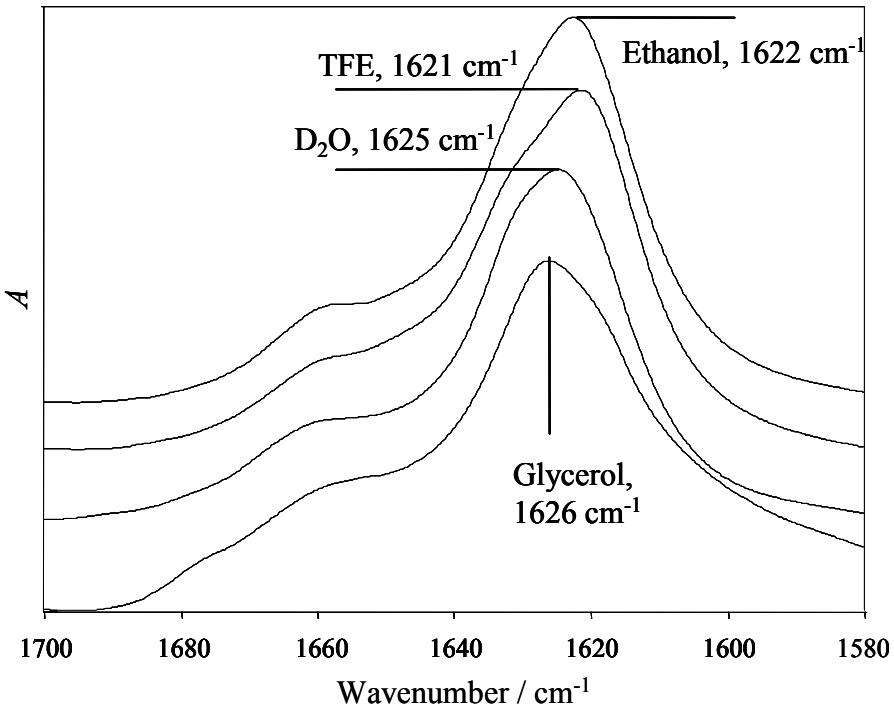

Figure 16: Amide I' band of final insulin amyloid aggregates in different co-solvents.

3.1.2. Sonication of amyloid fibrils

0.5 % insulin was dissolved in HCl, pH 2, and incubated for 40 hours at 60°C to induce formation of fibers (Fig. 17A). The sample was subjected to an ultrasonic bath (45 kHz, 30W) for different times. This leads to braking of fibers into shorter pieces (Figs. 17B and C).

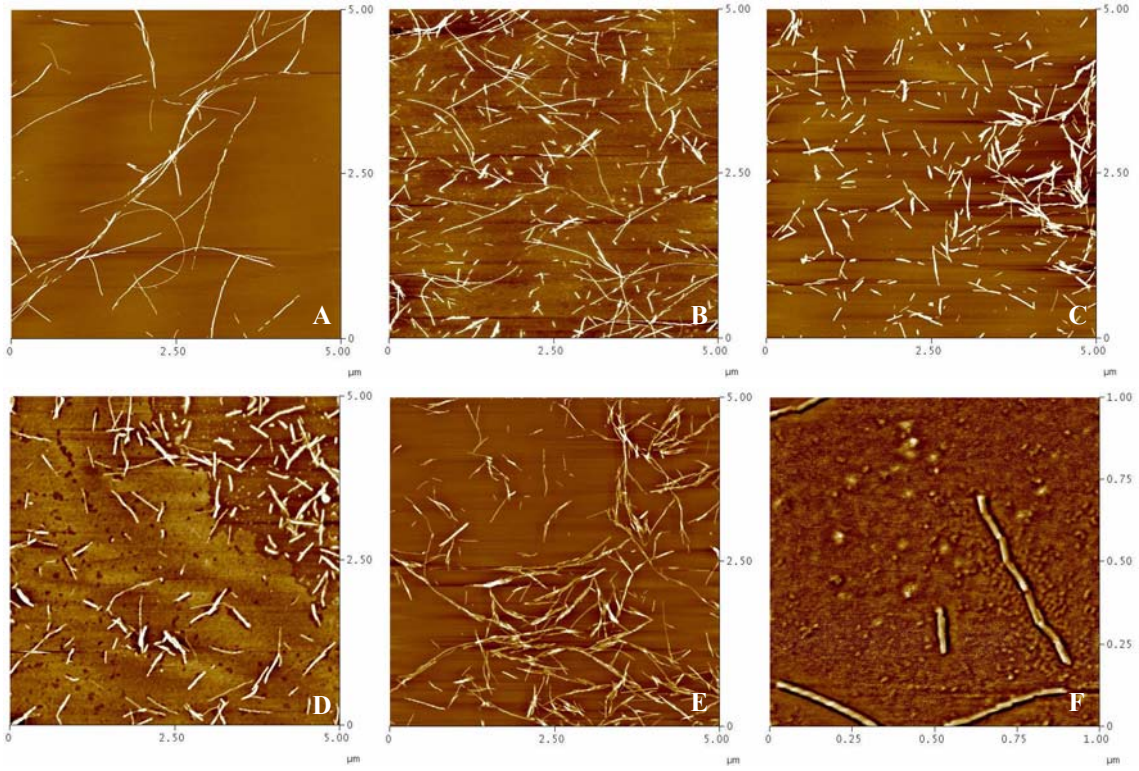

Figure 17: AFM pictures of insulin amyloid fibrils. Before sonication (A); after 30 min sonication (B); 3 hours sonication (C); 24 hours (D), 72 hours (E) and 168 hours (F) incubation at room temperature.

Sonicated fibers were kept at room temperature for a week to check if broken pieces could reconnect together. The process of fibrils sticking together is rather slow – there were no long fibrils found after 24 hours of incubation (Fig. 17D). Though further incubation leads to formation of colonies, including fibril-like particles (Fig. 17E) of a similar length as the fibrils have before sonication (Fig. 17A). A closer look at the AFM pictures shows that most of the broken fibrils stick together via their ends (Fig. 17F), suggesting that broken fibrils are probably more prone to attach additional particles and thus elongate.

3.1.3. Seed induced aggregation

The seed-induced aggregation of bovine insulin at pD 1.9 and 25°C was followed by time-resolved FTIR spectroscopy (Fig. 18A). The infrared spectra show a gradual shift of the amide I' band to 1625 (in acidified D_2O) or 1622 (acidified 20% (v/v)

ethanol in D_2O) cm^{-1}, accompanied by a marked narrowing of the peak, both of which reflect the complete transition of the native structure into nonnative aggregated β-strands. The amyloidal character of the final insulin aggregates was confirmed by atomic force microscopy scans, which exhibit typical fibrils (Fig. 18B).

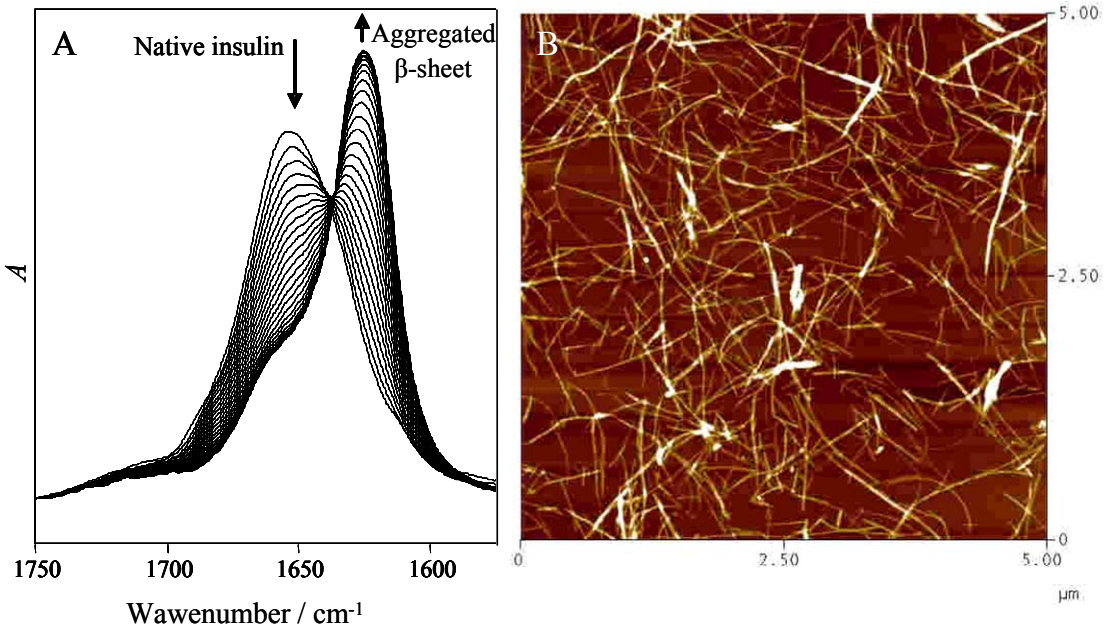

Figure18: Seeds-induced aggregation of insulin. (A) Time-dependent changes in FT-IR spectra show the gradual evolution of the amide I' band of insulin reflecting the structural transition from the native form to amyloid: 2% (w/w) bovine insulin in 0.1 M NaCl in D_2O, pD1.9, seeded at 25°C at a 20:1 weight ratio with preformed seeds. The total elapsed time between the first and the final spectrum was 20 h. Arrows show directions of the spectral changes. (B) A height-scan AFM image of the final insulin aggregate.

The position of the amide I' band at 1622 or 1625 cm^{-1} is the fundamental spectral difference between insulin amyloids grown spontaneously (unseeded) at 60°C in the presence or absence of 20% (v/v) d_1-deuterated ethanol (EtOD), respectively (Fig. 19A). Although in either case, the band's shapes and positions are characteristic for the amyloid's parallel β-sheet structure, it is red-shifted for EtOD-grown samples (1622 versus 1625 cm^{-1} for D_2O-grown amyloid (Fig. 19A)). According to corresponding second derivative spectra (Fig. 19B), this shift should be specifically attributed to an increasing β-sheet fraction at 1620 cm^{-1}. The mature amyloid fibrils do not exhibit any spectral changes after being resuspended in an alternative solvent (data not shown).

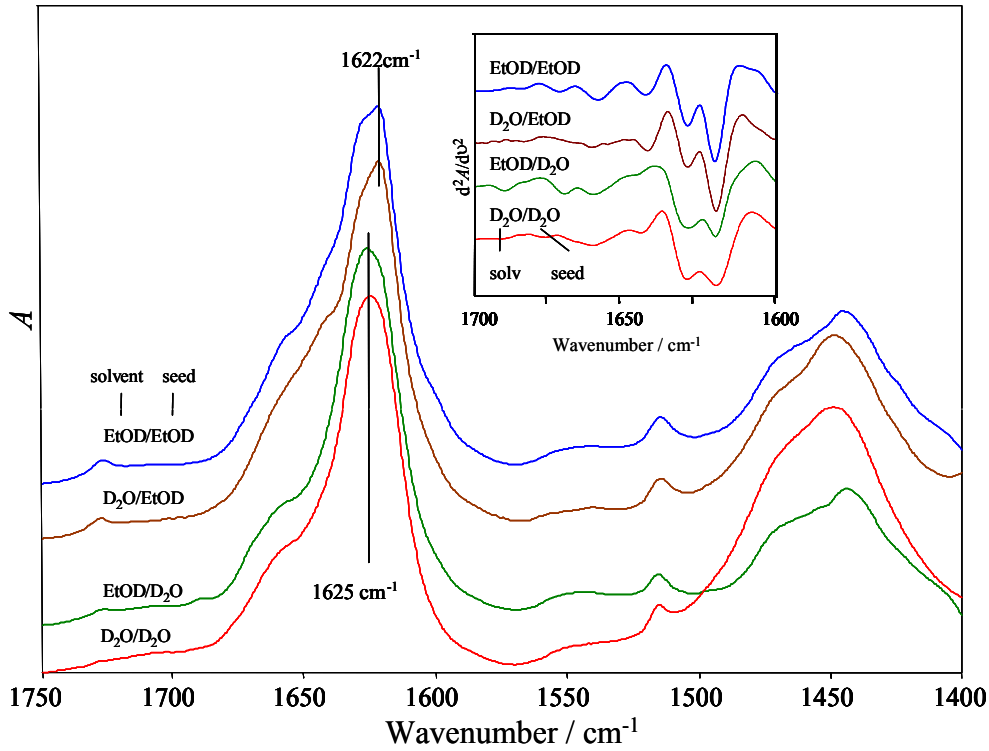

Figure 19: The type of the original template determines the infrared spectral features of the grown amyloid. The amide I' infrared band of insulin amyloids seeded homogeneously and heterogeneously. The original absorption FTIR spectra and 2nd derivatives (solvent/seed): D_2O, 0.1 M NaCl in D_2O (p D1.9); EtOD, 20% (v/v) EtOD in 0.1 M NaCl in D_2O (pD 1.9).

Insulin amyloid was seeded by mixing a small amount (5% (w/w) of the total protein content) of sonicated [Saborio et al., 2001] fibrils of either preparation with fresh insulin solution (either with or without 20% (v/v) EtOD). Should the insulin solution be the same as the one originally used for spontaneous growth of the seeds, this would be "homogenous seeding," as opposed to the "heterogeneous seeding" with alternative amyloid fibrils type. The infrared spectra of each amyloid obtained through the homogenous seeding are very similar to the spectra of the spontaneously formed precursor seeds (Fig. 16). Minor differences are visible at ~1660 cm^{-1}, namely, in the spectral region assigned to turns. Interestingly, templates of each type induce practically identical amyloid (in terms of its spectral features), when used for heterogeneous seeding (Fig. 19). This means that the critical factor, which determines spectral characteristics of growing amyloid is the preformed template, rather than the current solvent conditions. The FTIR data were subsequently used for plotting time dependencies of the amide I' band position (Fig. 20A), its bandwidth at half height (Fig.

20B), and the relative change of the β-sheet content (Fig. 20C). The plots show that the spectral changes occur immediately after doping the native insulin with the amyloid. The fastest conformational transition takes place in the homogenously seeded ethanol-containing insulin solutions. Apparently, each type of seed acts as a more effective catalysts in the insulin solution of its original growth. Figure 20, A and B, shows that both the peak position and bandwidth of the final amyloid depend on the seed, rather than the cosolvent. On the other hand, the presence of ethanol leads to a more pronounced (by roughly 2 to 3 cm^{-1}) broadening of the amide I' band at an intermediate stage of the aggregation process (Fig. 20B). The relative spectral intensity at 1625/1622 cm^{-1} quantifies the actual amount of the aggregated β-strands (Fig. 20C). The plots calculated for the homogenously seeded amyloids show a linear time-dependent accumulation of the aggregated protein, and the other two corresponding to the heterogeneously seeded amyloids display some curvature. Especially, seeding insulin dissolved in 20% (v/v) EtOD with D_2O-grown amyloids evokes a sigmoid-like shape of the corresponding curve in figure 20C.

The second derivative spectra reveal that the EtOD type of amyloid has a higher fraction of the strongly hydrogen-bonded component of the β-sheet at 1620 cm^{-1}. The different energy of the inter-β-sheet hydrogen bonding is likely to reflect subtle structural differences between the two types of fiber. The fact that the spectra of once-formed amyloid remain intact after resuspending in another solvent, demonstrates that its spectrally distinguishable structural features are well conserved within the fiber. Furthermore, as protein aggregation is said to drive the protein molecules to the "real" global energy minimum, the fact that slow spontaneous aggregation results in particularly tuned β-sheet conformation suggests that, under given solvent conditions, this structure corresponds to such an energy minimum [Gazit, 2002]. The experiments with homogenous seeding have shown that, under conditions favoring particular amyloid structure and in the presence of seeds spontaneously formed under similar conditions, the growing amyloid will only maintain the fold of its initial template. Compared with the seeded aggregation at 25°C, the higher temperature (60°C) required for the spontaneous growth of amyloid appears to promote turns. Thus, it seems reasonable to attribute the presence of such less-ordered structural components to increased thermal fluctuations of the polypeptide chains, which are expected to hamper

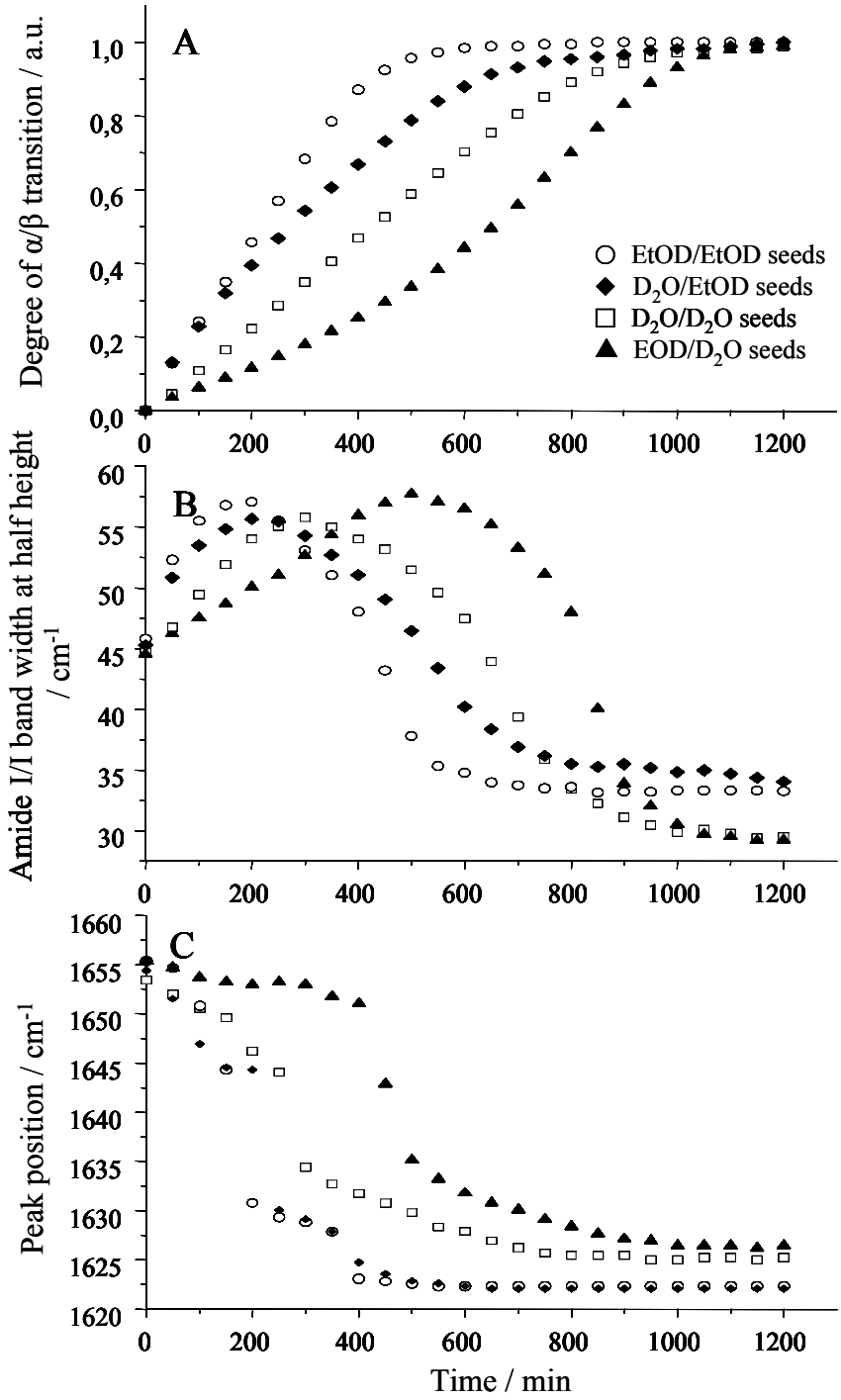

Figure 20: Kinetics of the homogeneously and heterogeneously seeded aggregation of insulin at 25°C followed by the maximum of the amide I' band (A), the amide I' band's width at half-height (HHBW; B), and the relative absorption of the spectral component assigned to β-sheets (C).

an ideal packing of the insulin molecules within the fibrils. Interestingly, the heterogeneous seeding experiments concluded in figure 19 prove that a slightly altered

structure of the foreign seed is capable of changing the protein conformation by pushing it off the preferential aggregation pathway.

Recent studies have shown evidence that the "strains" reflect multiple distinct conformations of the prion (e.g., human [Wadsworth et al., 1999], hamster [Peretz et al., 2002], yeast [Chien and Weissman, 2001; Chien et al., 2003]). Both insulin amyloid types obtained from the single protein propagate, maintaining the original infrared features even under conditions favoring a different fold in the β-sheet fibers (Fig. 20A, B). In light of these facts, the two distinct conformations of insulin amyloid appear to have "strain"-like character.

When comparing the kinetics of seed-induced aggregation of insulin in D_2O and in 20% (v/v) EtOD, one must take into account that insulin dimers predominate in the former case [Whittingham et al., 2002], and the presence of ethanol promotes formation of monomers [Millican and Brems, 1994]. The water-grown seeds are more effective in insulin solutions containing dimers than in the presence of monomer-inducing ethanol, which sheds light on a possible mechanism of the aggregation. Namely, although (under different conditions) human insulin has been shown to aggregate through a monomeric intermediate [Ahmad et al., 2003], the cross-seeding kinetic data presented in figure 20 would easily fit to an aggregation scenario involving two parallel pathways: through a monomer (preferential pathway in 20% (v/v) ethanol) or through a dimer (preferential pathway in water). A similar case of a protein capable of aggregating through a dimeric intermediate is transthyretin [Serag et al., 2001]. Nevertheless, other factors such as structural fluctuations may play a role in the controlling kinetics of amyloidogenesis. The relative intensity of the β-sheet spectral component plotted as a function of time quantifies the progress of the aggregation. The deviation from linearity observed for the heterogeneously seeded amyloids is puzzling. The sigmoidal shape of the plot corresponding to the aggregation of insulin in the presence of ethanol initiated with water-grown amyloid reflects an increasing rate of the structural conversion. It could be hypothesized that such an enhancing effect stems from newly formed second-generation amyloid gradually acquiring a higher affinity to the abundant monomeric substrate, therefore becoming a more effective aggregation catalyst in the EtOD solutions. The kinetic obstacles revealed in the heterogeneous seeding experiments remind one of barriers facing prion cross-species propagation [Chien and Weissman, 2001; Peretz et

al., 2002; Chien et al., 2003]. On the other hand, the time-dependent enhancement of the catalytic properties of foreign fibrils appears to parallel the observation that a heterogeneously seeded second generation of AApoAII(B) protein fibrils grown in vivo induced a faster and more severe disease in mice [Xing et al., 2002]. In other words, the sigmoidal shape of the α/β-transition curve in EtOD/D_2O-seed aggregation is likely to mirror refining catalytic properties of the growing amyloid. Despite these changes, the final FT-IR spectra continue to reflect the initial template (Fig. 19).

Figure 20B depicts time-dependencies of the amide I' bandwidth, which is a yardstick of structural fluctuations of a protein molecule. Increasing conformational fluctuations, which lead to disorder and unfolding of a protein, result in a marked broadening of the amide I' band [Dzwolak et al., 2003]. By the same token, a reversed process of protein folding and subsequent assembling of native monomers into a compact and stable quaternary structure is expected to reduce, or simply damp, the fluctuations, leading to a narrowing of the band. This has been confirmed in a very recent Raman spectroscopic study, which specifically coupled narrowing of the amide I band to the damping of conformational fluctuations in insulin molecules, upon their assembly into higher oligomers, as well as a result of amyloid formation [Dong et al., 2003]. Figure 20B shows that the aggregation initially causes broadening of the amide I' band up to 57 cm^{-1}, which should be attributed to the spectral separation between the transiently coexisting native α-helices and β-sheet. However, it seems quite likely that partly unfolded aggregation-intermediate states contribute to the broadening of the spectral band as well [Ahmad et al., 2003]. The EtOD-grown seeds render the final half height bandwidth (HHBW) larger by ~5 cm^{-1}, suggesting a sustained degree of conformational fluctuations in the fibrils.

3.1.4. Aggregation and seeding under high pressure

To study insulin aggregation and seeding under high hydrostatic pressure we used a thermostated high pressure chamber for the incubation of samples and transmission FTIR spectroscopy for determining the secondary structures before and after incubation. 0.5 % insulin solution in D_2O, pH 2 (from now on pH in D_2O solutions means pH-meter readout), containing 0.1 M NaCl, were incubated at two different temperatures, 25°C

and 60°C, and at two different pressures, 1 bar and 1000 bar in the absence and presence of 5% sonicated seeds, respectively (Fig. 21).

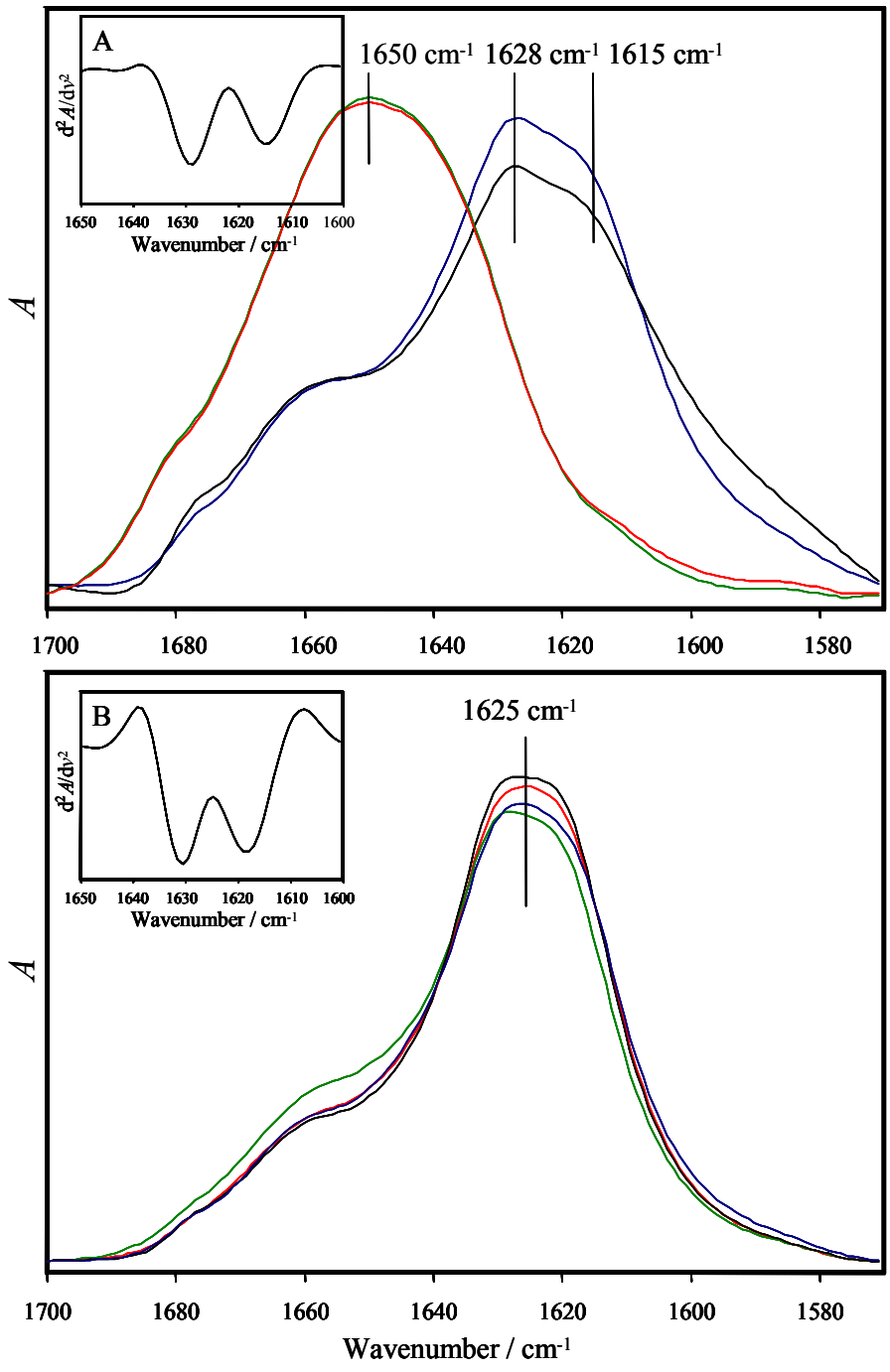

Figure 21: FTIR spectra of insulin structures in the absence (A) and presence (B) of seeds after 24 hours incubation at different temperatures and pressures. Red color represents 1 bar pressure and 25°C, green – 1000 bar and 25°C, blue – 1 bar and 60°C, and black – 1000 bar, 60°C. Inserts show the 2nd derivative FTIR spectra of the final aggregates.

Figure 21A shows predominantly α-helical structure (amide I' band maximum at 1650 cm^{-1}) after 24 hours incubation at 25°C, not much different from the sample kept under 1000 bar pressure, and dominant β-sheet structures after incubation at 60°C. Contrary to previous data of high pressure FTIR, using a diamond anvil cell [Dzwolak et al., 2003], β-sheet-rich aggregates were formed under 1000 bar pressure too. The final spectra of the samples at 60°C are very similar under ambient and high pressure conditions, both showing the same two types of β-sheet, represented by an amide I' band maximum around 1628 cm^{-1} and a shoulder around 1615 cm^{-1}, respectively, with just a bit broader peak in the case of 1000 bar pressure.

Figure 21B shows β-sheet rich structures in each of the different conditions used. The final spectra at each temperature and pressure conditions are very similar, showing an amide I' band maxima around 1625 cm^{-1}, with the second derivative showing two minima around 1630 cm^{-1} and 1619 cm^{-1}, respectively. During the process of sonication strong hydrogen bonds (1615 cm^{-1}) of spontaneously formed β-structures are partially destroyed (Fig. 22) and the new bonds formed in the process of fibril elongation are weaker (1619 cm^{-1}). That is the reason for the differences found in the spectra of spontaneously formed and seed-induced insulin amyloid.

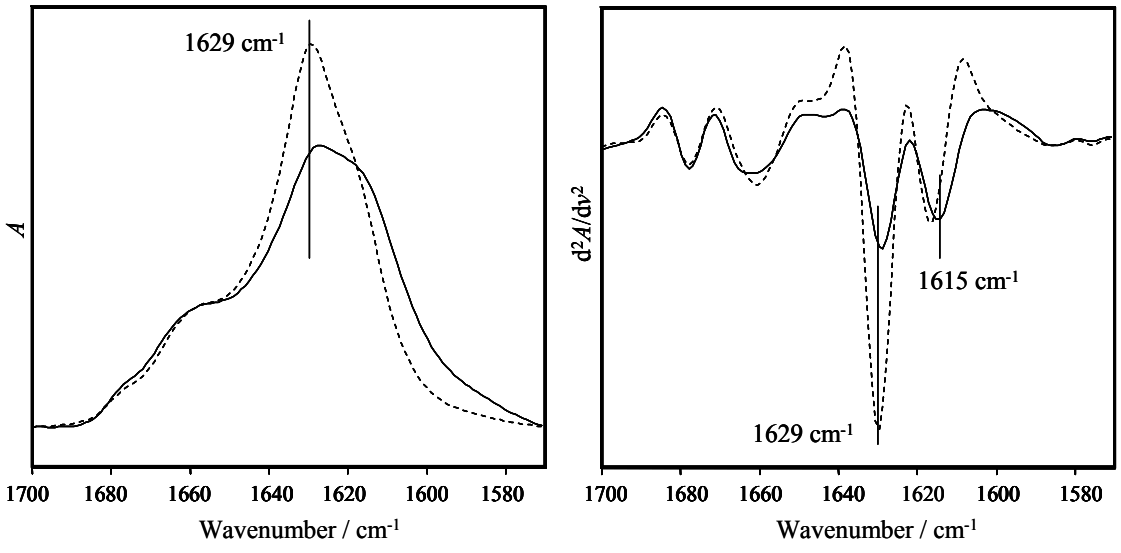

Figure 22: FTIR spectra (A) and corresponding 2nd derivative spectra (B) of insulin fibrils before (solid line) and after (broken line) sonication.

In order to check if high pressure changes the seeding kinetics, fluorescence spectroscopy measurements were performed. 0.5 % insulin solution in H_2O, pH 2, in the presence and absence of 0.1 M NaCl, respectively, were mixed with Thioflavine T (ThT), 5% seeds were added and samples were incubated at 37°C (this temperature was chosen due to the aggregation being too fast at 60°C and too slow at 25°C), continuously measuring the emission at 482 nm.

Figure 23 shows the impact of pressure on the kinetics of seed-induced insulin aggregation. In the presence of salt (Fig. 23A), the application of higher pressures seems to increase the initial rate of elongation. The rate of aggregation at ambient pressure is constant (~linear increase) until around 80% of the insulin is aggregated, and then it levers off due to shortage of substrate. At higher pressures the initial rate is much higher and no linear behavior of the growth rate is observed. Such behavior may be explained by the higher reactivity in the pressure-assisted aggregation process. In the absence of salt (Fig. 23B) the process of aggregation is much longer and differences between ambient and high pressure are hardly seen.

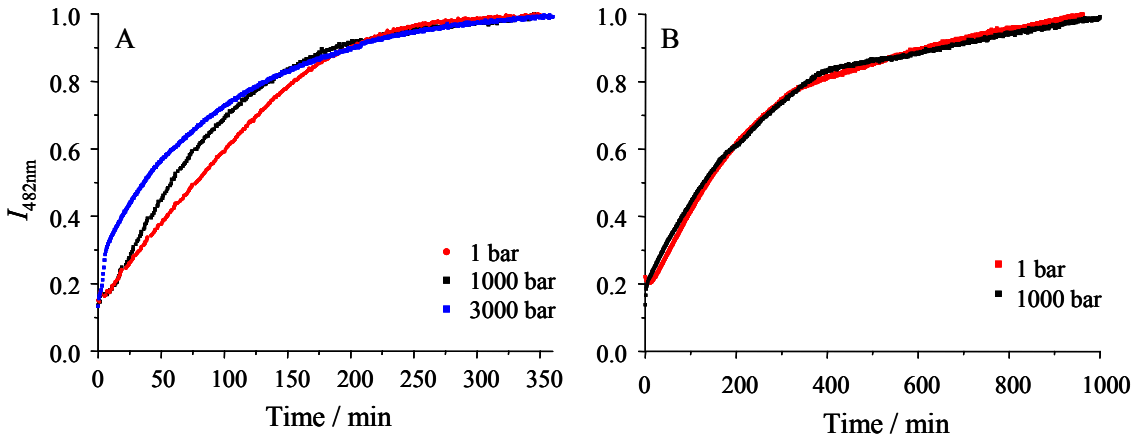

Figure 23: Kinetics of seed induced insulin aggregation at different pressures in the presence (A) and absence (B) of 0.1 M NaCl.

3.1.5. Compressibility of amyloid

From the thermodynamic standpoint, the partial protein volume and its temperature and pressure derivatives, as well as enthalpy and volume fluctuations are the parameters determining protein stability, unfolding and aggregation behavior. These

parameters can be monitored by differential scanning (DSC) and pressure perturbation (PPC) calorimetry, densitometry and ultrasound velocimetry [Gekko and Hasegawa, 1986, 1989; Taulier and Chalikian, 2002; Chalikian, 2003]. Through such a combination of methods a detailed thermodynamic description of an aggregating protein can be obtained, linking its thermodynamics to the generic behavior of proteins implicated in conformational diseases. Samples were prepared by dissolving insulin in H_2O at 2 wt % concentration. The pH of the sample was adjusted to 1.9 with diluted HCl.

Recently, molecular fluctuations of proteins and their coupling to the surrounding solvent have been receiving much interest [Fenimore et al., 2002]. Protein fluctuations permit conformational motions, such as flips of side chains and backbone motions, facilitating transitions between various substates. As the volume, enthalpy and electrical dipole moment fluctuations in the hydration shell and of the exposed amino acid residues are coupled to the surrounding solvent, the term "slaving" has been coined [Fenimore et al., 2002]. Thus the solvent emerges as an active participant in protein dynamics and folding. The fluctuations are given by the relevant susceptibilities, the specific heat capacity c_p at constant pressure, and the isothermal compressibility, β_T:

$$\left\langle (\Delta H)^2 \right\rangle = k_{\mathrm{B}} T^2 m\, c_p , \tag{22}$$

$$\left\langle (\Delta V)^2 \right\rangle = k_{\mathrm{B}} T\, V \beta_T . \tag{23}$$

Here, k_{B} is the Boltzmann constant and V and m are the volume and mass of the protein, respectively. Combined enthalpy and volume fluctuations are related to the coefficient of thermal expansion [Cooper, 1984]:

$$< (\Delta H)(\Delta V) > = k_{\mathrm{B}} T^2 V \alpha . \tag{24}$$

Volume fluctuations are a yardstick of protein flexibility, further related to its packing, void volume and solvational properties, and, in the end, to its biological function. On the several stages of the transition from the native state to the amyloid - destabilization, unfolding, aggregation, fibrillation -, volume fluctuations are expected to play a significant role [Dzwolak et al., 2004b; Grudzielanek et al., 2005] and are therefore discussed in this study.

Typically, small or negative values of β_S are obtained for the acid-, base- or guanidinium hydrochloride-induced denaturation processes of proteins [Gekko and

Hasegawa, 1986, 1989; Taulier and Chalikian, 2002; Chalikian, 2003]. The existing data have indicated that the compressibility of a protein can be divided into at least two components of opposite sign. Because of compressible cavities and voids in the protein interior, a first component is the protein intrinsic compressibility, $\beta_{S,\mathrm{intr}}$, which is positive. The second term, $\beta_{S,\mathrm{hyd}}$, is the contribution to the compressibility due to hydration and bound water. As the compressibility of single amino acids and small peptides in solution is negative [Gekko and Hasegawa, 1986, 1989; Taulier and Chalikian, 2002; Chalikian, 2003], $\beta_{S,\mathrm{hyd}}$ is negative.

Calculations of the volume fluctuations of the system by using expression (23) implies that V is the actual intrinsic volume of the protein, which represents the geometric volume of its solvent-inaccessible interior, and β_T is the actual coefficient of isothermal compressibility of the protein interior [Chalikian, 2003]. This equation cannot be directly used for computing partial molar volume or compressibility data as determined here, because these still contain hydrational contributions. However, qualitative conclusions can be drawn.

The actual aggregation of insulin is preceded by an endothermic unfolding of the native protein around 50 ^{o}C, which is accompanied by complete H/D exchange [Dzwolak et al., 2003]. In the native state, v^{o} and the apparent coefficient of thermal expansion, α, show the typical temperature dependence of a native protein. Around 50 ^{o}C, in the pretransitional range, α increases slightly and decreases significantly again above ~60 ^{o}C, when the aggregation of the protein sets in (Fig. 24A). These observations are in good agreement with previous PPC data suggesting that the abrupt decrease of α upon aggregation is directly related to the release of water from shrinking solvent accessible surface area (SASA) of the fibrillating protein [Heerklotz, 2004; Dzwolak et al., 2004]. The initial increase of α points to a minor conformational change of the protein, accompanied by a slight increase of the solvent accessible surface area and hydration, both factors known to contribute to a positive α.

Whereas β_S does not change markedly with temperature, β_T increases steadily up to ~50 ^{o}C, where a slight change in the slope is visible. The increasing isothermal compressibility data and hence mean square volume fluctuations may result from an increased imperfect packing of the amino acid residues and the dynamic character of a partially destabilized polypeptide. No drastic increase of β_T is observed in the

pretransition region, which indicates that no expanded protein conformation is formed in this temperature range, which would lead to a significant increase in β_T value [Mitra et al., 2006; Ravindra et al., 2004]. Also the PPC data point to a slight change in ASA and hydration of the protein, only. Upon unfolding and during the initial aggregation step at 60 ^{o}C, v^{o} and β_T decrease slightly with respect to the initial linear temperature dependence of v^{o} and β_T, respectively. The character of the temperature-dependencies of α and β_T in the pre-aggregation period can be easily reconciled with the topological properties of the early, aggregation competent intermediates, which are bulky, solvent-exchanged, and as yet are lacking any defined morphological motifs [Jansen et al., 2005].

Figure 24B presents the thermodynamic properties measured as a function of time, i.e., under the conditions when the time-dependent aggregation and fibrillation are taking place. These molecular processes result in significant changes in all the measured physicochemical properties, which are associated with formation of fibrillar topologies by the orderly-stacking insulin molecules [Jansen et al., 2005]. The data presented in this figure conveys a coherent picture of a "volumetric" catastrophe, which accompanies the amyloidogenesis: volume collapse, abrupt reduction of area of the protein-water interphases, and the simultaneous decrease of the compressibility of the protein. The drastic decrease of v^{o} with time can be ascribed to a decrease of void volume. Furthermore, also the ASA and the hydration contribution diminishes, which are known to render α smaller. Also β_T decreases substantially over the first 100 min of aggregation, indicating that the mean square volume fluctuations, which are highest at the early stage of the aggregation reaction, are drastically damped when the aggregation and fibrillation process proceeds. Upon subsequent aggregation and formation of mature fibrillar aggregates, as indicated by the Fourier transform FT-IR spectroscopic data acquired under corresponding sample conditions and heating regimes [Dzwolak et al., 2003], significant dehydration and compaction occurs, whereby water molecules at the protein surface are released, rendering v^{o}, α, β_S and β_T values constant after 150 min. The combined contributions of enthalpy and volume fluctuations, $<(\Delta H)(\Delta V)>$, as revealed by α, increases by ~ 2 % at the pretransition, and decreases overall by about

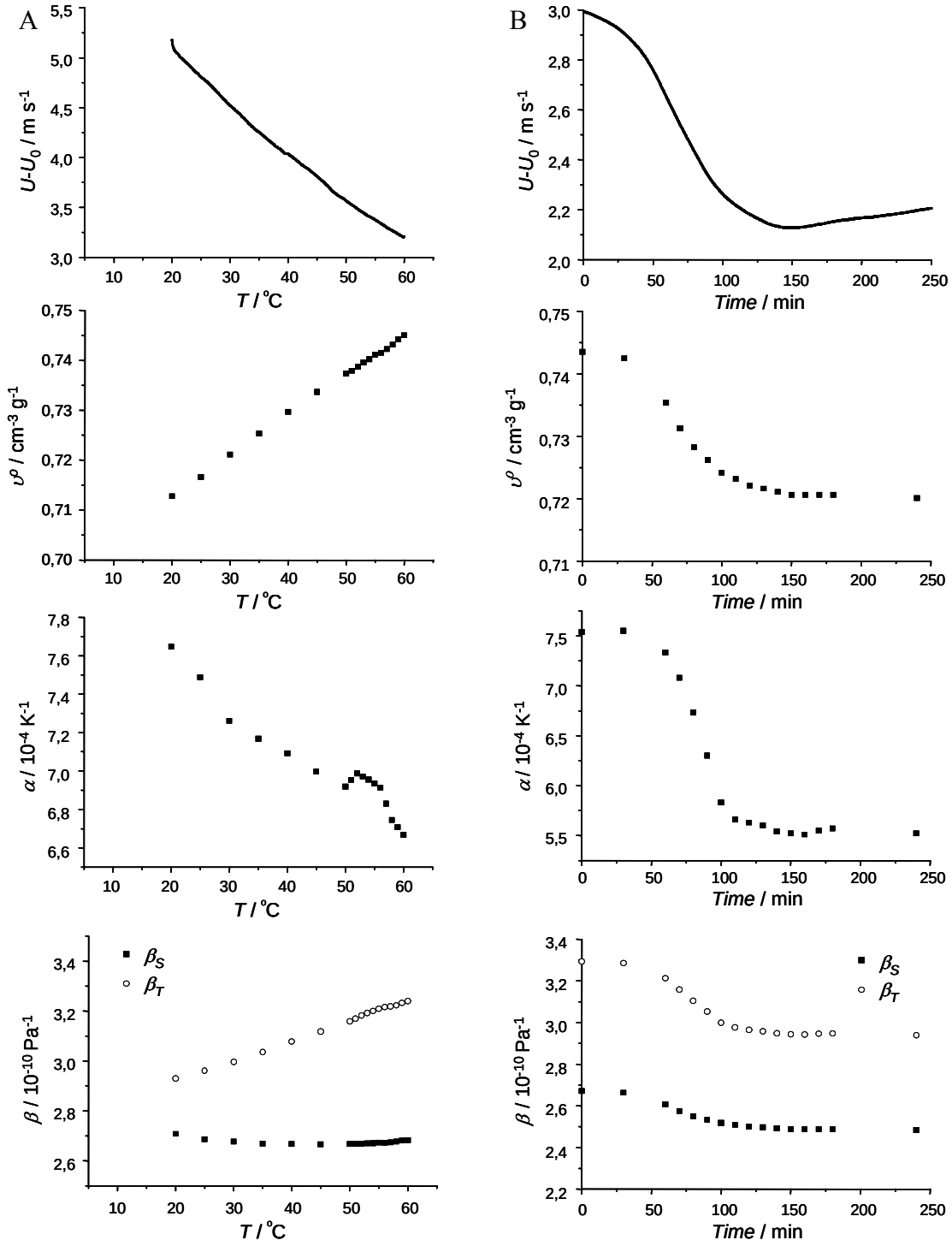

Figure 24: (A) Results from measurements of the ultrasound velocity, specific protein volume, thermal expansion coefficient, adiabatic compressibility β_S and isothermal compressibility β_T of insulin as a function of temperature. (B) Results from measurements of the ultrasound velocity, specific protein volume, thermal expansion coefficient, adiabatic compressibility β_S and isothermal compressibility β_T at 60 °C as a function of time.

30% during the aggregation and fibrillation process, the reduction in volume fluctuations being ~7%. The tight packing of β-sheets and depletion of internal cavities in the late fibrillar aggregates leads to a compaction and hence ~ 3% reduction of the final value of the partial specific protein volume. The decrease in solvent accessible surface area is also reflected in the negative C_p change of -2 kJ mol^{-1} K^{-1} as determined by DSC, recently [Dzwolak et al., 2003].

In comparison to β_S, β_T is always more positive above and below the transition point and displays a more pronounced temperature dependence in the α-to-β transition region. The larger magnitude and changes of β_T may be attributed to the additional contribution of slower structural relaxation processes compared to β_S, which essentially reflects fast (e.g., hydrational) relaxation processes. The slow structural relaxation processes detected by β_T in the transition region may be due to structural relaxation processes of the highly flexible and dynamic transient oligomeric and smaller aggregate entities, and cease upon maturation of fibrils. Rather large differences in β values are also observed at low temperatures, before unfolding and aggregation sets in. Such behavior may be due to the large contribution of slow relaxation processes in combination with monomer-dimer and dimer-oligomer equilibria shifting with increasing temperature.

3.1.6. Impact of NaCl on aggregation

To study the impact of salt, a 0.5 % insulin solution in D_2O, pH 2 with and without 0.1 M NaCl was used. Samples were incubated at 60°C, simultaneously taking FTIR spectra every 5 minutes.

The aggregation process is accompanied by the conversion of the native α-helical-rich secondary structure to a β-sheet-rich structure within the amyloid fibril. This conversion finally gives rise to a prominent FTIR band at 1627 cm^{-1}, characteristic for parallel-stacked, intermolecular β-strands [Bouchard et al., 2000], which develops progressively with time. The kinetic data (Fig. 25) show clearly that, in the presence of 0.1 M NaCl, this process proceeds via an observable intermediate phase. The

intermediate phase vanishes when NaCl is absent, and the overall aggregation is by far slower and follows a simple sigmoidal time-course.

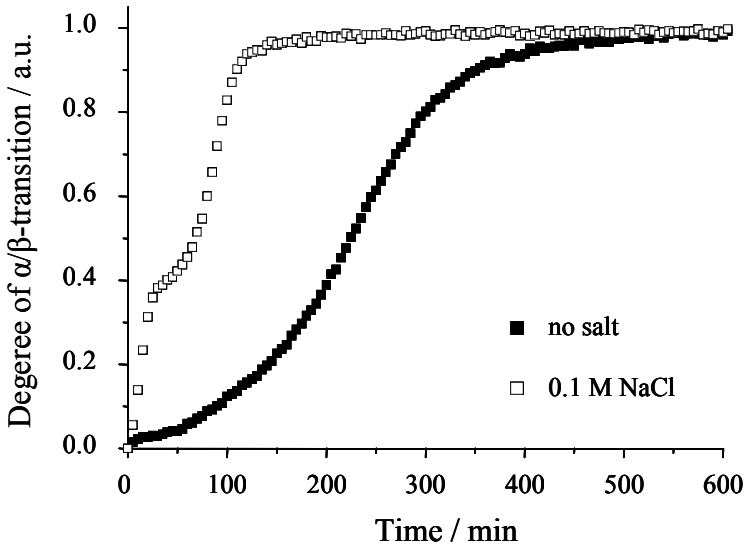

Figure 25: Degree of α/β-transition of insulin, kept at 60 °C (data derived from FTIR spectra).

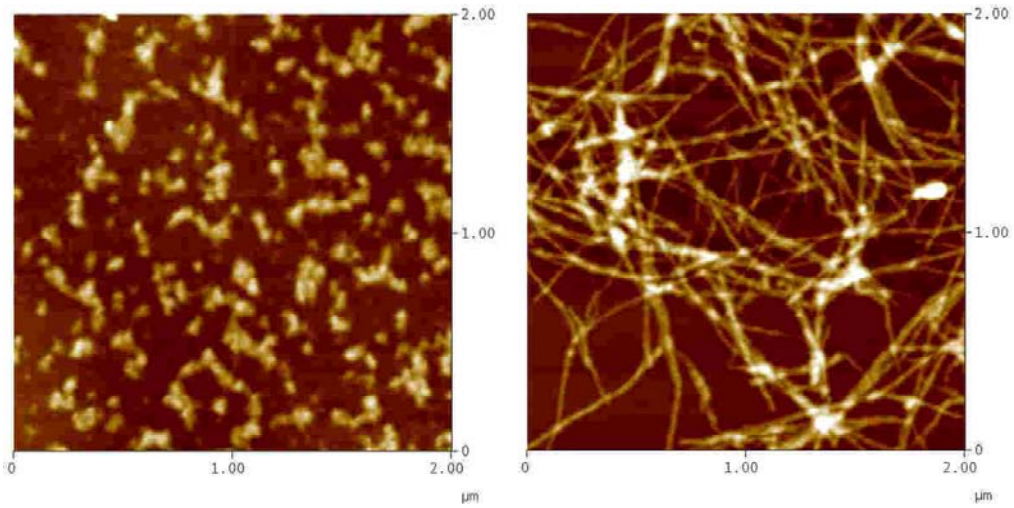

Figure 26: AFM images of insulin aggregates in presence of 0.1 M NaCl. Amorphous aggregates (or oligomers) formed after 35 min (left) and amyloid fibrils formed after 2 hours (right) of incubation at 60 °C.

Figure 26 shows atomic force microscopy images of the insulin species that have formed after incubation at 60 °C for 35 min and for 120 min, i.e., within the pre-transition region and at the end of the main transition in the temporal FTIR profiles, respectively. The image after 35 min shows small amorphous aggregates (or oligomers)

besides coagulated elongated structures. The elongated species are of about 1 nm in height and consist largely of spherical particles that are attached to each other. According to the hierarchical assembly model for amyloid fibrils [Khurana et al., 2003], these resemble precursors of protofilaments. However, it is questionable whether these species transform directly into protofilaments or whether they have to dissociate first to re-enter the amyloid pathway. In contrast, after 120 min, a network of fibrillar species is observed. The fibrillar species appear as straight rod-like objects with varying lengths up to several micrometers and heights between approximately 3 and 10 nm. The former value corresponds to mature insulin fibrils, and the latter corresponds to laterally twisted coils of fibrils [Khurana et al., 2003].

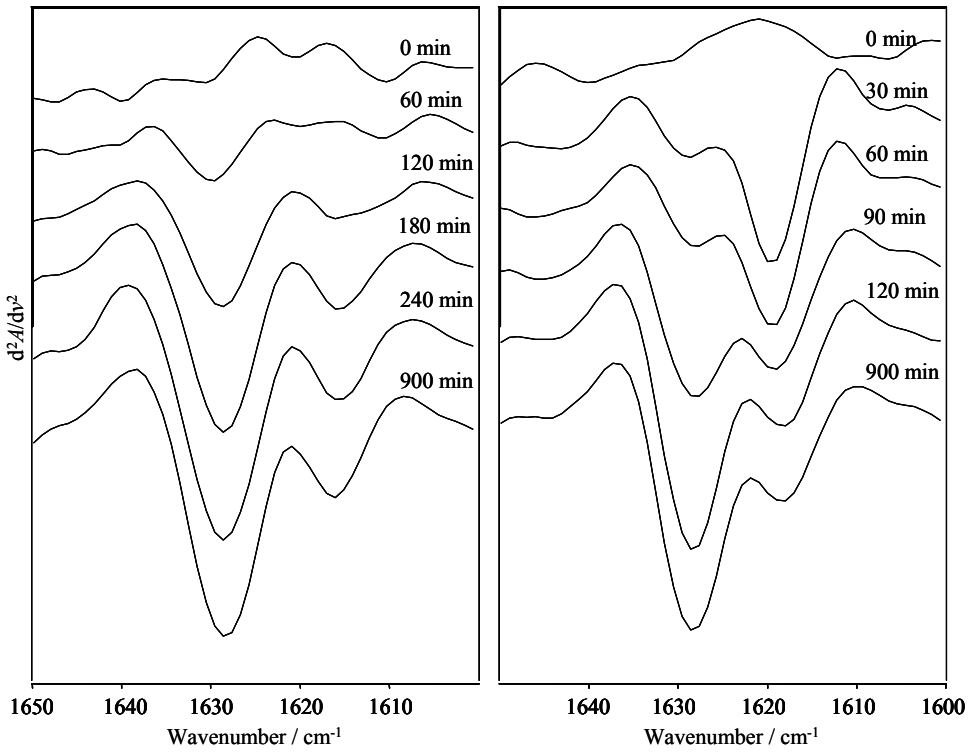

Figure 27: The second derivative FTIR spectra reflect insulin aggregation at 60 °C in the absence (left) and presence (right) of 0.1 M NaCl.

A closer inspection of the amide I' region of the second derivative FTIR spectra (Fig. 27) reveals at least two modes of intermolecular β-strand hydrogen bonding. In the absence of 0.1 M NaCl, a major band at 1627 cm^{-1} develops progressively, accompanied by the simultaneous appearance of a minor component at 1617 cm^{-1}. The increase of the latter band, however, does not proceed beyond approx. 4 h. In contrast, a

single low-frequency band develops at 1619 cm^{-1} in the presence of 0.1 M NaCl within 40 min, i.e., within the pretransition time-range. During the subsequent main aggregation transition, this band shifts slightly, to 1617 cm^{-1}, and reduces in favour of a higher frequency band developing at 1627 cm^{-1}, which dominates the spectrum of the completely aggregated, matured sample.

The amide I' band arises mainly from the carbonyl stretching vibration of the protein backbone amide groups, the frequency of which correlates with the strength of the hydrogen bonds these groups are involved in [Krimm and Bandekar, 1986]. We may refer to the low-frequency band as "strongly hydrogen bonded" amide groups and to the band at 1627 cm^{-1} as "weakly hydrogen bonded" amide groups. According to our data, relatively strong, but presumably few, hydrogen bonds are formed during the pre-transition in 0.1 M NaCl. The formation of these bonds likely reflects the struggle of partially unfolded insulin monomers to saturate "dangling" hydrogen bonds [Thirumalai et al., 2003], which is feasible upon their electrostatically and hydrophobically driven assembly to non-native oligomers. On the other hand, amyloid nucleus formation and subsequent growth are accompanied by a substantial structural rearrangement into extended β-strands within the growing fibril. Owing to the rigidity of mature fibrils, intra-fibrillar hydrogen bonds are thought to underlie considerable geometrical constraints, especially within twisted fibrillar structures. Such constraints would be reflected in weakened hydrogen bonds that manifest in the high-frequency FTIR band at 1627 cm^{-1}. In fact, the frequency of the prominent β-sheet FTIR band for fibrils has been shown to correlate partly with the twist angle of the β-sheet, in that higher twist angles give rise to higher FTIR frequencies [Zandomeneghi et al., 2004].

We showed that 0.5% insulin pH 2 in the presence of 0.1M NaCl can aggregate in two steps, first forming amorphous aggregates and later amyloid fibrils while in the absence of salt direct fiber formation can be observed [Grudzielanek et al., 2006]. But neither FTIR, or fluorescence spectroscopy, nor AFM were able to tell much about physical properties of the aggregates. To get a deeper insight into differences in the process of insulin aggregation in the presence and absence of 0.1M NaCl, simultaneous measurements using FTIR spectroscoy, URT, densitometry and DSC were performed. To minimize time differences in aggregation times, due to the use of different measuring cells, volumes, and environmental conditions (e.g., weak ultrasound in URT

or tube vibration in the densitometer), the measurements were performed as temperature scans increasing the temperature from 25 to 85°C at a rate of 20°C/h.

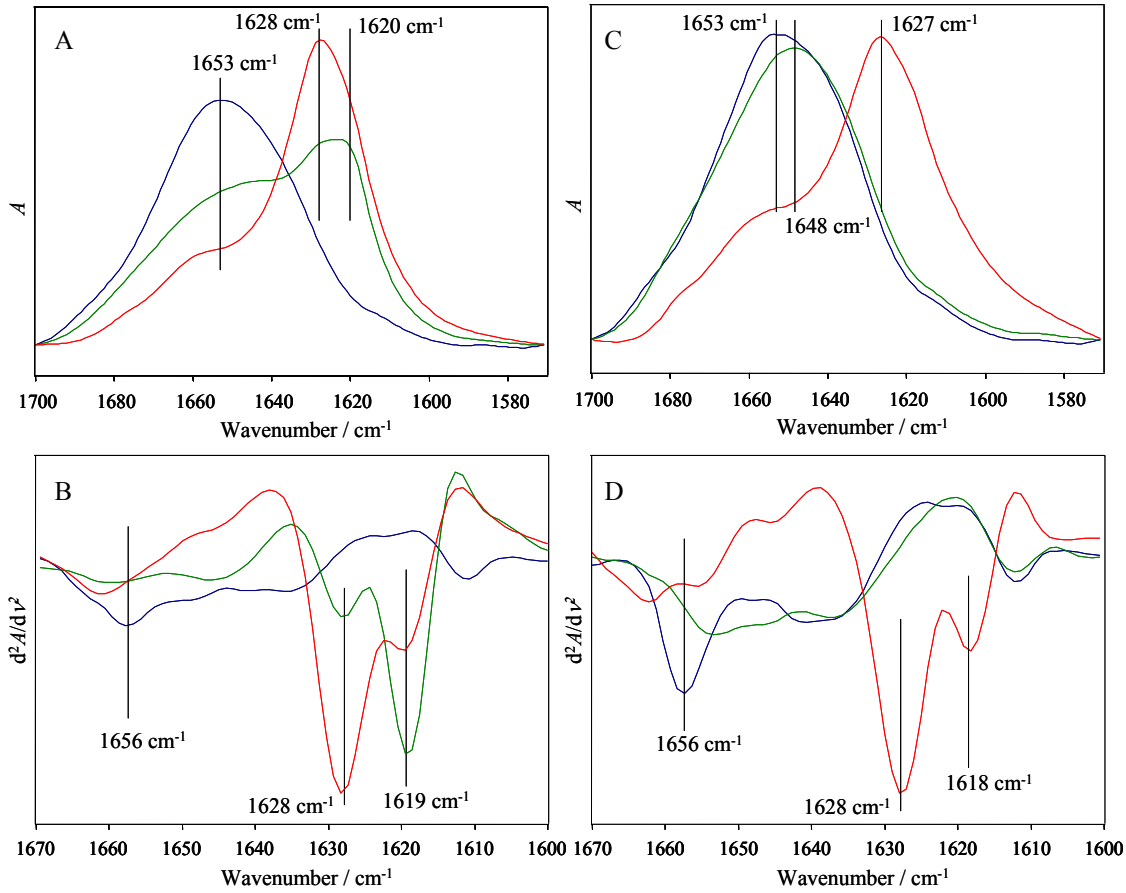

Figure 28: Amide I/I' region of FTIR spectra of 2% insulin in D_2O, pH 2, in the presence (A) and absence (C) of 0,1 M NaCl at different temperatures. B and D show second derivatives of these spectra. Blue lines are for 25°C, green lines for 65°C and red lines for 85°C.

The FTIR measurements (Fig. 28) reveal very similar initial spectra at 25°C with a maximum at 1653 cm^{-1} (minimum of 2nd derivative at 1656 cm^{-1}), which is typical for α-helical structures. The last spectra at 85°C also does not differ significantly; they show a maximum at 1628 cm^{-1} (minimum of 2nd derivative at 1628 cm^{-1} with a weaker one at 1619 cm^{-1}) in the presence of 0.1 M NaCl and a slightly broader peak at 1627 cm^{-1} (minimum of 2nd derivative at 1628 cm^{-1} with a weaker one at 1618 cm^{-1}) in its absence – both cases are typical for β-sheet rich secondary structures. The main difference is hidden in between. In the absence of NaCl, the spectrum at 65°C shows a maximum at 1648 cm^{-1} together with a broadening of the band (no pronounced minima

in the 2nd derivative), which shows the unfolding of the protein to a random coil secondary structures. Conversely, in the presence of salt we can see a completely different picture: a broad β-sheet peak with the maximum between 1620-1628 cm^{-1} (the main minimum of the 2nd derivative is at 1619 cm^{-1} with a weaker one at 1628 cm^{-1}) with a large broad shoulder within the range, characteristic for random coil secondary structures. All these spectra are comparable to the data of insulin aggregation at 60°C temperature, thus we can state, that the spectrum at 65°C in the presence of NaCl represents nonfibrillar aggregates (or oligomers) as found in AFM images, and both spectra at 85°C represent amyloid fibrils.

Further processing of the FTIR spectra allow to follow the relative changes of β-sheet rich structures with increasing temperature. Figure 29A displays the formation of preliminary aggregates, which takes place between 55 and 60°C, the lifetime of these aggregates between 60 and 75°C, and the formation of fibrils between 75 and 80°C in the presence of NaCl, respectively. Figure 29B shows a minor increase between 55 and 70°C, which is mainly caused by H-D exchange and a broadening of the band due to of protein unfolding, and subsequent formation of fibrils between 70 and 80°C in the absence of NaCl. Calorimetric measurements show that both the processes of preliminary aggregation in presence of salt (positive peak between 55 and 60°C (Fig. 29C)) and the unfolding in absence of salt (broad positive peak between 50 and 70°C (Fig. 29D)) are endothermic, whereas the following formation of fibrils (sharp negative peak between 75 and 80°C in presence of salt (Fig. 29C) with a negative peak between 70 and 85°C in absence of salt (Fig. 2D)) is exothermic.

Measured partial specific volumes together with sound velocity allow estimation of the partial adiabatic compressibility. The formation of nonfibrillar aggregates in the presence of NaCl leads to a small decrease in sound velocity (Fig. 29G) together with an increase in partial specific volume (Fig. 29E), which means a positive change in the partial adiabatic compressibility. As these preliminary aggregates occupy a larger volume than the native protein and are easier to compress, application of pressure should be able to prevent formation of such aggregates and should be able to dissociate them, in good agreement with recent pressure-dependent experiments [Grudzielanek et

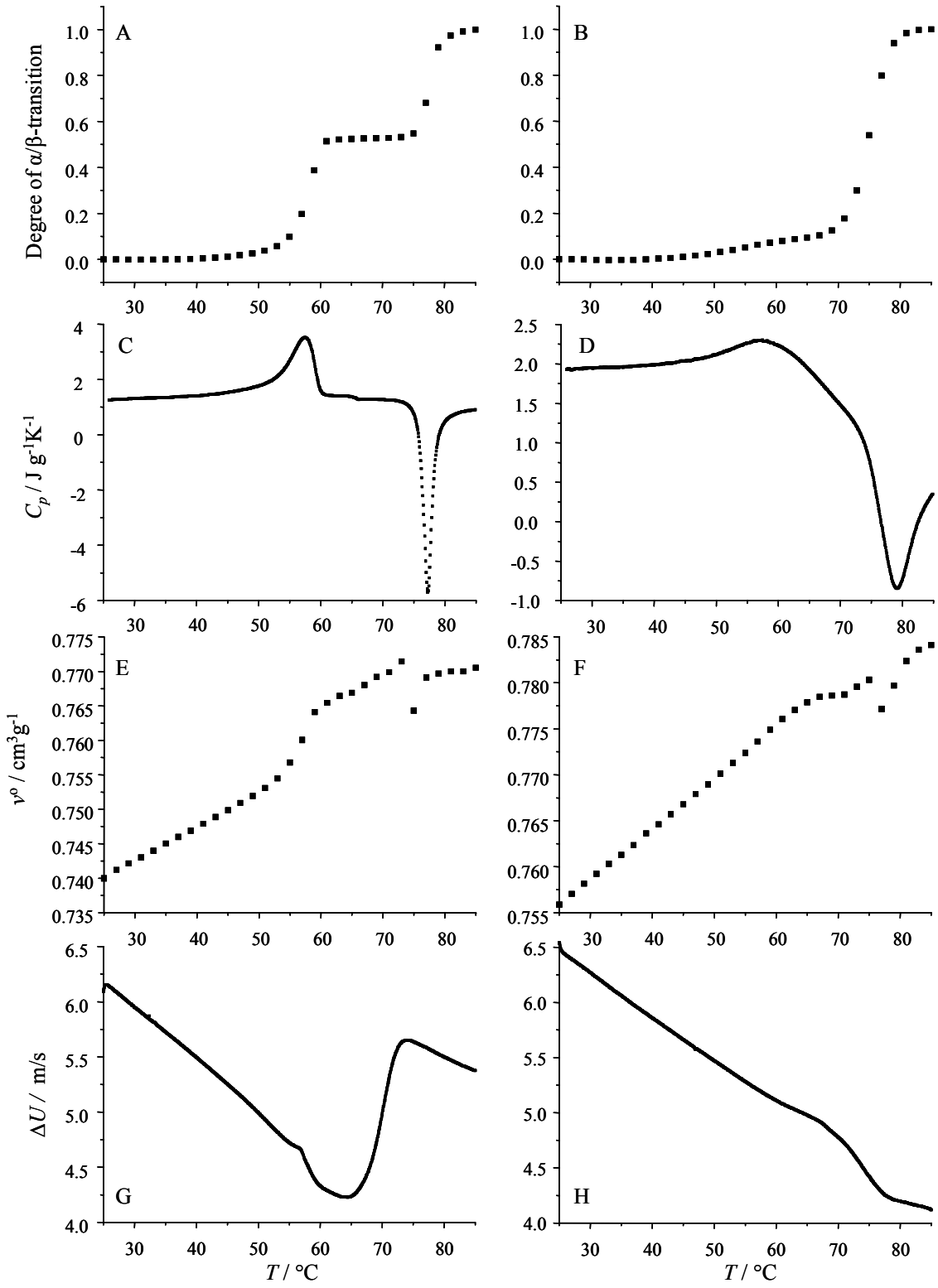

Figure 29: Relative increase in β-sheet structures derived from FTIR spectra (A and B), measured specific heat capacity (C and D), partial specific protein volume (E and F) and sound velocity (G and H) in the presence (left column) and the absence (right column) of 0.1 M NaCl.

al., 2006]. The formation of fibrils leads to a decrease of the partial specific volume and an increase in sound velocity, reflecting a negative change in partial adiabatic compressibility. It seems that the fibrils are much denser and less compressible than the intermediate aggregates. Minor fluctuations of the sound velocity between 65 and 70°C (Fig. 29H) together with a decrease in partial specific volume (Fig. 29E) result in a negative change of the partial adiabatic compressibility, which is common for protein unfolding [Chalikian et al., 1996]. Final fibrils occupy a comparable volume to the unfolded protein but the speed of sound is lower, which is due to a slightly higher compressibility.

Following the data for both samples (with and without NaCl), we can see that most of the differences in the mechanisms of aggregation take place before the start of fibril formation. Formation of nonfibrillar aggregates in one case and unfolding in the other one reflects the differences seen in the data obtained through each single technique. Putting the data together, we can become more certain of how the process is proceeding. No single technique was able to confirm the formation of stable nuclei, which should form before growing of fibrils according to the nucleation-elongation hypothesis. Before the final part of fibril formation is reached we observed two different pathways – via partially unfolded nonfibrillar aggregates (or oligomers) in the presence of NaCl and via partially unfolded (or possibly full unfolded) monomers or dimers in the absence of salt.

Differences in the process of fibril formation are not so well visible in most of experiments. FTIR data suggest similar secondary structure of the final fibrils, DSC suggests both processes being exothermic (with the only difference of a broader peak in the absence of NaCl, which could be due to a slower process). A fast decrease of the partial specific volume at the start of fibril formation, followed by an increase during the subsequent aggregation process was also observed in both samples. Such an unexpected behavior can be explained by the formation of very densely packed nuclei, followed by elongation of fibrils, which leads to a lower water accessible surface area and an increase of partial volume due to decreased hydration. The only technique, able to show such a significant difference in fibril formation between the samples, was URT. A large increase in sound velocity during fibril formation in the presence of NaCl leaves no doubts about the existence of different mechanisms of fibril formation, when

compared to the sample without salt, which shows a decrease in sound velocity upon forming fibrils, only.

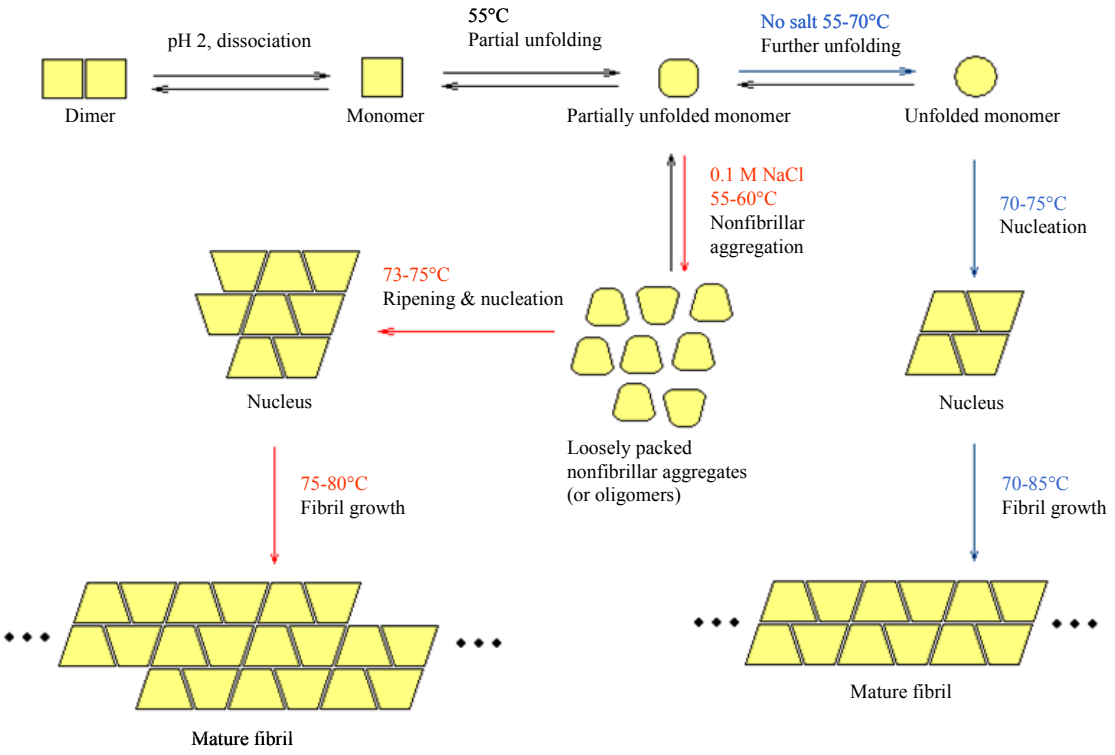

Figure 30: Proposed scheme for the temperature dependent insulin aggregation process in the presence and absence of salt, respectively.

The combined data from FTIR, URT, densitometry and DSC allows a proposal of the scheme for the temperature dependent insulin aggregation process in the presence and absence of 0.1 M NaCl (Fig. 30). We propose that in the absence of salt, insulin starts to unfold with increasing temperature, and, after reaching a certain level of unfolding (with dominating random coil secondary structure), it is able to form nuclei and grow into fibrils. In the presence of 0.1 M NaCl, insulin also partially unfolds (the fraction of random coil secondary structure is below 50%) with raising temperature, but around 55-60°C the protein forms partially unfolded nonfibrillar aggregates (or oligomers). Further increase of temperature leads to the formation of nuclei and growth of elongated fibrils.

Nuclei, formed from amorphous aggregates and final mature fibrils, formed in the presence of NaCl tend to stick together, which often causes problems in finding separate fibrils in AFM pictures (Fig. 31).

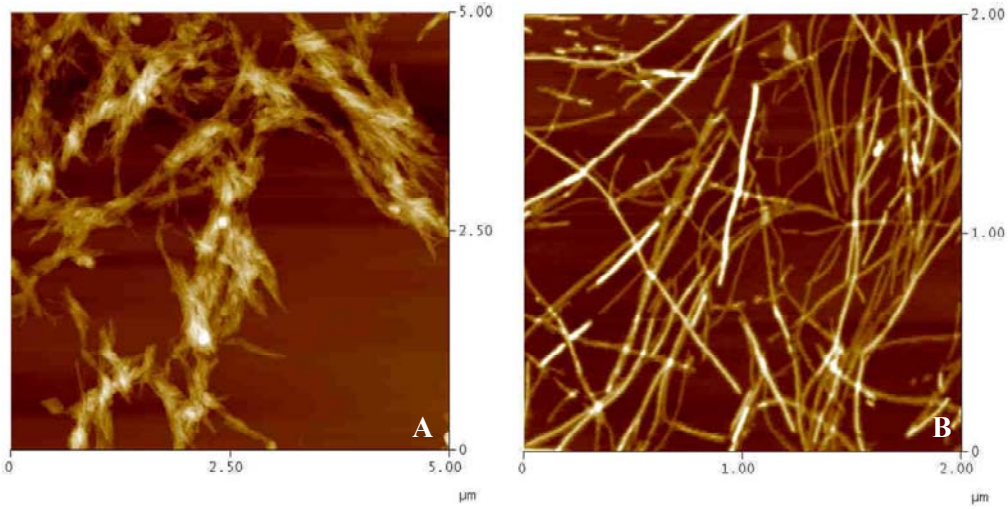

Figure 31: AFM pictures of typical insulin amyloid fibrils formed in the presence (A) or absence (B) of 0.1 M NaCl.

3.2. Thermodynamic properties underlying the α-helix-to-β-sheet transition, aggregation, and amyloidogenesis of polylysine

Samples were prepared by dissolving the polypeptide in H_2O at 2 wt % concentration. The pH of the sample was adjusted to 11.6 with diluted NaOH. Simultaneous measurements of the partial molar volume, the heat capacity, and the coefficients of thermal expansion, adiabatic and isothermal compressibility of the polylysine upon unfolding and aggregation, were performed (Fig. 32)

Recently, it was shown using DSC (Fig. 32B), PPC, and circular dichroism (CD) spectroscopic measurements [Dzwolak et al., 2004c] that the α/β-transition in poly-D- and poly-L-lysine starts at ~35 °C and is completed at 50 °C. As revealed by the increase of the specific protein volume and the isothermal compressibility (Fig. 32D), a temperature-induced destabilization of the polylysine's structure occurs just (~3 °C) before the onset of the unfolding and aggregation process. The increased isothermal compressibility data and hence mean-square volume fluctuations may result from an increased imperfect packing of the amino acid residues and the dynamic character of a

partially destabilized polypeptide, which is reminiscent of a molten globule kind of intermediate state, which has been shown to lead to a significant increase of compressibility values [Chalikian and Breslauer, 1996, 1998; Chalikian et al., 1996]. Upon unfolding and during the initial aggregation step, $v°$, β_S, and, most drastically, β_T decrease simultaneously, reaching minima around 35 °C. This can be ascribed to a release in void volume and – probably more importantly – an increased hydration of the protein surface, which is known to render β_S negative. Generally, the higher the total solvent-accessible surface area, the more negative is the hydration contribution. Hence,

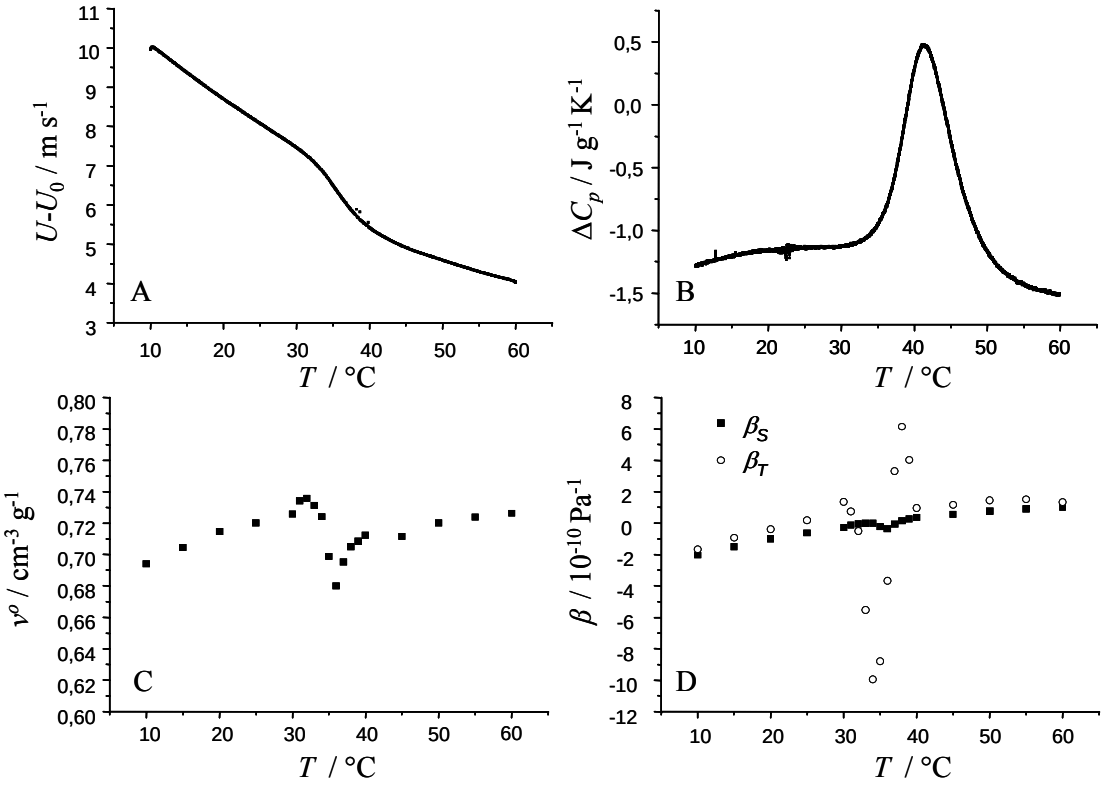

Figure 32: Results from measurements of the (A) ultrasound velocity, (B) heat capacity, (C) specific protein volume, and (D) adiabatic compressibility β_S and isothermal compressibility β_T of a 2 wt % polylysine solution at pH 11.6 as a function of temperature.

the mean-square volume fluctuations increase slightly before the onset of the unfolding/aggregation reaction and then decrease drastically in a rather cooperative manner when the unfolding and aggregation process sets in. Upon subsequent aggregation and formation of mature fibrillar aggregates, as indicated by the CD and FTIR spectroscopic data [Dzwolak et al., 2004], significant dehydration occurs,

whereby more densely packed water at the protein surface is released, leading to an increase of $v°$, β_S, and β_T again, which, at higher temperatures, are largely determined by the thermal volume effect [Chalikian and Breslauer 1996, 1998; Chalikian et al. 1996]. The large increase of β_T just after the transition (at ~38 °C) indicates that the early aggregates formed (which might well be still partially amorphous) still undergo large volume fluctuations, which rapidly decay upon formation of larger fibrils. The tight packing of β-sheets and depletion of internal cavities in the late fibrillar aggregatesleads to a compaction and hence 20% reduction of the final value of the partial specific protein volume. The decrease in solvent-accessible area is also reflected in the negative C_p change of -4 kJ mol^{-1} K^{-1} (Fig. 32B). In comparison to β_S, β_T is always slightly more positive above and below the transition and displays drastically more pronounced temperature dependence in the transition region, however. The larger changes of β_T may be attributed to the additional contribution of slower structural relaxation processes compared to β_S, which essentially reflects fast (hydrational) relaxation processes only. The slow structural relaxation processes detected by β_T in the transition region may be due to structural relaxation processes of the highly flexible and dynamic transient oligomeric and smaller aggregate entities.

3.3. Islet amyloid polypeptide (IAPP)

3.3.1. Effect of high hydrostatic pressure (HHP)

So far, there are no reports regarding the effects of HHP on IAPP. Owing to the fact that high hydrostatic pressure acts to disfavour hydrophobic and electrostatic interactions that cause protein aggregation, this parameter can be used as efficient tool to reveal new important information on the nucleation and growth processes of the protein. High-pressure coupled with Fourier-transform Infrared spectroscopic studies and atomic force microscopy measurements were carried out to reveal the changes in IAPP aggregate and fibril formation under pressure-perturbation.

For the samples before and after pressure treatment, we used 10 mM NaH_2PO_4 with 1 % residual TFE in D_2O at pH 7.4 and a protein concentration of 250 µM (~0.1 % w/w).

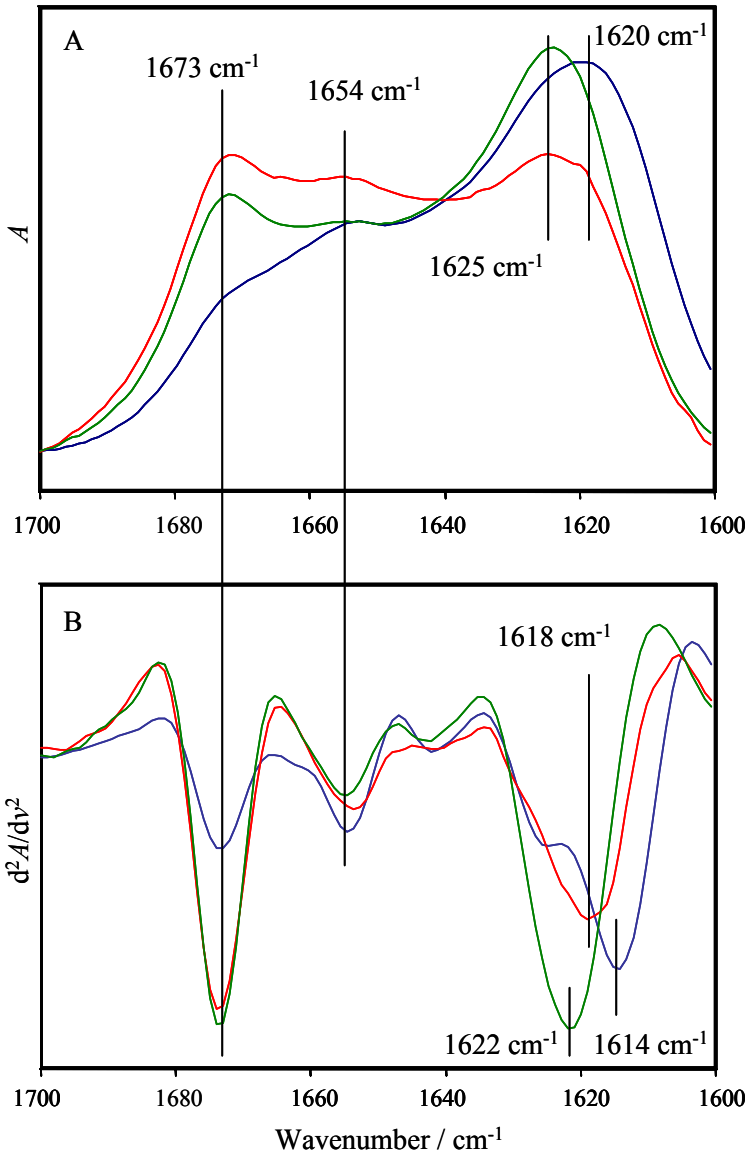

Figure 33: FTIR spectra (A) and second derivatives (B) of IAPP: 5 min after preparation (green), after 3 days of aggregation at ambient pressure (red) and after 3 days at 3.5 kbar (blue).

Figure 33 shows FTIR spectra of various IAPP samples: freshly dissolved IAPP and IAPP aggregated for 3 days at ambient pressure and at 3.5 kbar, respectively (all spectra were taken at room temperature, 25 °C). The FTIR spectrum of the freshly prepared IAPP sample at a concentration as high as 250 µM exhibits a IR band

appearing at ~1622 cm^{-1}, likely of intermolecular parallel β-sheet structures, and a pronounced peak at 1673 cm^{-1}, which is due to turns and residual trifluoracetic acid (TFA) in the sample. Such IR pattern is indicative of the aggregated state of IAPP according to the data of other amyloidogenic proteins, like insulin [Dzwolak et al., 2004a].

In order to reveal the different morphological structures formed, additional AFM measurements were carried out for this IAPP concentration (Fig. 34). Most of the aggregate structures seen in the sample that was not subjected to HHP are short (< 1 μm) fibrils with an average of 5 - 15 nm diameters as determined from the AFM height profile. Such rather short fibrillar structures probably appear due to a comparably fast nucleation process at this high protein concentration, whereas the elongation process seems to be comparably slow. The pressure treated sample still contains fibrils, but also a significant amount of smaller oligomeric particles (of 0.5 - 1.5 nm size).

Taking the FTIR spectroscopic and AFM results together, we may conclude that the sample subjected to the high pressure treatment shows less fibrillar β-sheet structures and a larger population of smaller amorphous aggregates with a different H-bonding pattern. The different fibrillar and non-fibrillar amorphous/oligomeric morphologies found for the high pressure treated sample indicate that not all IAPP aggregate structures are equally sensitive to pressure, hence suggesting the existence of pressure resistant fibrils with densely packed cores and a population that can be dissociated by HHP.

The conceptual framework for using such pressure axis experiments is as follows: The interior of proteins is largely composed of rather efficiently packed residues (with void volume on the order of 0.5 %), more likely hydrophobic than those at the surface. High hydrostatic pressure induces conformational fluctuations due to a decrease in the strength of hydrophobic interactions, finally leading to partially pressure-induced unfolding through transfer of water molecules into the protein interior, gradually filling cavities and leading to the dissociation of close hydrophobic contacts and subsequent swelling of the hydrophobic protein interior [Haberhold et al., 2004; Hummer et al., 1998]. According to the literature, aggregation of the C-terminal domain of IAPP (amino acid sequences 20-29 and 30-37) is thought to be most likely driven by hydrophobic interactions. The distinctly amyloidogenic region 20-29 has been pointed

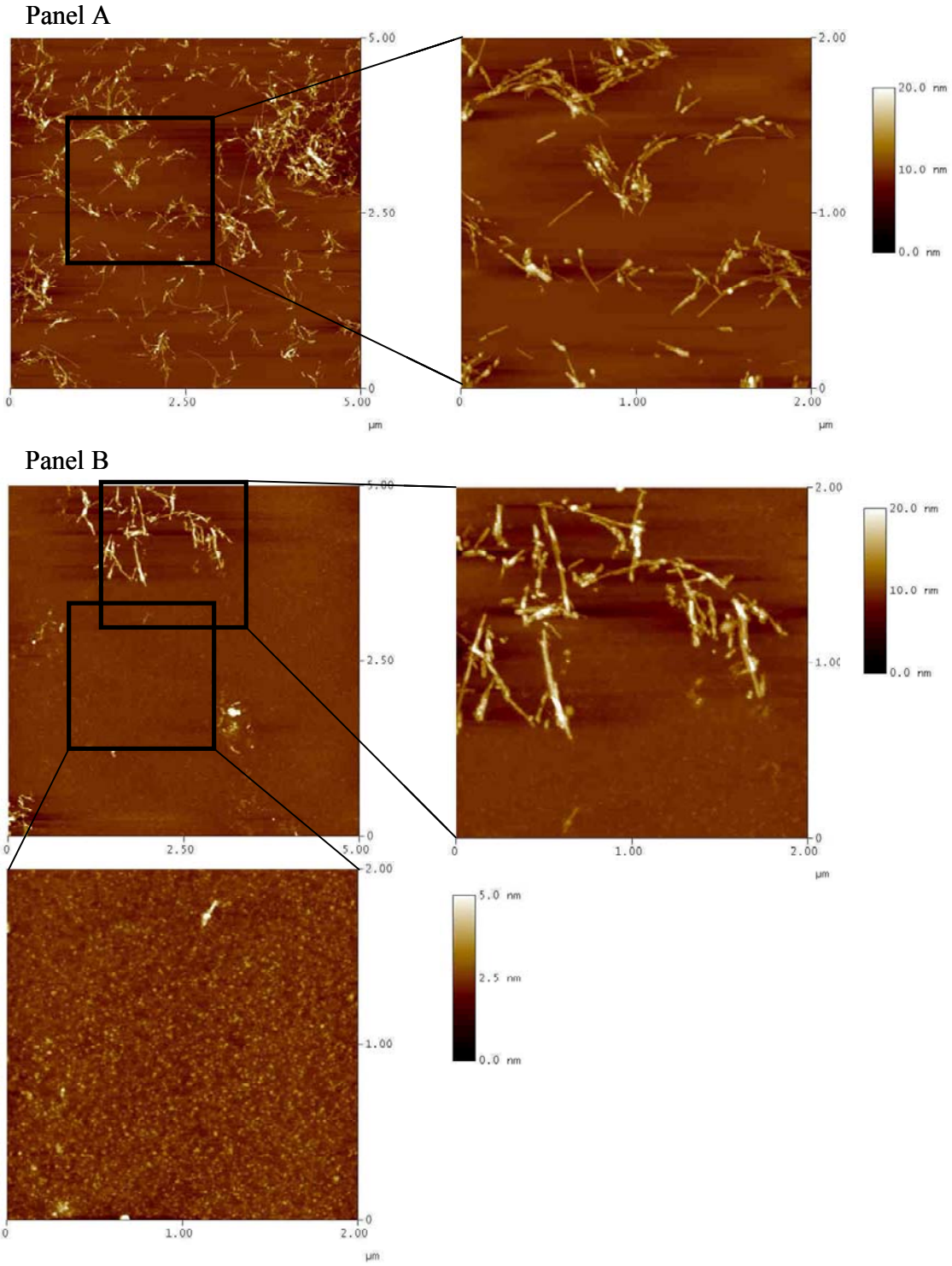

Figure 34: AFM height images of 250 µM IAPP aggregates after 3 d without (panel A) and with pressure treatment at 3.5 kbar (panel B).

out to be a key fibril-forming region [Ma et al., 2001]. Hence it is conceivable that the C-terminus of IAPP, spanning residues 20 to 37, forms a β-sheet. The secondary

structure predictions of human IAPP indicate that there is one potential α-helical region between amino acid residues 8-14, and three potential β-strand regions. A β-turn has been predicted at Asn31, which would result in two adjacent β-strands (32-37 and 24-29); a third β-strand is proposed to exist in region 18-23 [Jaikaran et al., 2001].

According to these data, it may be concluded that IAPP has not only one but several amyloidogenic cores that are interacting to form an organized aggregate structure, and that hydrophobic interactions may drive the initial stage of the aggregation process. As HHP is acting to weaken or even prevent hydrophobic self-organization, we may expect that the amyloidogenic "cores" cannot be arranged and packed the same way upon aggregation as they are able to do under ambient pressure conditions, thus leading to the formation of a more heterogeneous population of fibrils and smaller amorphous/oligomeric species.

Taken all data together, a hypothetical model for IAPP fibril formation may be suggested: i) IAPP undergoes fast nucleation (due to several amyloidogenic "cores"), largely driven by hydrophobic interactions. Hence, formation and packing of fibrils is not perfect and mixed-registry β-sheet structures might exist, in particular at high protein concentrations, which can be partially dissociated by pressure leading to smaller aggregate structures and oligomers. HHP already as low as 3.5 kbar is sufficient to weaken and (at least partially) disrupt the hydrophobic cores thus leading to formation of a heterogeneous population of fibrillar aggregates with IR amide I' bands in the low wavenumber region (which is typical of a more strongly H-bonding pattern of intermolecular β-sheets) and a large amount of non-fibrillar smaller aggregates and oligomers, as detected by AFM (with IR amide I' bands in the larger wave number region around 1620 cm^{-1}). ii) Our data also indicate that the early IAPP fibrils are sensitive to high hydrostatic pressure, similar to amorphous aggregates and inclusion bodies [St John et al., 1999; Foguel and Silva, 2004]. Considering the fact that high hydrostatic pressure is an effective means in disturbing ionic and hydrophobic interactions but not hydrogen bonds, we can conclude that these former two types of interaction are important for the stability of IAPP fibrillar aggregates, as also suggested in work using denaturing agents [Kayed et al., 1999]. The results may be physiologically relevant and may have important implications regarding the stability of

the IAPP fibrils against degradation, a fact that can contribute to the development of antagonists of the pathogenesis of type II diabetes mellitus.

3.3.2. Aggregation in trifluorethanol (TFE)

TFE is one of the solvents used for preparing stock solutions for IAPP studies [Lopes et al., 2004, 2007]. To check if a high concentration stock solution can be kept for longer times, 0.5% of IAPP was dissolved in trifluorethanol and incubated at room temperature for 7 weeks, taking FTIR spectra after 1, 7, 14 and 52 days of incubation. The second derivative FTIR spectra shown in figure 35 illustrate changes of secondary structure during incubation.

IAPP just dissolved in TFE shows a dominant 2nd derivative peak at 1626 cm^{-1}, which can be assigned to β-sheet structures and a smaller peak at 1652 cm^{-1}, typical for α-helices. Minima at 1674 cm^{-1}, observed in all spectra, are assigned to residual trifluoracetic acid in the sample (Fig. 35). After one day, a decrease of the β-sheet signal with a simultaneous increase in α-helical structures is observed. During the next 2 weeks, α-helical structures become dominant. After 14 days, the initial β-sheet structures (represented by a minimum at 1626 cm^{-1}) are completely dissociated, but a new type of β-strands (minima at 1630 and 1616 cm^{-1}) starts to form. And finally after 52 days, α-helices are completely converted into the new type of β-strands.

Hence, during the incubation process of IAPP, two transitions have been observed: the first one is a non-amyloid β-sheet conversion into α-helices which is induced by TFE; the second one leads to aggregation of the non-native α-helices into amyloidogenic β-sheet structures. This suggests that α-helical structures are an on-pathway intermediate to the amyloidogenesis of IAPP. Transient α-helical structures have in fact been shown to occur in some natively unstructured amyloid-forming proteins including IAPP [Lopes et al., 2007; Williamson and Miranker, 2007; Kirkitadze et al., 2001]. Hence, reported data are further indication that α-helices may be a rather common intermediate formed before the amyloid formation by natively unstructured peptides takes place [Lopes et al., 2007].

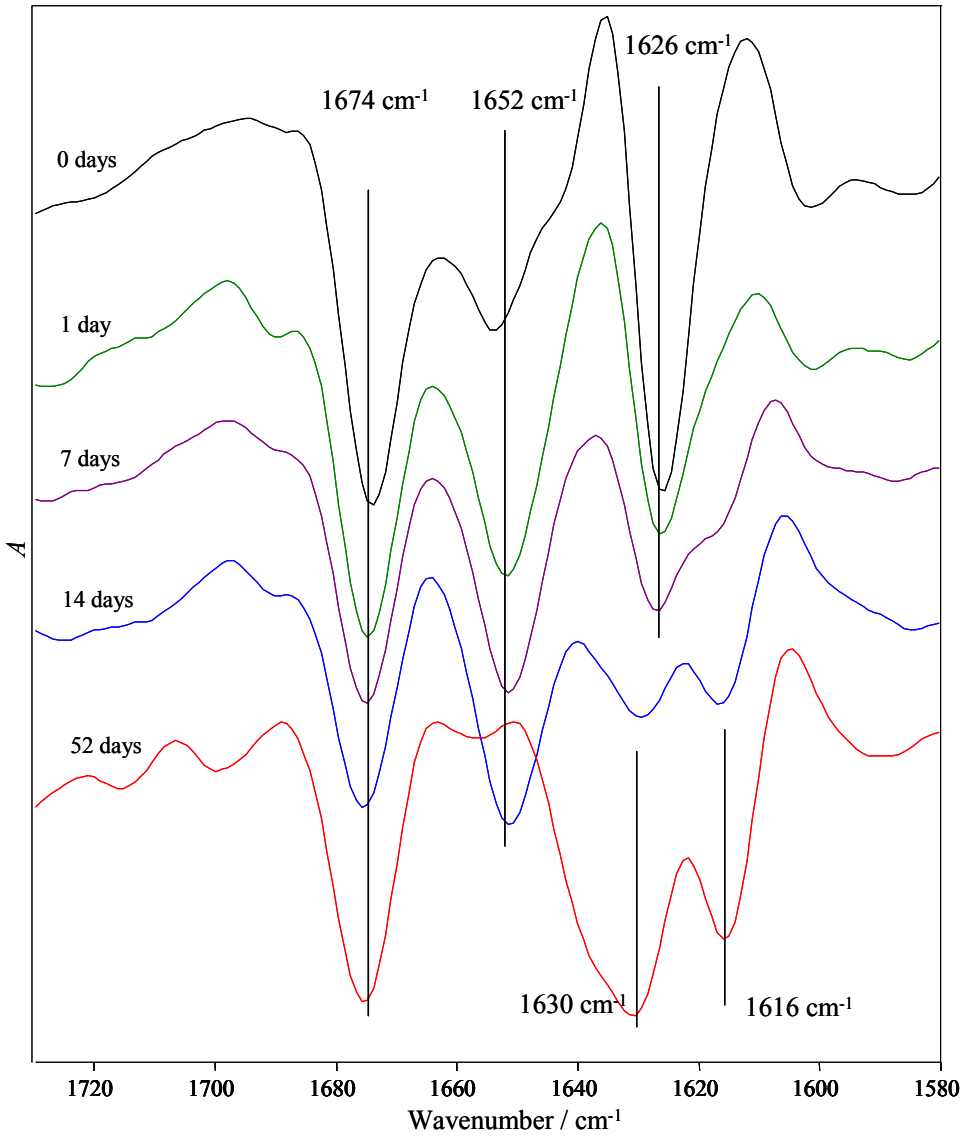

Figure 35: Second derivative FTIR spectra showing changes in secondary structure of IAPP solution in TFE during incubation at room temperature.

4. Summary

The number of people affected by different neurodegenerative diseases is considerable and increases every year. One of the characteristic hallmarks of these diseases is the deposition of ordered proteinacious aggregates, called amyloid. Not only disease-related proteins are able to form amyloid-like structures; In fact it was suggested that formation of amyloid fibrils can be considered a generic feature of polypeptide chains. Thus simple and cheaper peptides and proteins can be used as models for studying amyloidogenesis. Insulin and polylysine, which have been used in this study, are among the most common model proteins and peptides.

A thorough study of the amyloidogenesis of insulin has been conducted. Such work provides a coherent and precise description of the changes of the structure of the protein, the partial specific volume, heat capacity, the coefficient of thermal expansion, as well as the adiabatic and isothermal compressibility of the protein upon partial unfolding, aggregation and fibril formation. Additionally, a thermodynamic study upon partial unfolding, aggregation and fibril formation of polylysine, and a pressure and TFE perturbation study of IAPP, which plays a major role in the diabetes mellitus type II disease, were performed. This was possible due to the application of ultrasound velocimetry and pressure perturbation calorimetry, complemented by differential scanning calorimetry, FTIR and fluorescence spectroscopy, as well as atomic force microscopy studies.

The work starts with a solvational perturbation study of the insulin aggregation process. Three model co-solvents (ethanol, TFE and glycerol) were used for the FTIR study. It was shown that the presence of 20% ethanol speeds up the aggregation kinetics, while 20% of TFE and 20% of glycerol stabilize α-helical structures and slow down the aggregation process. Moreover, the secondary structures of the final aggregates, formed in the presence of the different co-solvents, were found to be different from those formed under ambient, co-solvent-free conditions. This suggests that several distinct amyloid states may be induced *in vitro* from a single protein (Fig. 36 A and B).

Insulin amyloid fibrils can be broken into smaller pieces by using ultrasound treatment. Most of the broken fibrils can stick together via interactions between their

ends. Possibly, the termini of broken fibrils are prone to attach additional particles and are able to elongate effectively in such a way.

Sonicated insulin fibrils, added to the native insulin solution at low pH, are able to induce the formation of amyloid (seeding-effect) under conditions, which are not common for nuclei formation. Moreover, two distinct insulin amyloid states, formed under co-solvent free conditions and in the presence of 20% ethanol, replicate their structure-hallmarking infrared features (Fig. 36 C and D). The cross-seeding specificity and the kinetic features of both amyloid types appear to mirror certain aspects of the prion strains phenomenon and kinetic traits observed in other amyloidosis. This suggests that the strain-dependent infectivity of prions is an inherent feature of protein amyloids and, as such, remains in accordance with the protein-only molecular basis of prion diseases.

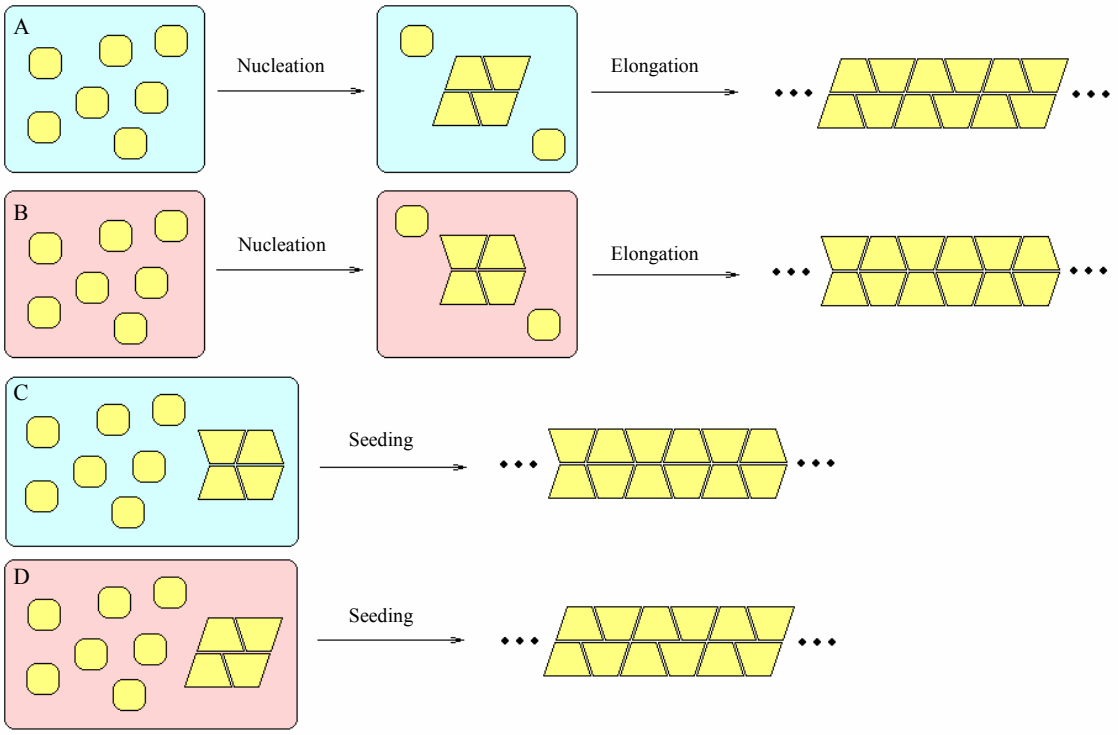

Figure 36: Formation of insulin amyloid "strains" and cross-seeding. At low pH and high temperatures insulin forms amyloid fibrils. The fibrils exhibit different structures when formed in pure water (A) and in the presence of 20% ethanol (B). Short pieces of fibrils, subjected to insulin solution, are able to induce the formation of amyloid (seeding-effect) even at ambient temperature. The presence of seeds negates the environmental factor: amyloid particles, formed in the presence of 20% ethanol, are able to replicate when subjected to insulin solution in pure water (C), and amyloid particles formed in pure water are able to replicate when subjected to insulin solution in the presence of 20% ethanol (D).

The study of insulin aggregation under different pressures showed no major differences between samples aggregated under 1 and 1000 bar. The only minor differences were observed in the kinetics of aggregation.

A precise and simultaneous determination of the thermodynamic variables v^o, C_p, α, β_S, and β_T upon unfolding and aggregation of insulin and polylysine was performed. It permits devising a unified thermodynamic picture of the time-dependent aggregation process, with highlighting the importance of volume fluctuations during unfolding and amyloidogenesis of the protein. The volume fluctuations appear to stem largely from changes in the flexibility of the protein, which is related to void volume and hydration changes during the various phases of the structural transformation of the protein: destabilization and partial unfolding of the monomer, oligomerisation, early aggregation and maturation of fibrils.

A series of measurements in the absence and presence of 0.1 M NaCl revealed two distinctly different pathways of insulin aggregation. In the absence of screening ions (salt), with increasing temperature insulin starts to destabilize and unfold, and, after reaching a significant level of unfolding (random coil secondary structures are dominating), it forms compact nuclei that grow into fibrils. In the presence of 0.1 M NaCl, partial unfolding (the contents of disordered, random coil-like secondary structures is below 50%) occurs with raising temperature, forming partially unfolded nonfibrillar aggregates (or oligomers) around 55-60 °C. Further increase of temperature leads to a reorganization of the aggregate structure and formation of more compact nuclei which allow growth of elongated mature fibrillar species. As revealed by AFM, the latter process which fosters reorganization, ripening and formation of more compact nuclei from amorphous oligomers, leads to more crowded aggregate morphologies.

The study of the disease-related islet amyloid polypeptide revealed its sensitivity to high pressure. The results may be physiologically relevant and may have important implications regarding the stability of the IAPP fibrils against degradation, a fact that can contribute to the development of antagonists of the pathogenesis of type II diabetes mellitus. IAPP aggregation in TFE showed a novel β-to-α-to-β secondary structural transition. The data indicate that formation of α-helices may be a rather common event preceeding amyloid formation from natively-unstructured peptides.

5. Zusammenfassung

Die Anzahl der Personen, die an unterschiedlichen neurodegenerativen Erkrankungen leiden, ist erheblich und steigt jedes Jahr weiter an. Eines der charakteristischen Merkmale solcher Krankheiten ist das Vorkommen von geordneten Protein-Aggregaten, so genannten Amyloiden. Aber nicht nur mit Krankheiten assoziierte Proteine sind in der Lage, Amyloid-Strukturen auszubilden. Es wurde vermutet, dass Polypeptidketten generell Amyloid-Fibrillen bilden können. Daher werden einfache und kostengünstige Peptide und Proteine als Modellsubstanzen dazu genutzt, die Amyloidogenese zu studieren. Insulin und Polylysin, die in dieser Studie verwendet wurden, gehören zu den gebräuchlichsten Modellproteinen und – peptiden.

In dieser Arbeit wurde eine umfassende Untersuchung der Amyloidogenese des Insulins durchgeführt, die eine schlüssige und präzise Beschreibung der Veränderungen der Proteinstruktur, des spezifischen partiellen Volumens, der Wärmekapazität, des thermischen Ausdehnungskoeffizienten so wie der adiabatischen und isotermen Kompressibilität des Proteins bei seiner partiellen Entfaltung, Aggregation und Fibrillbildung liefert.

Zusätzlich wurde eine thermodynamische Untersuchung der partiellen Entfaltung, Aggregation und Fibrillbildung von Polylysin durchgeführt und der Einfluss von Druckänderungen und TFE auf die Aggregation von IAPP studiert. Dies war durch den Einsatz von Ultraschallgeschwindigkeitsmessungen und der Druckperturbations-kalorimetrie, ergänzt durch DSC, FTIR- und Fluoreszenz-Spektroskopie sowie Rasterkraftmikroskopie möglich.

Zunächst wurde der Einfluss verschiedener Co-Lösungsmittel auf die Insulinaggregation untersucht. Drei Modell-Cosolventien wurden für die FTIR-Untersuchungen benutzt: Ethanol, TFE und Gylcerol. Es konnte gezeigt werden, dass die Anwesenheit von 20% Ethanol die Aggregations-Kinetik beschleunigt, während 20% TFE und besonders 20% Glycerol α-helikale Strukturen stabilisieren und somit die Aggregationsrate herabsetzen. Des Weiteren ist die Sekundärstruktur, die in Anwesenheit von Cosolventien ausgebildet wird, unterschiedlich von der ohne diesen

Substanzen gebildeten Struktur. Dies lässt darauf schließen, dass es in vitro mehrere verschiedene Amyloid-Zustände für ein einzelnes Protein gibt (Abb. 36 A und B).

Insulinfibrillen können mittels Ultraschallbehandlung in kleinere Stücke gebrochen werden. Die meisten gebrochenen Fibrillen können an ihren Enden zusammenhängen. Möglicherweise besitzen die Enden der gebrochenen Fibrillen eine erhöhte Affinität für die Anlagerung weiterer Partikel und sind so in der Lage, sich effizient zu verlängern.

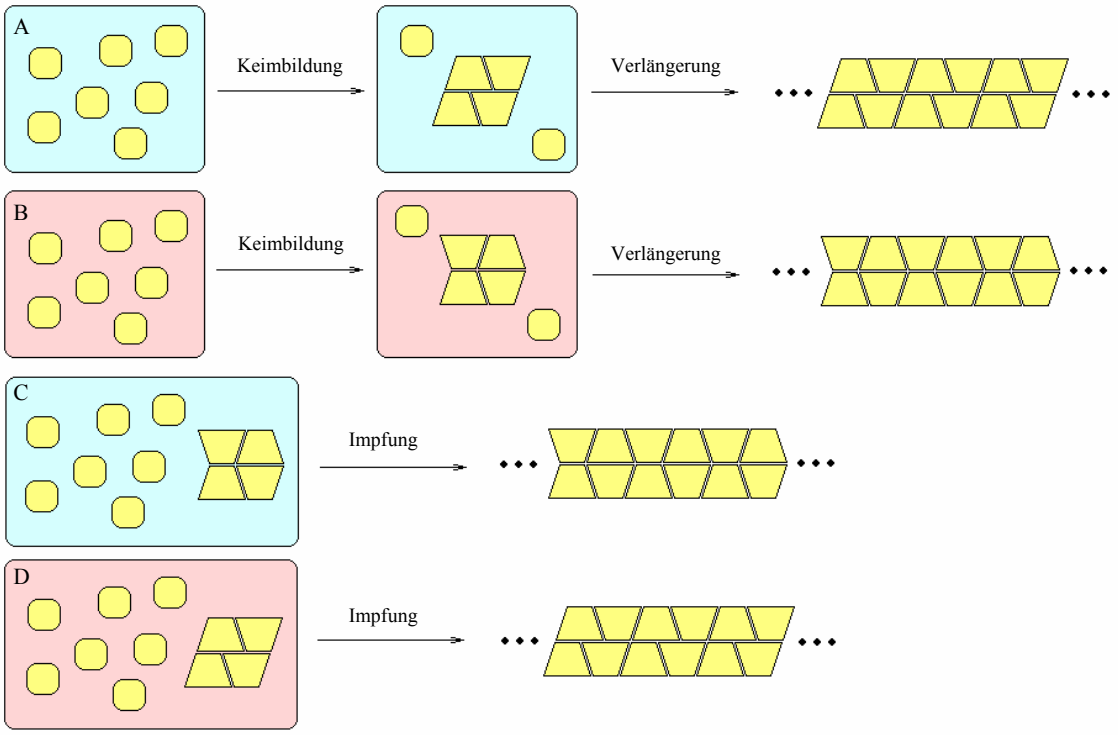

Abbildung 36: Bildung von Inulin-Amyloid-„Strängen" und „cross-seeding". Bei niedrigem pH und hoher Temperatur bilden sich Insulinfibrillen. Die Form von in reinem Wasser (A) und in Anwesenheit von 20% Ethanol (B) gebildeten Fibrillen ist unterschiedlich. Kurze Stücke von Fibrillen, induziert in eine Insulinlösung, können selbst bei Raumtemperatur die Bildung von Amyloid induzieren. Der Effekt von solchen Kristallisationskeimen ist erheblich stärker als Faktoren der Umgebung: Amyloidpartikel, die in einer Lösung mit 20% Ethanol gebildet wurden, können sich, in eine Insulinlösung in reinem Wasser gegeben, vervielfältigen (C) und Amyloidpartikel, die in reinem Wasser entstanden, wachsen, ihre Struktur beibehaltend, weiter in einer Insulinlösung, die 20% Ethanol enthält (D).

Zu einer nativen Insulinlösung mit geringem pH-Wert hinzugefügte ultraschallbehandelte Insulinfibrillen induzieren strukturgleiche Amyloide selbst unter Lösungsmittel-Bedingungen, die für die Ausbildung von Fibrillkeimen ungünstig sind.

Darüber hinaus bleiben die strukturkennzeichnenden Infraroteingenschaften dieser beiden Amyloidzustände auch in der jeweils anderen Lösung erhalten (Abb. 36 C und D). Diese „cross-seeding"-Spezifität und die kinetischen Eigenschaften dieser beiden Amyloidtypen scheinen das bereits bekannte „Prion-Strain-Phänomen" und die kinetischen Charakteristika widerzuspiegeln, die bereits bei anderen amyloidbildenden Proteinen gefunden wurden. Daraus lässt sich schließen, dass es sich bei dem strangabhängigen Wachstum von Prionen um eine inhärente Eigenschaft von Proteinamyloiden handelt.

Die Untersuchung von Insulin bei unterschiedlichen Drücken zeigte keine wesentlichen Unterschiede der Aggregation bei 1 bar und 1000 bar. Einzig ein geringer Unterschied in der Kinetik der Aggregation konnte beobachtet werden.

Die thermodynamischen Größen v^{o}, C_p, α, β_S, und β_T bei der Entfaltung und Aggregation des Insulins und des Polylysins wurden gemessen. Daraus konnte ein einheitliches Bild der zeitabhängigen Aggregation entwickelt werden, das die Wichtigkeit von Volumenfluktuationen während des Enfaltungsprozesses und der Amyloidogenese der Proteine hervorhebt. Diese Fluktuationen scheinen hauptsächlich durch Änderungen der Flexibilität des Proteins, die eng mit dem Leervolumen und Hydratationsänderungen während der zahlreichen Phasen der Strukturänderung (Destabilisierung und partielle Entfaltung des Monomers, Oligomerisierung, erste Aggregation und Wachstum der Fibrillen) verbunden sind, hervorgerufen zu werden.

Schließlich zeigten sich in einer Reihe von Messungen ohne und mit 0,1 M NaCl zwei völlig verschiedene Wege der Aggregation von Insulin. In Abwesenheit ladungsabschirmender Ionen (Salz) wird das Insulin mit steigender Temperatur destabilisiert und entfaltet. Wenn ein gewisses Maß an Entfaltung erreicht ist (wenn die ungeordneten Bereiche dominieren), bildet das Insulin kompakte Keime, die dann zu Fibrillen anwachsen. In Anwesenheit von 0,1 M NaCl kommt es mit steigender Temperatur zu einer partiellen Entfaltung (der „random-coil"-Anteil liegt unter 50%) und zur Bildung von partiell entfalteten nicht-fibrillaren Aggregaten (oder Oligomeren) bei etwa 55-60 °C. Eine weitere Erhöhung der Temperatur führt zu einer Reorganisation der Aggregatstruktur und der Bildung kompakterer Keime, die ein Wachstum längerer Fibrillen erlauben. Die AFM-Messungen zeigen, dass der letzte Prozess, die

Reorganisation, Reifung und Bildung kompakterer Keime aus amorphen Oligomeren zu einer dichteren Aggregatmorphologie führt.

In der Untersuchung an IAPP trat eine besondere Sensitivität des Proteins für hohen Druck zum Vorschein. Die gewonnen Ergebnisse sind möglicherweise physiologisch relevant und wichtig für das Verständnis der Stabilität von IAPP-Fibrillen. Die daraus gewonnenen Kenntnisse lassen sich möglicherweise für die Entwicklung von Antagonisten der Krankheit Diabetes Mellitus Typ II nutzen. Die Aggregation von IAPP in TFE zeigte einen interessanten β-zu-α-zu-β Sekundärstrukturübergang. Dies ist ein Hinweis darauf, dass die transiente Ausbildung von α-Helices wahrscheinlich ein allgemeines Phänomen bei der Amyloidbildung nativ-unstrukturierter Peptide ist.

6. Appendix

6.1. The shape of amyloid fibrils

Several years ago, the existence of circular-shaped amyloid, promoted by high pressure was shown [Jansen et al., 2004]. But can such a shape be observed only after high pressure treatment? And will the same conditions always promote the same shape of fibrils?

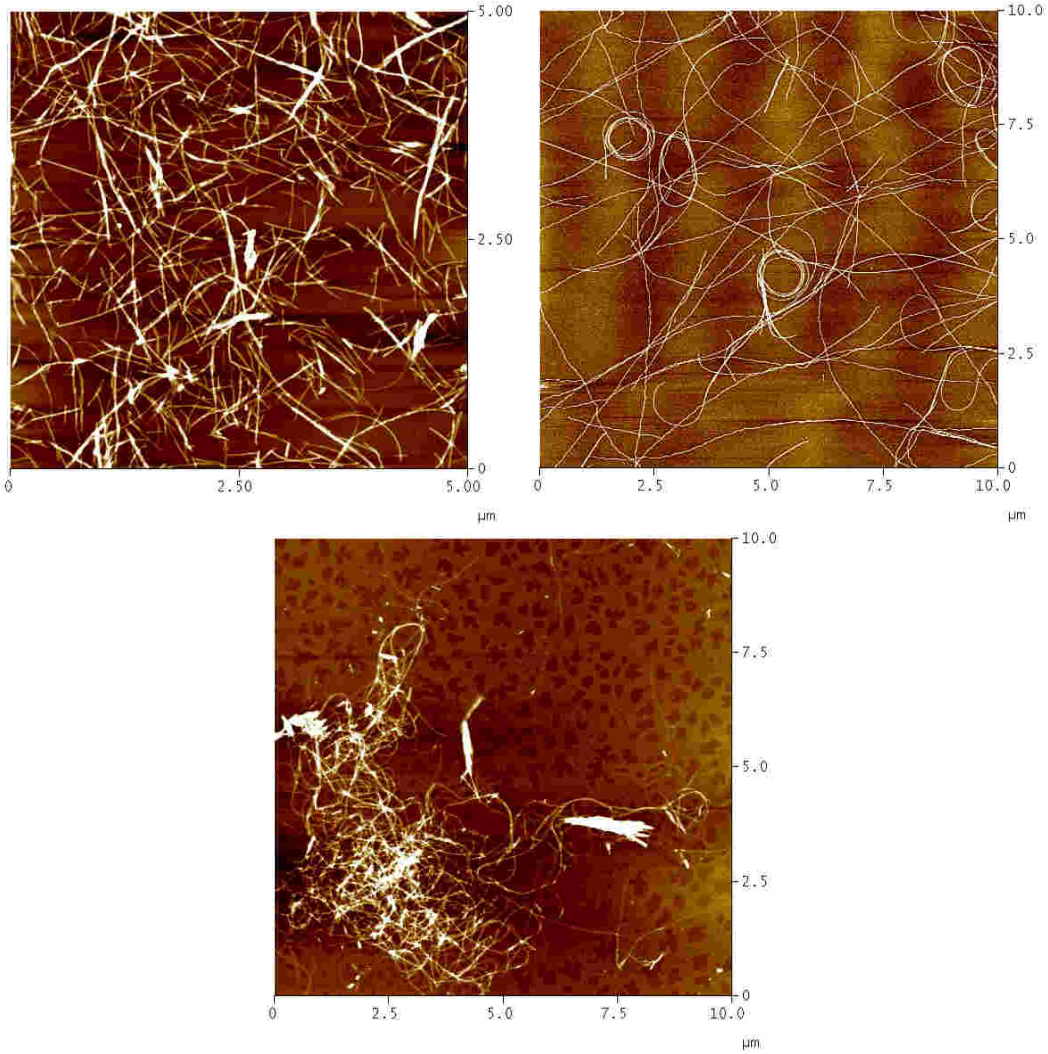

Figure 36: Insulin amyloid fibrils, formed in pH 2, at 60 °C. Straight fibrils, some circles and even some kind of network tructure can be formed under similar conditions.

Figures 36 and 37 show different shapes of insulin amyloid fibrils, grown in water (pH 2) or in presence of 20% TFE. The diversity of shapes of fibrils, formed under the same experimental conditions reflects the stochastic nature of the process and the high degree of polymorphism present in this ???.

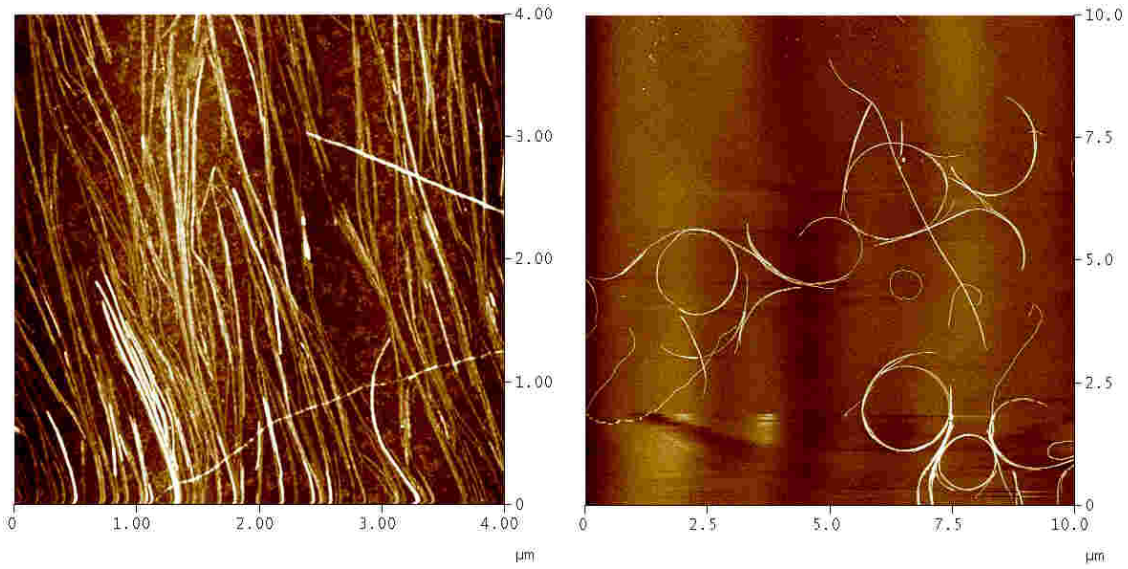

Figure 37: Insulin amyloid fibrils, formed at pH 2, in the presence of 20% TFE at 60 °C. Most of the samples show straight unbranched fibrils, but samples with circular fibrils were also observed.

6.2. Handedness of insulin amyloid

Studies of the insulin fibril structure suggest that insulin is able to form left-handed fibrils [Jimenez et al., 2002]. Most of the microscopy studies are able to confirm it. But there are several articles, showing a model (Fig. 2) [Kurnana et al., 2003] or even AFM images [Jansen et al., 2005] of right-handed insulin amyloid fibrils. Do right-handed insulin fibrils exist, and are there any special conditions to form such fibrils?

Figures 38 and 39 exhibit many of left-handed fibrils and the only right-handed one that I was able to find during 3 years. The inability to find more right-handed fibrils in the same sample and in other samples, prepared the same way, suggests that formation of right-handed fibrils may not depend on environmental conditions, but may be formed at any conditions, with a much lower probability than left handed ones, however. Moreover, it was recently reported that insulin possesses the ability to form aggregates with uniformly biased chiral moieties, which bind and twist likewise an

achiral dye [Dzwolak et al., 2007]. Perhaps these findings can lead to the discovery of the special conditions needed to form different handedness of fibrils.

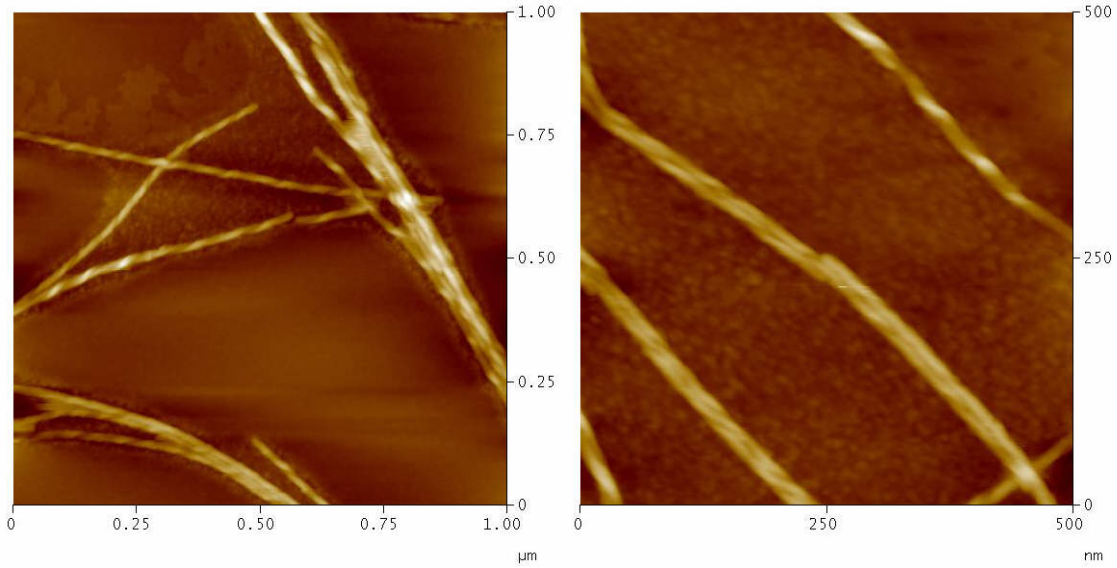

Figure 38: Fibrils, formed by insulin are left-handed…

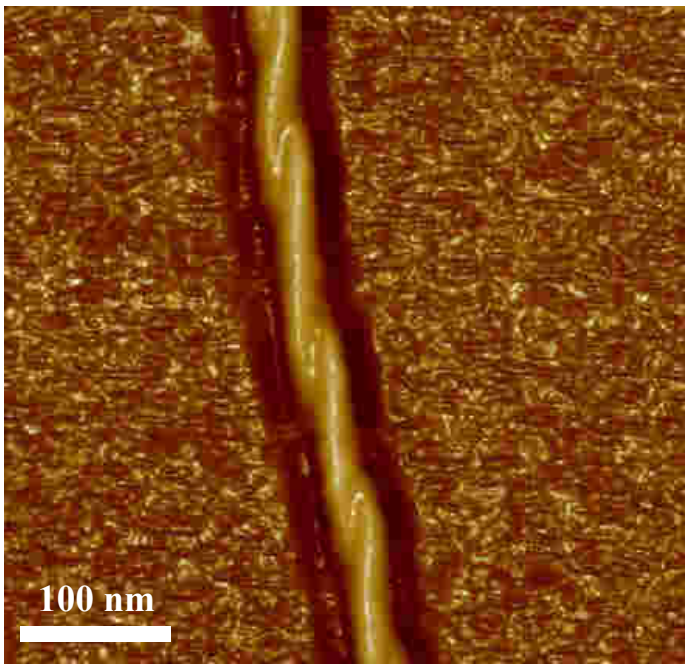

Figure 39: …but occasionally right-handed fibril can be formed s well.

6.3. Layers of IAPP fibrils

While carrying one AFM measurement on IAPP amyloid fibrils I have observed that amyloid fibrils are able to form densely packed monolayers (Figs. 40-41). 5µM IAPP was kept under 3000 bar pressure at 37°C for 3 days, diluted 5 times, put on the mica and left to dry. Upon drying the pressure-treated protein started aggregation directly on the mica, leading to layers of fibrils (Fig. 40). Such behavior of IAPP after pressure treatment was spotted only once, subsequent samples subjected to the same treatment did not show any similar behavior.

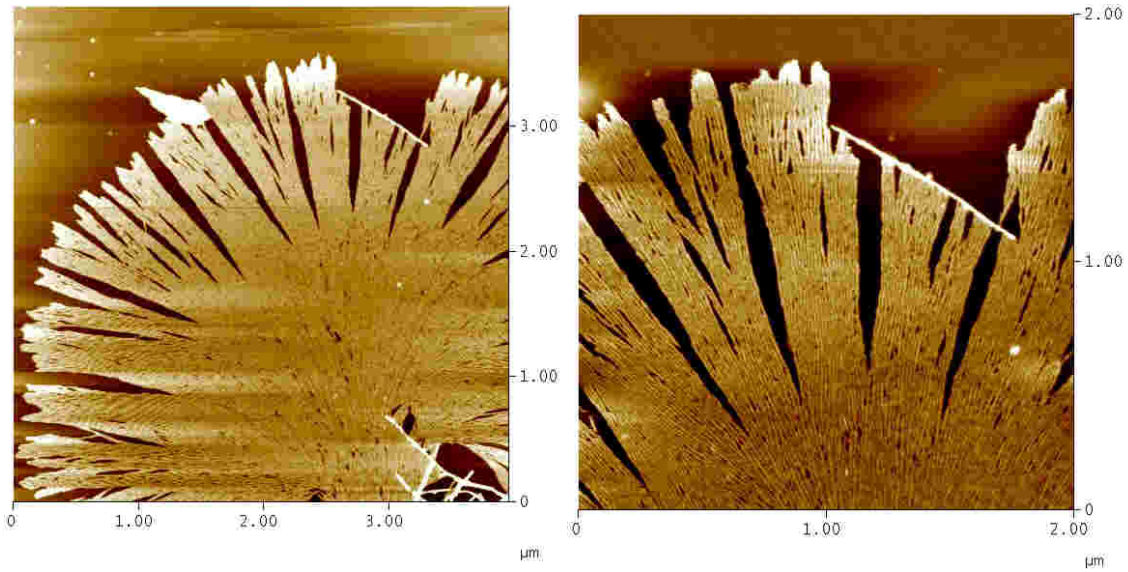

Figure 40: Layers of IAPP fibrils, formed on the mica after pressure treatment.

Additionally, similar layers of fibrils were observed in samples of IAPP, subjected to sonication before applying to mica and leaving to dry (Fig. 42). These findings suggest that IAPP subjected to critical conditions (e.g. high pressure or ultrasonic waves), which lead to the partial break-up into smaller, highly reactive species, has the tendency of fast elongation and the ability to form layer-like structures, when drying at planar solid supports.

In both cases, layers are formed from highly uniform, ~4 nm diameter fibrils. A deeper look into the images reveals that the fibrils tend to grow in a tree-like manner, with dividing into branches during the growth process. Such branching mechanism of

growth was proposed for fibrils of the prion protein [Baskakov 2007] and is typical for diffusion-limited aggregation reactions.

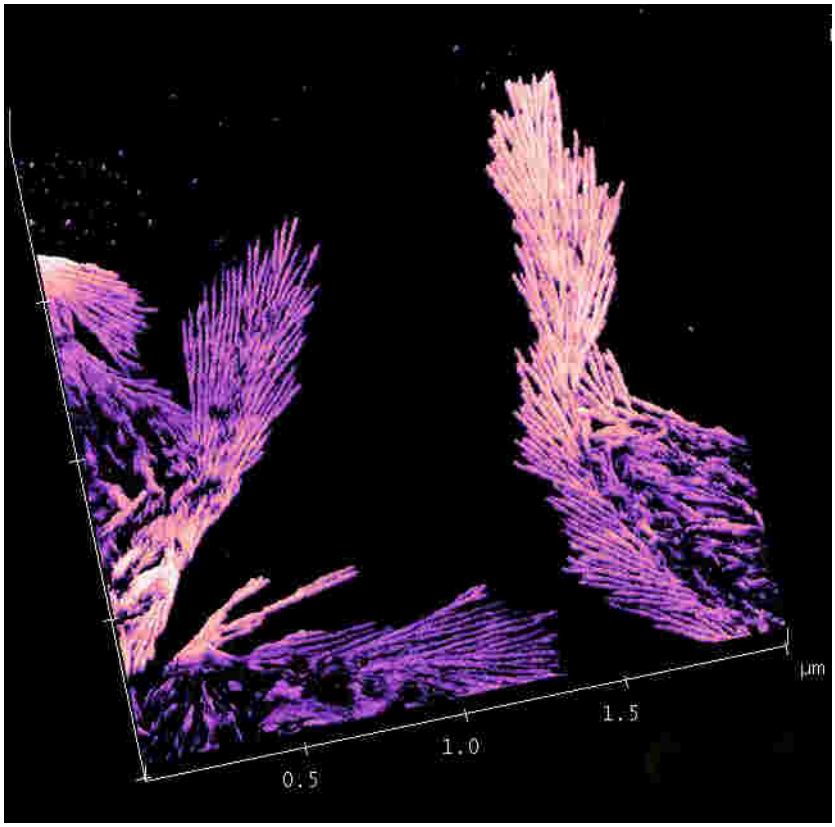

Figure 41: The art of amyloid fibrils. Fibrils of IAPP, grown on mica after sonication.

7. References

Ahmad A, Millett IS, Doniach S, Uversky VN, Fink AL: Partially folded intermediates in insulin fibrillation. BIOCHEMISTRY-US 42 (39): 11404-11416, 2003.

Ban T, Yamaguchi K, Goto Y: Direct observation of amyloid fibril growth, propagation, and adaptation. ACC CHEM RES 39 (9): 663-670, 2006.

Barth A: The infrared absorption of amino acid side chains. PROG BIOPHYS MOL BIO 74 (3-5): 141-173, 2000.

Baskakov IV: Branched chain mechanism of polymerization and ultrastructure of prion protein amyloid fibrils. FEBS J 274 (15): 3756-3765, 2007.

Baumketner A and Shea JE: Free energy landscapes for amyloidogenic tetrapeptides dimerization. BIOPHYS J 89 (3): 1493-1503, 2005.

Bessen RA and Marsh RF: Distinct PrP properties suggest the molecular-basis of strain variation in transmissible mink encephalopathy. J VIROL 68 (12): 7859-7868, 1994.

Bouchard M, Zurdo J, Nettleton EJ, Dobson CM and Robinson CV: Formation of insulin amyloid fibrils followed by FTIR simultaneously with CD and electron microscopy. PROTEIN SCI 9 (10): 1960-1967, 2000.

Bousset L, Thomson NH, Radford SE and Melki R: The yeast prion Ure2p retains its native alpha-helical conformation upon assembly into protein fibrils in vitro. EMBO J 21 (12): 2903-2911, 2002.

Brookmeyer R, Johnson E, Ziegler-Graham K and Arrighi HM: Forecasting the Global Burden of Alzheimer's Disease. ALZHEIMER'S AND DEMENTIA 3: 186-191, 2007.

Bruce ME and Dickinson AG: Biological evidence that scrapie agent has an independent genome. J GEN VIROL 68: 79-89, 1987.

Bruce ME, McBride PA and Farquhar CF: Precise targeting of the pathology of the sialoglycoprotein, PrP, and vacuolar degeneration in mouse scrapie. NEUROSCI LETT 102 (1): 1-6, 1989.

Chalikian TV and Breslauer KJ: Compressibility as a means to detect and characterize globular protein states. P NATL ACAD SCI USA 93 (3): 1012-1014, 1996.

Chalikian TV, Totrov M, Abagyan R and Breslauer KJ: The hydration of globular proteins as derived from volume and compressibility measurements: Cross correlating thermodynamic and structural data. J MOL BIOL 260 (4): 588-603, 1996.

Chalikian TV and Breslauer KJ: Thermodynamic analysis of biomolecules: a volumetric approach. CURR OPIN STRUC BIOL 8 (5): 657-664, 1998.

Chalikian TV: Volumetric properties of proteins. ANNU REV BIOPH BIOM 32: 207-235, 2003.

Canet D, Last AM, Tito P, Sunde M, Spencer A, Archer DB, Redfield C, Robinson CV and Dobson CM: Local cooperativity in the unfolding of an amyloidogenic variant of human lysozyme. NAT STRUCT BIOL 9 (4): 308-315, 2002.

Chien P and Weissman JS: Conformational diversity in a yeast prion dictates its seeding specificity. NATURE 410 (6825): 223-227, 2001.

Chien P, DePace AH, Collins SR, and Weissman JS: Generation of prion transmission barriers by mutational control of amyloid conformations. NATURE 424 (6951): 948-951, 2003.

Chiti F and Dobson CM: Protein misfolding, functional amyloid, and human disease. ANNU REV BIOCHEM 75: 333-366, 2006.

Cooper A: Protein fluctuations and the thermodynamic uncertainty principle PROG BIOPHYS MOL BIO. 44 (3): 181-214, 1984.

Cooper GJS, Day AJ, Willis AC, Roberts AN, Reid KBM and Leighton B: Amylin and the amylin gene - structure, function and relationship to islet amyloid and to diabetes-mellitus. BIOCHIM BIOPHYS ACTA 1014 (3): 247-258, 1989.

Cooper GJS, Willis AC and Leighton B: Amylin hormone. NATURE 340 (6231): 272-272, 1989.

DeArmond SJ, Mobley WC, DeMott DL, Barry RA, Beckstead JH and Prusiner SB: Changes in the localization of brain prion proteins during scrapie infection. NEUROLOGY 37 (8): 1271-1280, 1987.

Dickinson AG, Meikle VMH and Fraser H: Identification of a gene which controls the incubation period of some strains of scrapie agent in mice. J COMP PATHOL 78 (3): 293-9, 1968.

Dobson CM: Protein misfolding, evolution and disease. TRENDS BIOCHEM SCI 24 (9): 329-332, 1999.

Dobson CM: Protein folding and misfolding. NATURE 426 (6968): 884-890, 2003.

Dobson CM: Principles of protein folding, misfolding and aggregation. SEMIN CELL DEV BIOL 15 (1): 3-16, 2004.

Dong J, Wan ZL, Popov M, Carey PR, and Weiss MA: Insulin assembly damps conformational fluctuations: Raman analysis of amide I linewidths in native states and fibrils. J MOL BIOL 330 (2): 431-442, 2003.

Dzwolak W, Ravindra R, Lendermann J and Winter R: Aggregation of bovine insulin probed by DSC/PPC calorimetry and FTIR spectroscopy. BIOCHEMISTRY-US 42 (38): 11347-11355, 2003.

Dzwolak W, Smirnovas V, Jansen R and Winter R: Insulin forms amyloid in a strain-dependent manner: An FT-IR spectroscopic study. PROTEIN SCI 13 (7): 1927-1932, 2004a.

Dzwolak W, Ravindra R and Winter R: Hydration and structure - the two sides of the insulin aggregation process. PHYS CHEM CHEM PHYS 6 (8): 1938-1943, 2004b.

Dzwolak W, Ravindra R, Nicolini C, Jansen R and Winter R: The diastereomeric assembly of polylysine is the low-volume pathway for preferential formation of beta-sheet aggregates. J AM CHEM SOC 126 (12): 3762-3768, 2004c.

Dzwolak W, Loksztejn A, Galinska-Rakoczy A, Adachi R, Goto Y and Rupnicki L: Conformational indeterminism in protein misfolding: Chiral amplification on amyloidogenic pathway of insulin. JOURNAL OF THE AMERICAN CHEMICAL SOCIETY 129 (24): 7517-7522, 2007.

Fändrich M, Fletcher MA and Dobson CM: Amyloid fibrils from muscle myoglobin - Even an ordinary globular protein can assume a rogue guise if conditions are right. NATURE 410 (6825): 165-166, 2001.

Fändrich M and Dobson CM: The behaviour of polyamino acids reveals an inverse side-chain effect in amyloid structure formation. EMBO J 21 (21): 5682-5690, 2002.

Fenimore PW, Frauenfelder H, McMahon BH and Parak FG: Slaving: Solvent fluctuations dominate protein dynamics and functions. P NATL ACAD SCI USA 99 (25): 16047-16051, 2002.

Fink AL: Protein aggregation: folding aggregates, inclusion bodies and amyloid. FOLD DES 3 (1): R9-R23, 1998.

Foguel D and Silva JL: New insights into the mechanisms of protein misfolding and aggregation in amyloidogenic diseases derived from pressure studies. BIOCHEMISTRY-US 43 (36): 11361-11370, 2004.

Fuhrhop JH, Krull M and Büldt G: Precipitates with beta-pleated sheet structure by mixing aqueous-solutions of helical poly(d-lysine) and poly(l-lysine). ANGEW CHEM INT EDIT 26 (7): 699-700, 1987.

Gazit E: The "Correctly folded" state of proteins: Is it a metastable state. ANGEW CHEM INT EDIT 41 (2): 257-259, 2002.

Geddes AJ, Parker KD, Atkins ED and Beighton E: Cross-beta conformation in proteins. J MOL BIOL 32 (2): 343-358, 1968.

Gekko K and Hasegawa Y: Compressibility structure relationship of globular-proteins. BIOCHEMISTRY-US 25 (21): 6563-6571, 1986.

Gekko K and Hasegawa Y: Effect of temperature on the compressibility of native globular-proteins. J PHYS CHEM-US 93 (1): 426-429, 1989.

Glenner GG: Amyloid deposits and amyloidosis. The beta-fibrilloses. NEW ENGL J MED 302 (23): 1283-1292 and 302 (24): 1333-1343, 1980.

Green JD, Goldsbury C, Kistler J, Cooper GJS and Aebi U: Human amylin oligomer growth and fibril elongation define two distinct phases in amyloid formation. J BIOL CHEM 279 (13): 12206-12212, 2004.

Grudzielanek S, Jansen R and Winter R: Solvational tuning of the unfolding, aggregation and amyloidogenesis of insulin. J MOL BIOL 351 (4): 879-894, 2005.

Grudzielanek S, Smirnovas V and Winter, R: Solvation-assisted pressure tuning of insulin fibrillation: From novel aggregation pathways to biotechnological applications. J MOL BIOL 356 (2): 497-509, 2006.

Hayden MR: Pancreatic islet amyloid in type 2 diabetes mellitus: a clinical and historical review. MO MED 99:495–498, 2002.

Heerklotz H: The microcalorimetry of lipid membranes. J PHYS-CONDENS MAT 16 (15): R441-R467, 2004.

Herberhold H, Royer CA and Winter R: Effects of chaotropic and kosmotropic cosolvents on the pressure-induced unfolding and denaturation of proteins: An FT-IR study on staphylococcal nuclease. BIOCHEMISTRY-US 43 (12): 3336-3345, 2004.

Hummer G, Garde S, Garcia AE, Paulaitis ME and Pratt LR: The pressure dependence of hydrophobic interactions is consistent with the observed pressure denaturation of proteins. P NATL ACAD SCI USA 95 (4): 1552-1555, 1998.

Inouye H, Domingues FS, Damas AM, Saraiva MJ, Lundgren E, Sandgren O and Kirschner DA: Analysis of x-ray diffraction patterns from amyloid of biopsied vitreous humor and kidney of transthyretin (TTR) Met30 familial amyloidotic polyneuropathy (FAP) patients: axially arrayed TTR monomers constitute the protofilament. AMYLOID 5 (3): 163-174, 1998.

Jaikaran ET, Higham CE, Serpell LC, Zurdo J, Gross M, Clark A and Fraser PE: Identification of a novel human islet amyloid polypeptide beta-sheet domain and factors influencing fibrillogenesis. J MOL BIOL 308 (3): 515-525, 2001.

Jansen R, Grudzielanek S, Dzwolak W and Winter R: High pressure promotes circularly shaped insulin amyloid. JOURNAL OF MOLECULAR BIOLOGY 338 (2): 203-206, 2004.

Jansen R, Dzwolak W and Winter R: Amyloidogenic self-assembly of insulin aggregates probed by high resolution atomic force microscopy. BIOPHYS J 88 (2): 1344-1353, 2005.

Jarrett JT and Lansbury PT: Seeding one-dimensional crystallization of amyloid - a pathogenic mechanism in alzheimers-disease and scrapie. CELL 73 (6): 1055-1058, 1993.

Jiménez JL, Tennent G, Pepys M and Saibil HR: Structural diversity of ex vivo amyloid fibrils studied by cryo-electron microscopy. J MOL BIOL 311 (2): 241-247, 2001.

Jiménez JL, Nettleton EJ, Bouchard M, Robinson CV and Dobson CM: The protofilament structure of insulin amyloid fibrils. P NATL ACAD SCI USA 99 (14): 9196-9201, 2002.

Jin LW, Claborn KA, Kurimoto M, Geday MA, Maezawa I, Sohraby F, Estrada M, Kaminsky W and Kahr B: Imaging linear birefringence and dichroism in cerebral amyloid pathologies. P NATL ACAD SCI USA 100 (26): 15294-15298, 2003.

Johnson KH, O'Brien TD, Betsholtz C and Westermark P: Islet amyloid polypeptide - mechanisms of amyloidogenesis in the pancreatic-islets and potential roles in diabetes-mellitus. LAB INVEST 66 (5): 522-535, 1992.

Kayed R, Bernhagen J, Greenfield N, Sweimeh K, Brunner H, Voelter W and Kapurniotu A: Conformational transitions of islet amyloid polypeptide (IAPP) in amyloid formation *in vitro.* J MOL BIOL 287 (4): 781-796, 1999.

Kayed R, Sokolov Y, Edmonds B, McIntire TM, Milton SC, Hall JE and Glabe CG: Permeabilization of lipid bilayers is a common conformation-dependent activity of soluble amyloid oligomers in protein misfolding diseases. J BIOL CHEM 279 (45): 46363-46366, 2004.

Khurana R, Ionescu-Zanetti C, Pope M, Li J, Nielson L, Ramírez-Alvarado M, Regan L, Fink AL, Carter SA: A general model for amyloid fibril assembly based on morphological studies using atomic force microscopy. BIOPHYS J 85 (2): 1135-1144, 2003.

Kirkitadze MD, Li H, Condron MM, Zagorski MG, Teplow DB: Formation of an alpha-helix-containing, oligomeric intermediate is an obligatory step in amyloid beta-protein fibrillogenesis. BIOPHYS J 80 (1): 667, 2001.

Kraineva J, Smirnovas V and Winter R: Effects of lipid confinement on insulin stability and amyloid formation. LANGMUIR 23 (13): 7118-7126, 2007.

Krimm S and Bandekar J: Vibrational spectroscopy and conformation of peptides, polypeptides, and proteins. ADV PROTEIN CHEM 38: 181-364, 1986.

Krishnan R, Lindquist SL: Structural insights into a yeast prion illuminate nucleation and strain diversity. NATURE 435 (7043): 765-772, 2005.

Lazo ND and Downing DT: Amyloid fibrils may be assembled from beta-helical protofibrils. BIOCHEMISTRY-US 37 (7): 1731-1735, 1998.

Lopes D, Meister A, Gohlke A, Hauser A, Blume A and Winter R: Mechanism of IAPP Fibrillation at Lipid Interfaces Studied by Infrared Reflection Absorption Spectroscopy (IRRAS). BIOPHYS J Published ahead of print on July 27, 2007 as doi:10.1529/biophysj.107.110635.

Lopes D, Colin C, Degaki TL, de Sousa ACV, Vieira MNN, Sebollela A, Martinez AMB, Bloch C, Ferreira ST and Sogayar MC: Amyloidogenicity and cytotoxicity of recombinant mature human islet amyloid polypeptide (rhIAPP). J BIOL CHEM 279 (41): 42803-42810, 2004.

Lopez de la Paz M, Goldie K, Zurdo J, Lacrois E, Dobson CM, Hoenger A and Serrano L: De novo designed peptide-based amyloid fibrils. P NATL ACAD SCI USA 99 (25): 16052-16057, 2002.

Lorenzo A and Yankner BA: Beta-amyloid neurotoxicity requires fibril formation and is inhibited by congo red. P NATL ACAD SCI USA 91 (25): 12243-12247, 1994.

Ma Z, Westermark GT, Sakagashira S, Sanke T, Gustavsson A, Sakamoto H, Engstrom U, Nanjo K and Westermark P: Enhanced in vitro production of amyloid-like fibrils from mutant (S20G) islet amyloid polypeptide. AMYLOID 8 (4): 242-249, 2001.

Makhatadze GI, Clore GM and Gronenborn AM: Solvent isotope effect and protein stability. NAT STRUCT BIOL 2 (10): 852-855, 1995.

Makin OS and Serpell LC: Structures for amyloid fibrils. FEBS J 272 (23): 5950-5961, 2005.

Makin OS, Atkins E, Sikorski P, Johansson J and Serpell LC: Molecular basis for amyloid fibril formation and stability. P NATL ACAD SCI USA 102 (2): 315-320, 2005.

Mastrianni JA, Nixon R, Layzer R, Telling GC, Han D, DeArmond SJ and Prusiner SB: Prion protein conformation in a patient with sporadic fatal insomnia. NEW ENGL J MED 340 (21): 1630-1638, 1999.

McKinley MP, Meyer RK, Kenaga L, Rahbar F, Cotter R, Serban A and Prusiner SB: Scrapie prion rod formation in vitro requires both detergent extraction and limited proteolysis. J VIROL 65 (3): 1340-1351, 1991.

Millican RL and Brems DN: Equilibrium intermediates in the denaturation of human insulin and two monomeric insulin analogs. BIOCHEMISTRY-US 33 (5): 1116-1124, 1994.

Mitra L, Smolin N, Ravindra R, Royer C and Winter R: Pressure perturbation calorimetric studies of the solvation properties and the thermal unfolding of proteins in solution - experiments and theoretical interpretation. PHYS CHEM CHEM PHYS 8 (11): 1249-1265, 2006.

Modler AJ, Gast K, Lutsch G and Damaschun G: Assembly of amyloid protofibrils via critical oligomers - A novel pathway of amyloid formation. J MOL BIOL 325 (1): 135-148, 2003.

Morozova-Roche LA, Zurdo J, Spencer A, Noppe W, Receveur V, Archer DB, Joniau M and Dobson CM: Amyloid fibril formation and seeding by wild-type human lysozyme and its disease-related mutational variants. J STRUCT BIOL 130 (2-3): 339-351, 2000.

Munishkina LA, Phelan C, Uversky VN and Fink AL: Conformational behavior and aggregation of alpha-synuclein in organic solvents: Modeling the effects of membranes. BIOCHEMISTRY-US 42 (9): 2720-2730, 2003.

Nelson R, Sawaya MR, Balbirnie M, Madsen AO, Riekel C, Grothe R and Eisenberg D: Structure of the cross-beta spine of amyloid-like fibrils. NATURE 435 (7043): 773-778, 2005.

Nielsen L, Khurana R, Coats A, Frokjaer S, Brange J, Vyas S, Uversky VN and Fink AL: Effect of environmental factors on the kinetics of insulin fibril formation: Elucidation of the molecular mechanism, BIOCHEMISTRY-US 40: 6036-6046, 2001.

Nielsen L, Frokjaer S, Carpenter JF and Brange J: Studies of the structure of insulin fibrils by Fourier transform infrared (FTIR) spectroscopy and electron microscopy. J PHARM SCI 90 (1): 29-37, 2001.

Padrick SB and Miranker AD: Islet amyloid polypeptide: Identification of long-range contacts and local order on the fibrillogenesis pathway. J MOL BIOL 308 (4): 783-794, 2001.

Padrick SB and Miranker AD: Islet amyloid: Phase partitioning and secondary nucleation are central to the mechanism of fibrillogenesis. BIOCHEMISTRY-US 41 (14): 4694-4703, 2002.

Pan KM, Baldwin M, Nguyen J, Gasset M, Serban A, Groth D, Mehlhorn I, Huang Z, Fletterick RJ, Cohen FE and Prusiner SB: Conversion of alpha-helices into beta-sheets features in the formation of the scrapie prion proteins. P NATL ACAD SCI USA 90 (23): 10962-10966, 1993.

Peretz D, Williamson RA, Legname G, Matsunaga Y, Vergara J, Burton DR, DeArmond SJ, Prusiner SB and Scott, MR: A change in the conformation of prions accompanies the emergence of a new prion strain. NEURON 34 (6): 921-932, 2002.

Perutz MF, Finch JT, Berriman J and Lesk A: Amyloid fibers are water-filled nanotubes. P NATL ACAD SCI USA 99 (8): 5591-5595, 2002.

Petterson RF: Presentation speech of the Nobel Committee at the Karolinska Institute, December 10, 1997.

Prusiner SB: Molecular-biology of prion diseases. SCIENCE 252 (5012): 1515-1522, 1991.

Prusiner SB: Prion diseases and the BSE crisis. SCIENCE 278 (5336): 245-251, 1997.

Prusiner SB: Prions. P NATL ACAD SCI USA 95 (23): 13363-13383, 1998.

Prusiner SB: Shattuck lecture - Neurodegenerative diseases and prions. NEW ENGL J MED 344 (20): 1516-1526, 2001.

Quintas A, Vaz DC, Cardoso I, Saraiva MJM and Brito RMM: Tetramer dissociation and monomer partial unfolding precedes protofibril formation in amyloidogenic transthyretin variants. J BIOL CHEM 276 (29): 27207-27213, 2001.

Raetz CR and Roderick SL: A left-handed parallel beta helix in the structure of UDP-N-acetylglucosamine acyltransferase. SCIENCE 270 (5238): 997-1000, 1995.

Ravindra R and Winter R: On the temperature - Pressure free-energy landscape of proteins. CHEMPHYSCHEM 4 (4): 359-365, 2003.

Ravindra R, Royer C and Winter R: Pressure perturbation calorimetic studies of the solvation properties and the thermal unfolding of staphylococcal nuclease. PHYS CHEM CHEM PHYS 6 (8): 1952-1961, 2004.

Ridley RM and Baker HF: To what extent is strain variation evidence for an independent genome in the agent of the transmissible spongiform encephalopathies? NEURODEGENERATION 5 (3): 219-231, 1996.

Ross CA and Poirier MA: Protein aggregation and neurodegenerative disease. NAT REV NEUROSCI : S10-S17, 2004.

Saborio GP, Permanne B and Soto C: Sensitive detection of pathological prion protein by cyclic amplification of protein misfolding. NATURE 411 (6839): 810-813, 2001.

Safar J, Wille H, Itri V, Groth D, Serban H, Torchia M, Cohen FE and Prusiner SB: Eight prion strains have PrP^{Sc} molecules with different conformations. NAT MED 4 (10): 1157-1165, 1998.

E. Schreiner, C. Nicolini, B. Ludolph, R. Ravindra, N. Otte, A. Kohlmeyer, R. Rousseau, R. Winter, D. Marx, Folding and unfolding of an elastinlike oligopeptide:

"Inverse temperature transition," reentrance, and hydrogen-bond dynamics. PHYS REV LETT 92 (14): 148101, 2004.

Scott MR, Groth D, Tatzelt J, Torchia M, Tremblay P, Dearmond SJ and Prusiner SB: Propagation of prion strains through specific conformers of the prion protein. J VIROL 71 (12): 9032-9044, 1997.

Seemann H, Winter R and Royer CA: Volume, expansivity and isothermal compressibility changes associated with temperature and pressure unfolding of staphylococcal nuclease. J MOL BIOL 307 (4): 1091-1102, 2001.

Serag AA, Altenbach C, Gingery M, Hubbell WL and Yeates TO: Identification of a subunit interface in transthyretin amyloid fibrils: Evidence for self-assembly from oligomeric building blocks. BIOCHEMISTRY-US 40 (31): 9089-9096, 2001.

Serio TR, Cashikar AG, Kowal AS, Sawicki GJ, Moslehi JJ, Serpell L, Arnsdorf MF and Lindquist SL: Nucleated conformational conversion and the replication of conformational information by a prion determinant. SCIENCE 289 (5483): 1317-1321, 2000.

Sipe JD and Cohen AS: Review: History of the amyloid fibril. J STRUCT BIOL 130 (2-3): 88-98, 2000.

Smirnovas V, Winter R, Funck T and Dzwolak W: Thermodynamic properties underlying the alpha-helix-to-beta-sheet transition, aggregation, and amyloidogenesis of polylysine as probed by calorimetry, densimetry, and ultrasound velocimetry. J PHYS CHEM B 109 (41): 19043-19045, 2005.

St John RJ, Carpenter JF and Randolph TW: High pressure fosters protein refolding from aggregates at high concentrations. P NATL ACAD SCI USA 96 (23): 13029-13033, 1999.

Stefani M and Dobson CM: Protein aggregation and aggregate toxicity: new insights into protein folding, misfolding diseases and biological evolution. J MOL MED-JMM 81 (11): 678-699, 2003.

Sunde M, Serpell LC, Bartlam M, Fraser PE, Pepys MB and Blake CCF: Common core structure of amyloid fibrils by synchrotron X-ray diffraction. J MOL BIOL 273 (3): 729-739, 1997.

Taulier N and Chalikian TV: Compressibility of protein transitions. BBA-PROTEIN STRUCT M 1595 (1-2): 48-70, 2002.

Telling GC, Parchi P, DeArmond SJ, Cortelli P, Montagna P, Gabizon R, Mastrianni J, Lugaresi E, Gambetti P and Prusiner SB: Evidence for the conformation of the pathologic isoform of the prion protein enciphering and propagating prion diversity. SCIENCE 274 (5295): 2079-2082, 1996.

Thirumalai D, Klimov DK and Dima RI: Emerging ideas on the molecular basis of protein and peptide aggregation. CURR OPIN STRUC BIOL 13 (2): 146-159, 2003.

Tycko R: Insights into the amyloid folding problem from solid-state. NMR BIOCHEMISTRY-US 42 (11): 3151-3159, 2003.

Tycko R: Solid-state NMR as a probe of amyloid fibril structure. CURR OPIN CHEM BIOL 4 (5): 500-506, 2000.

Uversky VN and Fink AL: Conformational constraints for amyloid fibrillation: the importance of being unfolded. BBA-PROTEINS PROTEOM 1698 (2): 131-153, 2004.

Virchow R: Weitere Mittheilungen über das Vorkommen der pflanzlichen Cellulose beim Menschen. VIRCHOWS ARCH 6: 268-271, 1854.

Wadsworth JDF, Hill AF, Joiner S, Jackson GS, Clarke AR and Collinge J: Strain-specific prion–protein conformation determined by metal ions. NAT CELL BIOL 1 (1): 55-59, 1999.

Waugh DF, Thompson RE and Weimer RJ: Assay of insulin invitro by fibril elongation and precipitation. J BIOL CHEM 185 (1): 85-95, 1950.

Waugh DF: A fibrous modification of insulin. I. the heat precipitate of insulin. J AM CHEM SOC 68 (2): 247-250, 1946.

Westermark P and Wilander E: Influence of amyloid deposits on islet volume in maturity onset diabetes-mellitus. DIABETOLOGIA 15 (5): 417-421, 1978.

Westermark P, Benson MD, Buxbaum JN, Cohen AS, Frangione B, Ikeda S, Masters CL, Merlini G, Saraiva MJ and Sipe JD: Amyloid: Toward terminology clarification. Report from the Nomenclature Committee of the International Society of Amyloidosis. AMYLOID 12 (1): 1-4, 2005.

Westermark P: Aspects on human amyloid forms and their fibril polypeptides. FEBS J 272 (23): 5942-5949, 2005.

Wetzel R, Shivaprasad S and Williams AD: Plasticity of amyloid fibrils. BIOCHEMISTRY-US 46 (1): 1-10, 2007.

Whittingham JL, Scott DJ, Chance K, Wilson A, Finch J, Brange J and Dodson GG: Insulin at pH 2: Structural analysis of the conditions promoting insulin fibre formation. J MOL BIOL 318 (2): 479-490, 2002.

Williamson JA and Miranker AD: Direct detection of transient alpha-helical states in islet amyloid polypeptide. PROTEIN SCI 16 (1): 110-117, 2007.

Xing YM, Nakamura A, Korenaga T, Guo ZJ, Yao JJ, Fu XY, Matsushita T, Kogishi K, Hosokawa M, Kametani F, Mori M and Higuchi K: Induction of protein conformational change in mouse senile amyloidosis. J BIOL CHEM 277 (36): 33164-33169, 2002.

Zandomeneghi G, Krebs MRH, McCammon MG and Fandrich M: FTIR reveals structural differences between native beta-sheet proteins and amyloid fibrils. PROTEIN SCI 13 (12): 3314-3321, 2004.